UNIVERSITÀ DEGLI STUDI DI TRIESTE

XXX CICLO DEL DOTTORATO DI RICERCA IN

NANOTECNOLOGIE

Engineered DNA nanostructures for targeted breast cancer therapy

Settore scientifico-disciplinare: **BIO/14**

DOTTORANDO
STEFANO PALAZZOLO

COORDINATORE
PROF. LUCIA PASQUATO

SUPERVISORE DI TESI
DR. GIUSEPPE TOFFOLI

CO-SUPERVISORE
DR. FLAVIO RIZZOLIO

ANNO ACCADEMICO 2016/2017

INDEX OF CONTENTS

ABBREVIATIONS 3

1. INTRODUCTION 6

1.1 Chemotherapy 6

1.1.1 History 6

1.1.2 Action and side effects 8

TABLE 1 11

1.2 BREAST CANCER 14

1.3 NANOTECHNOLOGY 16

1.4 ORGANIC NPS IN NANOMEDICINE 18

1.4.1 Polymeric NPs 18

TABLE 2 [80] 21

1.4.2 Micelles 28

TABLE 3 [80] 30

1.4.4 Liposomes 35

TABLE 4 [80] 37

1.4.5 Exosomes 48

1.5 INORGANIC NPS IN NANOMEDICINE 51

TABLE 6 52

1.6 DNA NANOTECHNOLOGY 54

1.6.1 Former DNA nanostructures 54

1.6.2 DNA origami 58

1.6.3 DNA-based drug delivery 63

TABLE 7 68

2. RATIONALE 75

3. AIM 76

4. MATERIALS AND METHODS 77

4.1 REAGENTS 77

4.2 SELF-ASSEMBLING OF DNA ORIGAMI 77

4.3 DNA ORIGAMI PURIFICATION 77

4.4 AGAROSE GEL ELECTROPHORESIS (AGE) 77

4.5 TEM ANALYSIS 78

4.6 DNA ORIGAMI QD LABELING 78

4.7 DNA ORIGAMI STABILITY 78

4.8 DLS ANALYSIS 78

4.9 LIPOSOME PREPARATION AND DNA ORIGAMI INTERNALIZATION AND PURIFICATION 78

4.10 DOXORUBICIN INTERCALATION INTO DNA ORIGAMI, LSTDO AND RELEASE 79

4.11 CELL VIABILITY ASSAY 80

4.12 HISTOPATHOLOGY 80

4.13 ELISA TEST 81

4.14 MOUSE XENOGRAFT 81
4.15 BIODISTRIBUTION 81
4.16 STATISTICAL ANALYSIS 82

5. RESULTS 83
5.1 DNA ORIGAMI SYNTHESIS, CHARACTERIZATION AND STABILITY 83
5.2 THREE STAGE NANOVECTOR (LSTDO) SYNTHESIS AND CHARACTERIZATION 84
5.3 LOADING-RELEASE AND CELL VIABILITY 85
5.4 ACUTE TOXICITY EVALUATION 86
5.5 HISTOPATHOLOGY ANALYSIS 87
5.6 ANTITUMOR EFFICACY 87
5.7 ELISA TEST 88
5.8 THP1 ACTIVATION EXPERIMENT 89

6. DISCUSSION 90

7. CONCLUSIONS 95

BIBLIOGRAPHY 97

Abbreviations

5-FU: 5-Fluorouracil

AFM: atomic force microscopy

AGE: agarose gel electrophoresis

AIM2: absent in melanoma 2

ALL: acute lymphoblastic leukemia

AuNPs: gold nanoparticles

BAL: bronchoalveolar lavage

BC: breast cancer

cGAS: Cyclic GMP-AMP synthase

CHL: Cholesterol

CMC: critical micelle concentration

CMF: combination of cyclophosphamide, methotrexate and 5-fluorouracil

CRC: colorectal cancer

CSF: cerebrospinal fluid

DCs: dendritic cells

DDS: drug delivery system

DLS: dynamic light scattering

DPPE-PEG: 1,2-Dipalmitoyl-sn-glycero-3-phosphoethanolamine-PEG 2000 (16:0)

DSPC: 1,2-distearoyl-*sn*-glycero-3-phosphocholine (18:0)

EPR: enhanced permeability and retention

ER: estrogen receptor

GA: glycolic acid

H&E: hematoxylin and eosin

HTS: high-throughput screening

IFI16: interferon-inducible genes 16

IV: intravenous

L-PAM: L-phenylalanine mustard

LA: lactic acid

LSTDO: lisposome short tube DNA origami

LTDO: long tube DNA origami

MDR: multiple drug resistance

MPS: mononuclear phagocyte system

MRN: Mre11-Rad50-Nbs1

MVE: multivesicular endosomes

NNI: National Nanotechnology Initiative

NPs nanoparticles

ON: over night

ORR: overall response rate

PAA: poly acrylic acid

PEG: polyethylene glycol

PGA: poly glycolic acid

PGR: progestin receptor

PK: pharmacokinetic

PLA: poly lactic acid

PLGA: poly(lactide-co-glycolide)

QDs: quantum dots

RES: reticuloendothelial system

ROS: reactive oxygen species

STDO: short tube DNA origami

TEM: transmission electron microscopy

TLR: Toll-like receptor

TrDO: Triangle DNA origami

Abstract

In this work, I am presenting my PhD project accomplished during three years in nanotechnology. In this dissertation, we address the challenge of developing a drug delivery system based on DNA nanotechnology effective at preclinical stage on breast cancer (BC). In the last decades, DNA has drawn attention of many research groups as a smart nanomaterial. High stability, easy custom synthesis, mechanical rigidity and high loading efficiency are strong suitable properties of DNA to setup a drug delivery system. Unfortunately, the application of DNA nanotechnology *in vivo* is limited. Once in the bloodstream, DNA is quickly recognized as exogenous material by the immune system and DNAses that favor its rapid degradation. To answer this challenge, we developed a new drug delivery system (DDS) based on *short tube* DNA origami (STDO) of 30 nm in length, precisely designed to fit inside pegylated liposomes (LSTDO). This hybrid system combines the properties of stealth liposome to freely circulate in the blood stream and DNA origami to interact with doxorubicin, an anthracycline utilized in the treatment of BC. *In vitro* and *in vivo* antitumor efficacy of LSTDOdoxo was assessed showing an effective improvement of the therapeutic index of doxorubicin. In particular, the LSTDOdoxo accumulates in the tumor taking advantage from the EPR effect and reduces the tumor burden. It was also demonstrated that the encapsulation of DNA origami inside PEGylated liposomes allowed us to develop a safe drug delivery system, which avoid the immune response induced by the administration of exogenous DNA.

1. Introduction

1.1 Chemotherapy

1.1.1 History

Chemotherapy together with surgery are the first line of treatment for many types of cancer[1,2]. Until the 1950, the only therapy recognized for cancer was surgery. In 1942, was employed the first chemical compound to treat a patient with non-Hodgkin lymphoma. The patient was treated with nitrogen mustard. This treatment was based on a discovery of a research group at the Yale School of Medicine that found a profound lymphoid hypoplasia and myelosuppression during autopsy from soldiers exposed to nitrogen mustard during the First World War. Goodman and Gilman speculated that measured doses of a similar treatment could cause a lymphatic tumor regression, conducting an experiment on mice bearing a lymphoid tumor. A tumor regression was shown by the experiment attracting the attention of another research group headed by Lindskog who was persuaded to treat mice with a related compound of "nitrogen mustard" that presented higher reactivity. By this experiment, he demonstrated that a chemical approach was an alternative way to treat the tumor.

A second step into the development of chemotherapy started shortly after in the late '30s at Harvard medical school and at Boston Children's Hospital where Sydney Farber and his research group studied the effect of folic acid on patients with leukemia. This molecule was discovered in 1937 and its deficiency, highlighted in a patient with megaloblastic anemia[3], seemed to stimulate proliferation of acute lymphoblastic leukemia (ALL) cells when administered to children with cancer. Starting by these evidences, at Lederle Laboratories the research of a drug able to block the enzymes involved in the folic acid cascade started. They developed molecules able to block the function of folate requiring enzymes and becoming the first drugs to successfully induce remission in children with ALL[4]. These drugs were analogs of folic acid, which included aminopterin and amethopterin, now known as methotrexate. Another large-scale program started in those years contemplated the screening of fermentation products by the pharmaceutical industry to isolate and synthesize antibiotics to treat wound infection. Initially, penicillin seemed to have antitumor properties but this preliminary data was never confirmed. In contrast, actinomycin D demonstrated to have antitumor activity on some pediatric tumors, establishing the start of a profound interest in the research for more active antitumoral antibiotics. The last program carried during the Second World War was conducted by the Committee on Medical Research of the Office of Scientific Research and Development resulting in the research, synthesis and production of an antimalarial drug. In 1951, starting by a compound able to inhibit the metabolism of purine, Hitchings and Elion developed two drugs, 6-

thioguanine and 6-mercaptopurine, which later would play a pivotal role in the treatment of acute leukemia[5,6]. In the middle 1950s, Charles Heidelberg and his research group at Wisconsin University developed a drug against non-hematological cancers[7]. They observed that there was a great uptake of uracil in the metabolism of rat hepatoma compared to normal tissue. By this observation, they synthesized an analog of uracil binding to the 5-position a fluorine atom obtaining 5-Fluorouracil (5-FU). This agent was found to have a very wide action in the treatment of solid tumors, and until nowadays remain a proof of concept in the treatment of colorectal cancer (CRC).

In the same period, the research group of Gordon Zubrod who centered all their research programs in the discovery of natural compounds to treat important diseases, started a broad program for collecting and testing plant and marine sources that conduct to the discovering of taxanes and camptothecins.

The use of chemotherapy as an aid to traditional therapies started at the beginning of the1960s in advanced breast cancer (BC)[8]. Since the study of this program was not possible, other two programs started. These contemplated the use of L-phenylalanine mustard (L-PAM) used alone and a combination of cyclophosphamide, methotrexate and 5-fluorouracil (CMF) as adjuvant therapy[9]. Both programs were carried out on patients presenting metastatic cancer. The results obtained with CMF were impressive for that period, overall response rate (ORR) was 50% and about 20% of patients actually underwent a complete remission. This was the very beginning of the road that conducts to the present. Nowadays, the challenges are to decrease the side effects of these potent drugs and to develop new strategies to target the tumor. The first and best example of target therapy is the developing of Imatinib, a Bcr-Abl tyrosine kinase inhibitor and it is employed in the treatment of chronic myelocytic leukemia[10,11,12]. The data published by genome sequencing suggests that many of the abnormalities associated with cancer are related to the function of protein kinases, and a major thrust of the current drug development has been to develop a series of kinase inhibitors[13]. A large number of these small molecules have been now approved by the U.S. Food and drug administration for the treatment of a broad of solid tumor hematologic malignancies[9,10,14].

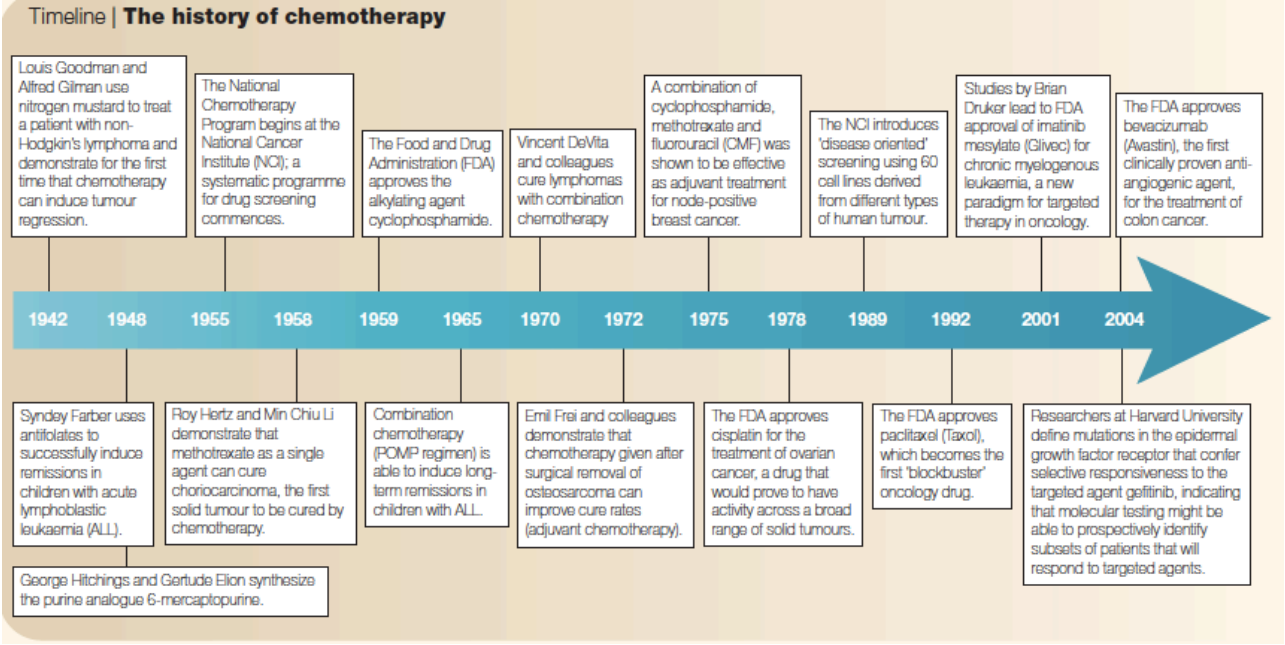

Fig. (1). Timeline of the key steps in the development of chemotherapy. Reproduced from reference [15].

1.1.2 Action and side effects

Cancer therapy has been improved over the past decade introducing a combination of drug regimens, adjuvants and targeted therapies. Nowadays, an increased number of patients are treated with successive chemotherapy lines showing a significantly increased survival. However, the spectrum of side-effects associated with chemotherapy results is wide, ranging from cardiotoxicity to neurological complications, due to the poor selectivity of these molecules (Table 1).

Cardiovascular complications of chemotherapy are uncommon but are higher in the presence of pre-existing coronary disease, in case of combinations of cardiotoxic drugs with previous or concomitant radiation therapy (especially radiotherapy for the left-sided breast carcinoma). For agents such as anthracyclines, cardiotoxicity results in dose-limiting side effects. The direct cardiotoxic effects include myocyte death and fibrosis with resultant cardiomyopathy and heart failure, induction of arrhythmias and coronary ischemia via vasospasm, thrombosis or vascular endothelial inflammation[16]. The family of anthracyclines is intercalating agents that are effective in many malignant diseases and are often used in BC treatment in combination with cyclophosphamide (AC). The antitumor activity of anthracyclines depends on several interconnected mechanisms including[17,18]:

- Cell penetration through the multiple drug resistance (MDR) pore and subsequent proteasome-mediated transport to the nucleus.
- Intercalation into nuclear DNA, elicited by the multiplanar ring structure of the drug, impairs transcription and protein synthesis.
- Inhibition of topoisomerase II blocks repair of disrupted DNA strands.
- Production of reactive oxygen species (ROS) follows nuclear drug binding and results in further injuries to DNA, as well as to cell membranes and mitochondria.

Apoptosis induced by anthracyclines is also initiated by ROS formation, which activates protein p53 and its subsequent fixation to DNA. In turn, p53 promotes transcription of the gene coding for Bax, a pro-apoptotic protein, which opens the mitochondrial pore, releases cytochrome c and initiates apoptosis. P53 also inhibits Bcl-xL, that codes for the related protein having an opposite effect.
Anthracyclines interact with p53 by facilitating its binding to DNA[18].Oxidative stress and induction of apoptosis are the main pathways involved in the action mechanism of anthracyclines. Anthracyclines side effects can be displayed early (within 1-6 months) or in the long-term (several years) and resulted in irreversible damages that conduct to death and cardiomyopathy[19].
Cardiovascular side effects are induced also by the treatment with cyclophosphamide, 5-FU and taxane. The mechanism of action of these compounds is summarized in Table 1. These drugs are frequently used in combination with anthracyclines so the patients treated with this regimen need a strict follow up of the side effect on their cardiovascular system.
Severe side effects due to the direct or indirect effect of chemotherapy affect also the central and peripheral nervous system with syndromes and injuries of different grades. Signs and symptoms can cause confusion with alternative tumor-related diagnosis such as cerebral metastatic disease, spinal cord compression, paraneoplastic syndromes or co-incidental diseases such as infective meningitis and primary epilepsy. Injuries to peripheral sensory and motor neurons are well-recognized as side effects of taxanes, thalidomide, vinca alkaloids and nucleoside analogs. Sensory neuropathies range from perioral numbness through peripheral paraesthesia to neuropathic burning pain. The family of Taxanes is generally linked with neuropathy that is often solved with a reduction of the drug, other compounds, such as thalidomide and vinca alkaloids may cause permanent irreversible damage and should be discontinued whenever signs of neurological injury are displayed. Motor neuropathies may also arise and would lead to reduction or discontinuation of the causative agent. Acute and subacute encephalopathy can be induced by Cytarabine treatment in a permanent form[20]. In contrast, if this drug is associated with methotrexate, encephalopathy is usually reversible[21]. Nevertheless, the

majority of neurotoxicities displayed by the treatment by different agents remain unpredictable. Another common adverse effect related to treatment with both cytotoxic and immunomodulatory chemotherapy is bone marrow suppression and immune deficiency[22]. The adverse effects are related to the fact that chemotherapeutic agents are more active on high proliferating cells as tumor cells, it targets the high mitotic rate of bone marrow (especially white cell precursor) cells too. These side effects may be dose-limiting or if stem cell harvest or bone marrow harvest has been undertaken before chemotherapy exposure, they may be ignored and the patient receives an autograft following chemotherapy. Consequently, patients undergo an immunosuppressive state that gets them susceptible to opportunistic infection requiring an antimicrobial prophylaxis to reduce the risk of sepsis and the reactivation of pre-existing infection is often displayed. Another severe event that can conduct patients to a very severe condition is represented by the hypersensitivity reaction due to the intravenous administration of chemotherapeutic drugs ranging from mild fever to fulminant anaphylaxis. This reaction is commonly caused by monoclonal antibody (Rituximab and Herceptin), but it is also frequently displayed in relation to asparaginase, carboplatin and etoposide.

The last group of most common and severe side effects concern gastrointestinal tract. Oro-pharyngeal mucositis may follow radiotherapy, chemotherapy or hemopoietic stem cell transplant and affects approximately 30–50% of the patient populations[23]. Chemotherapy-induced damage to the mucous membranes of the body occurs because of the relatively high turnover of cells in these tissues compared with others and results in local inflammation, cellular apoptosis and ulceration of the membrane with loss of barrier function and opportunistic secondary infection, especially with candida and herpes simplex virus. Mucositis is classified in a 5-grade[24] scale and the high scores should influence the decision to change the therapy. Certain drugs (5-fluorouracil, methotrexate, etoposide, doxorubicin and cytarabine) characteristically cause mucositis more frequently than others. Among side effects, nausea and vomiting remain the most distressing. They appear in the first 24 hours after the administration. Nausea and vomiting can be triggered by activation of the chemoreceptor trigger zone or via afferent inputs to the vomiting center of the brain in the nucleus tractus solitarius, which receives inputs from the gastrointestinal tract via the vagus nerve. Also, diarrhea is commonly associated with many different forms of chemotherapy in particular with antimetabolite and alkylating agents. Patients, who undergo these side effects need a quickly rehydration with the infusion of glucosate and saline solutions.

Table 1. Reproduced from Carr et al[25].

Drug group	**Mode of action**	**Characteristics toxicities**
Platinum analogues e.g. carboplatin, cisplatin	Selective inhibition of tumor DNA synthesis	Myelosuppression, nephro/oto/ neurotoxicity
Taxanes e.g. docetaxel, paclitaxel	Inhibits mitosis	Conduction defects, peripheral neuropathy, hypersensitivity
Topoismerase inhibitors e.g. irinotecan, topotecan	Inhibits DNA replication	Acute cholinergic syndrome
Immunomodulators Antiproliferatives Azathioprine Mycophenolate	Immunosuppressant	Myelosuppression
Immunosuppressors		
Cyclosporine	Calcineurin inhibitor	Nephrotoxic, hypertension, PRES, gum hyperplasia
Tachrolimus	Calcineurin inhibitor	Nephrotoxic, hypertension, PRES
Thalomide	Angiogenesis inhibitor, inhibiting cell growth	Teratogenic, peripheral neuropathy
Monoclonal antibodies		
bevacizumab	Inhibits VEGF, inhibiting cell growth	Mucocutaneous bleeding, GI perforation
Cetuximab	Binds To EGFR, inhibits cell division	Hypersensitivity
Rituximab	Causes lysis of B cell lymphocytes	Cytokine release syndrome
Trastuzumab (Herceptin)	Binds HER2 receptor, inhibits cell division	Cardiotoxicity, hypersensitivity
Alemtuzumab (Campath)	Causes lysis of mature lymphocytes	

Drug group	**Mode of action**	**Characteristics toxicities**
<u>Hormones</u>		
Oestrogens	Direct cytotoxic effect on tumour cells	Venous and arterial thromboses
Progestogens	Or suppress other hormone production	Mild (nausea, fluid retention)
Hormone antagonists		
Tamoxifen	Estrogen receptor antagonist	Thrombosis, endometrial Ca, strokes
Anastrozole	Aromatase Inhibitor	Post-menopausal symptoms
Gonadorelin analogues	Similar SE to menopause in women and orchidectomy in men	
Buserelin	Down regulate pituitary stimulation of Male and female gonads	

Drug group	**Mode of action**	**Characteristics toxicities**
Antiandrogens Cyproterone	Inhibit tumour ‘‘Flare’’	Hepatotoxicity
Miscellaneous antineoplastics Asparaginase	Breaks down asparagine to aspartic acid and ammonia	Anaphylaxis
Procarbazine	Causes free radical formation	Myelosuppression, hypersensitivity rash

1.2 Breast Cancer

BC is the most common cancer among women and is in the third place for mortality worldwide[26]. BC is a complex disease that includes different clinical, morphological and molecular facets. Great scientific, economic and social interest are involved in the research of BC to understand the causes of onset, identify the critical molecular players of progression, and define new lines of intervention in order to obtain more benefits and reduce the toxicity of the current therapies. BC can be subdivided into few subtypes based on their molecular profile and phenotype.

The luminal A BC representing the 50-60% of the case observed is the most common subtype. It is characterized by the expression of genes activated by estrogen receptor and a low expression of genes related to cell proliferation[27,28]. These features confer to this subtype a low-grade progression with patients' good prognosis; the relapse rate is lower than other subtypes with 27.8%[29], also time to relapse is longer with a median of 2.2 years.

Luminal B molecular profile is present in almost 20% of all BC. This subtype presents women with luminal B tumors, often diagnosed at a younger age than those with luminal A tumors[30,31] and, compared to luminal A tumors, they tend to have more aggressiveness with a worse prognosis, higher histological grade, proliferative index, larger tumor size, lymph node-positive, p53 gene mutations (about 30%), all factors that lead to a poorer prognosis[31,32]. The main biomolecular difference between luminal A and B is the increased expression of proliferative genes.

HER2 positive BC corresponds to 15-20% of all cases. They are characterized by the presence of extra copies of HER2 gene that induce the overexpression of this receptor and other associated with the HER2 pathway and/or HER2 amplicon located on the 17q12 chromosome. This subtype presents a particular high grade with a high proliferative profile associated with the 40% of case with the mutation of p53 that is translated in poor clinical prognosis for the patients. HER2 amplified BC can be subclassified into three different subtypes, one with a clearly worse prognosis with a 12% 10 years survival, and other two groups with 50–55% of survival.

Ten-twenty percent of all BC are represented by basal-like subtypes. They express genes that are usually present in breast myoepithelial cells; they are also characterized to be negative for three common markers represented by the key receptor of BC: estrogen receptor (ER), progestin receptor (PGR) and HER2. Clinically, they are characterized by an early stage appearance, high grade and high frequency of lymph nodes infection[33]. The high aggressiveness of this subtype can be related to the high frequency rate of p53 mutation (70%) and is often linked with a poor prognosis[27].

Normal BC represents 5-10% of all mammary carcinomas. They are not well characterized and they have been grouped into fibroadenomas and normal breast cancer[28]. The expressed genes are typical of adipose tissue; the prognosis is between luminal and basal-like and usually do not respond to neoadjuvant therapy. Due to the lack of ER, Pgr and HER2 expression, they can be classified as triple negative.

A new subtype called claudin-low was identified in 2007[34]. A low expression of genes involved in tight junctions and intercellular adhesion, including claudin-3, -4, -7 cingulin, occludin, and E-cadherin characterize this tumor. Claudin-low tumors even presenting the low expression of cell proliferation genes have a poor prognosis.

The importance of molecular classification for the therapeutic approach has been slowly recognized by the St. Gallen International Expert Consensus for Early Breast Cancer in 2011. Five clinicopathological definitions have been established by this Expert Consensus with a recommended therapeutic strategy for each subtype.

1.3 Nanotechnology

The application of nanotechnology in medicine is called nanomedicine and is the base to develop new drug formulations based on nanocarriers. In 2004, the European science foundation defines Nanomedicine as "the science and technology of diagnosing, treating and preventing diseases and traumatic injuries, of relieving pain, of preserving and improving human health, using molecular tools and molecular knowledge of the human body"[35]. Another definition of nanomedicine that explains better the working field of that discipline is the application of the nanoscale material in medicine that takes advantages of the nanomaterial's unique properties[36]. According to the federal US research and development program agency, the National Nanotechnology Initiative (NNI), nanotechnology involves the development of carriers devices or systems sized in 1 to 100 nm range although this limit can be extended up to 1000 nm[37]. In the last two decades, nanotechnology rapid developments have allowed the incorporation of multiple therapeutic, sensing and targeting agents into nanoparticles (NPs) in order to develop nanodevices able to detect, prevent and treat oncological disease. It is well known that chemotherapeutic agents present severe side effects including bone marrow suppression, cardiac and kidney toxicity, hair loss and mucositis; in addition, these drugs are poorly soluble in biological fluids, are quickly recognized by the mononuclear phagocyte system (MPS) and fast cleared from the body[38]. The binding or the encapsulation of drug to NPs can also modify chemical and physical properties such as poor water solubility, drug circulation half-life escaping the non-specific immune system, biodistribution and pharmacokinetic (PK)[39]. The application of nanotechnology to drug delivery has an enormous potential concerning the improvement of selectivity in targeting neoplastic cells by allowing the preferential delivery of drugs to tumors owing to the enhanced permeability and retention (EPR) effect of the leaky vasculature in tumors and inflamed tissue. Poorly aligned endothelial cells in the fast-growing, tumor vasculature with fenestration larger than 100 nm in size and reduced lymphatic drainage in tumor tissue result in preferred accumulation of nanocarriers in these tissues over healthy tissues. In that way, it is possible to reduce drug volume distribution while improving PK profile, and consequently, the anticancer efficacy. NPs, having a great surface to volume ratios, need a very high control of their surface properties in order to predict their behavior once in the blood stream[40]. The combination between size and surface properties can determine the fate of NPs within the body defining the interactions with their local environment. The sterical stabilization of NPs (for example by polyethylene glycol (PEG) polymers on their surface) and surface charges that are either slightly negative or slightly positive allows them to have minimal self–self and self–non–self interactions. For an *in vivo*

application, these properties represent a crucial point, since the inside surface of blood vessels and the surface of cells contain many negatively charged components, which would repel negatively charged NPs. The presence of a large surface charge (either positive or negative), increase and stimulate the macrophage to scavenge NPs and can lead to greater clearance by the reticuloendothelial system (RES). Thus, to minimize nonspecific interactions via steric stabilization and control, the surface charge covers a central role in order to prevent NPs loss to undesired locations. Summarizing, the drug encapsulation serves two purposes: to protect the body against off-site toxicities and to protect drug against body defense system.

Drug delivery system (DDS) and more generally nanovectors can be divided into three generations of compounds, according to whether or not they were developed to target a specific molecule which is expressed on the tumor cells or in the endothelium. First generation nanovectors are the simplest way to build a carrier nanoparticle, they are capable to accumulate by passive mechanisms exploiting EPR effect, or more specifically they extravasate through gaps in tumor neovasculature. Among the "first generation" vectors, liposomes based drug delivery is the most successfully used in the clinic, as demonstrated by liposomal doxorubicin for BC, ovarian cancer and Kaposi's sarcoma. The "second generation" of therapeutic nanovectors represent the natural evolution of the first generation, constructed with additional function including surface modification with ligands, able to bind specific biological molecules of the tumor cell[41]. The aim of these NPs is to deliver higher drug concentrations to pathologic tissues, sparing the normal ones in order to enhance the effect on the tumor, thereby reducing systemic toxicity. Moreover, they can possess advanced features including the possibility to co-deliver drugs and imaging agents, or can be modified in order to have a controlled or triggered release.

The so-called "third generation" of nanovectors has been developed and is based on a multi-stage strategy in order to overcome the numerous obstacles on their way to the tumor side. These carriers are made by diverse nanoparticles nested into a single vector to build a system that can avoid the biological barrier and at the same time possess tumor cytotoxic and target activity[42]. An example is represented by biodegradable silicon nanoparticle[43,44]. These particles possess the property to recognize specifically the pathologic endothelium through a mathematically driven recognition of the physic-chemical and geometrical surface features (first stage). The second stage nanoparticles are loaded into the first one and released inside tumor from the site of vascular adhesion. The size of these particles is <20 nm so they can easily cross the inter-endothelial junctions and extravasate in the tumor delivering the drugs.

The aforementioned strategies allowed the developing of more than 200 products that have been approved or are under clinical investigation[45]. In contrast with the large number of DDS that reached efficacy at a preclinical stage, recent studies demonstrate that development of a successful clinical translation is a very challenging process with about 10% of success rate of approval for therapeutics entering phase I trial[46].

1.4 Organic NPs in nanomedicine

Organic NPs can be described as solid particles composed of organic compounds (mainly lipids, proteins or polymers), and have been investigated for decades, providing a large variety of materials and exciting applications in nanomedicine[47].

1.4.1 Polymeric NPs

Polymeric NPs have been widely studied for their physical and chemical properties and used to encapsulate drugs. They are prepared from biocompatible polymers and can transport drugs in a controlled and targeted way through the surface modification[48]. Polymeric NPs can be synthesized from natural polymers, such as albumin[49], hyaluronic acid[50], and chitosan[51], and from synthetic polymers, such as, polyacrylic acid (PAA), polyglycolic acid (PGA), poly(lactide-co-glycolide) (PLGA), polylactic acid (PLA), dendrimers, and hyperbranched polymers[52]. Different methods of synthesis of polymeric NPs are investigated depending on the application and drug type. These methods include solvent evaporation, nanoprecipitation, and emulsion diffusion[53–55].

Albumin is the most abundant protein in plasma and used widely for the preparation of NPs due to its biodegradability, non-toxicity, availability, hydrophilicity, and easy to prepare[56]. The major advantage of albumin is its high binding capacity for different drugs due to multiple drug-binding sites[57]. The drugs can be loaded by electrostatic interaction on the surface of NPs, incorporated into the NPs matrix, or linked covalently to the protein due to the presence of surface reactive groups such as amines, thiols, and carboxylic acids[58], and released through hydrolysis, diffusion, or enzymatic degradation of NPs[59] (Figure 2).

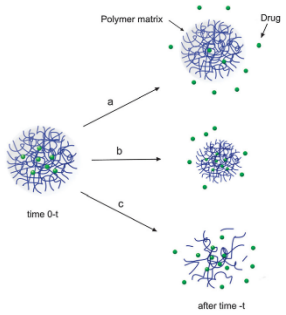

Fig. (2). Drug release mechanism from polymeric nanoparticles: (a) diffusion from the polymer matrix, (b) degradation of the polymer matrix, and (c) biodegradation of the polymer matrix due to the hydrolytic degradation. Reproduced with permission from reference [60].

Among the synthetic polymers, polyesters as PLA and PLGA, are commonly used in drug delivery due to their biocompatibility and controlled release through the hydrolysis of ester bonds[52,61].

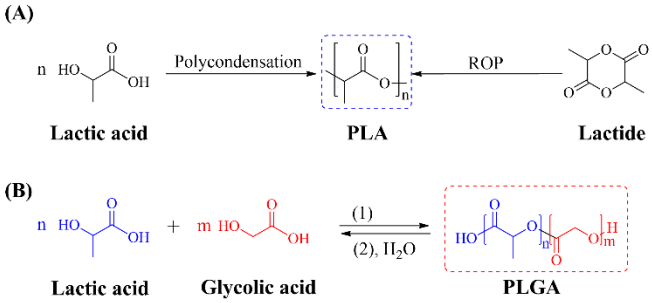

Fig. (1). (A) Synthesis of PLA by polycondensation of lactic acid or by ring-opening polymerization (ROP) of lactide. **(B)** (1) Synthesis of PLGA by polycondensation of lactic acid and glycolic acid, and (2) hydrolysis of PLGA.

PLA is a polyester homopolymer and synthesized by polycondensation of lactic acid or by ring-opening polymerization (ROP) of lactide (Figure 3A)[62]. PLA NPs have been used in drug delivery to encapsulate hydrophobic compounds and improve solubility limitations[63]. Due to its high crystallinity and low degradation rate, PLA NPs has slow drug release[64]. To overcome this limitation, researchers synthesized copolymers of lactides, PLGA and PEG-PLA[55]. PLGA is one of the most commonly used biodegradable polymers for the development of biocompatible NPs because it can be degraded by hydrolysis of ester bonds and break down into their monomers, lactic acid (LA) and glycolic acid (GA) which are excreted from the body[65] (Figure 3B).

The PLA to PGA ratio can be tuned to control the degradation of PLGA and release the drug molecule, due to the difference in hydrophobicity of PLA and PGA from the presence of methyl group in PLA[66]. The release rate of drugs can be adjusted from a scale of days to months[67–69].

In order to enhance the solubility and drug loading capacity of PLGA (or PLA), PEG has been copolymerized with PLGA (or PLA) to form PEG-PLGA (or PEG-PLA). The modification of the surface of NPS by PEG (PEGylation), make the NPs sterically stable, enables the NPs evasion of the reticuloendothelial system (RES) and improve blood circulation time[70–72].

Abraxane was the first drug formulation of this category approved by FDA in 2005 and is the most representative of the category we are describing. Abraxane is the albumin-bound (Nab) Paclitaxel formulation. Paclitaxel is a natural compound extracted from the bark of western yew (Taxus bifolia)[73] and is widely used for the treatment of breast, lung and advanced ovarian cancer[74]. The

high hydrophobicity of this drug limits its clinical application. To overcome this poor water solubility, it is formulated with the employment of lipid-based (Cremophor-EL) solvent. However, even this formulation is often related to the biological and pharmacological activity of lipid-based solvent that induces, during intravenous infusion, histamine release with consequent well-described hypersensitivity reaction and anaphylaxis in 20-40% phase I trials patients[74]. To avoid or minimize this side effects Paàl et al[75] research group made a new formulation based on non-covalent binding of paclitaxel to albumin. Albumin is the major component of plasma protein and is a natural carrier of hydrophobic molecules such as vitamins, hormones, and other water-insoluble plasma substances, that are bound in a reversible non-covalent manner[76,77]. In addition albumin is involved in endothelial transcytosis through cell surface receptor binding to a 60 kDa glycoprotein (gp60) called albondin[78]. It is also demonstrate that albumin is recognized by SPARC, *s*ecreted *p*rotein, *a*cidic and *r*ich in *c*ysteine, often present in some malignancies (breast, lung and prostate cancer), which could explain why albumin is known to accumulate in some tumors and can facilitate the accumulation of albumin-bound drugs[76]. Moreover, albumin stabilizes particles of 130 nm size that once in the circle rapidly dissociate in 8 nm paclitaxel coated albumin molecules which are able to prevent capillary obstruction risks and do not necessitate any particular infusion system or corticosteroid/antihistamine pretreatment before the intravenous administration[79]. Abraxane possesses a reduced treatment volume and time required for administration escaping the toxicity induced by Cremophor-EL. In the following table a summary of all polymeric nanoparticles that reach a clinical stage (Table 2).

Table 2 [80]**.** Polymeric Nanoparticles on the market and under clinical evaluation. Reproduced from Palazzolo et al.

Name [Refs]	Formulation	Bioactive compound	Company	Admin. Route	Size	Drug Loading/ Encapsulation (%)	Nanovector /Drug Ratio	Indications	Description	Conclusions	Clinical Trials Identifier (Phase, Status)
Abraxane [81–87]	Albumin	Paclitaxel	Abraxix Bioscience (Celgene)	Intravenous	130 nm	1:1		Metastatic breast cancer	To decrease toxicity of cremophor-based paclitaxel. Patients treated with Abraxane showed an increased OS and ORR, longer TTP.	Patients treated with Abraxane showed less toxicities compared to paclitaxel.	N/A (Approved FDA 2005, EMA 2008)
								NSCLC in combination with carboplatin		Patients treated with Abraxane in combination with carboplatin showed no toxicities compared to paclitaxel.	N/A (Approved FDA 2012)
								Metastatic pancreatic cancer in combination with gemcitabine		Patients treated with abraxane plus gemcitabine showed a major tumor accumulation of gemcitabine in tumor.	N/A (Approved FDA 2013)
								NSCLC in combination with Abraxane and Pembrolizumab	Determine the optimal dose of Abraxane to be safely administered in combination with pembrolizumab in patients with advanced inoperable NSCLC. The study is also aimed at evaluating the efficacy of the combination therapy.	No Study Results Posted.	NCT02733250 (Phase I/II)

Table 2. *(Continued)*

Name [Refs]	Formulation	Bioactive compound	Company	Admin. Route	Size	Drug Loading/ Encapsulation (%)	Nanovector /Drug Ratio	Indications	Description	Conclusions	Clinical Trials Identifier (Phase, Status)
Abraxane	Albumin	Paclitaxel	Abraxix Bioscience (Celgene)	Intravenous	130 nm	1:1		NSCLC in combination with Carboplatin/ nab-paclitaxel and Pembrolizumab	This trial is evaluating the combination of carboplatin, nab-paclitaxel, and pembrolizumab in metastatic non–small cell lung cancer (NSCLC) (mNSCLC)	Pembrolizumab in combination with carboplatin/nab-paclitaxel is safe and tolerable.	NCT02382406 (Phase I/II)
								Breast Cancer	Study of Neoadjuvant Chemotherapy with Nanoparticle Albumin Bound Paclitaxel, Doxorubicin and Cyclophosphamide (NAC) in Patients with Stages II-III Breast Cancer.	The highest tolerable dose of nab-paclitaxel (Abraxane) was assessed to be 100 mg/m^2 in combination with doxorubicin (Adriamycin) and cyclophosphamide in patients with stages II-III breast cancer in the neoadjuvant setting.	NCT01090128 (Phase I)
								Advanced Solid Tumors (Abraxane® (ABI-007) and Alimta® (Pemetrexed))	Evaluation of the safety and efficacy of combining pemetrexed and Abraxane with a focus on NSCLC for phase II expansion.	The phase II component demonstrated activity in second/third-line therapy of advanced NSCLC; response rate 14% and disease control rate 46%.	NCT00470548 (Phase I/II)
BIND-014	PEG-PL(G)A	Docetaxel	Bind Therapeutics	Intravenous	100 nm	Loading 10-13 %	N/A	Metastatic Cancer solid tumors	Primary outcome: to assess the DLTs and MTD of BIND-014	Treatment dose was establish at 75 mg/m^2	NCT01300533 (Phase I)

Table 2. *(Continued)*

Name [Refs]	Formulation	Bioactive compound	Company	Admin. Route	Size	Drug Loading/ Encapsulation (%)	Nanovector /Drug Ratio	Indications	Description	Conclusions	Clinical Trials Identifier (Phase, Status)
BIND-014	PEG-PL(G)A	Docetaxel	Bind Therapeutics	Intravenous	100 nm	Loading 10-13 %	N/A	Metastatic castration-resistant prostate cancer (mCRPC)	To evaluate the efficacy and safety of BIND-014. Primary outcome: to determine the efficacy of BIND-014 measured by radiographic PFS 6 months post treatment.	The most common treatment-related adverse events (TRAEs) were generally grade 1 and 2. BIND-014 is well-tolerated. Primary endpoint reached.	NCT01812746 (Phase II)
								NSCLC	To evaluate the efficacy and safety of BIND-014 in patients with advanced NSCLC treated once every 3 weeks. Primary outcome: to determine the efficacy by ORR.	The trial met its primary endpoint as measured by ORR.	NCT01792479 (Phase II)
CALAA-01	Cyclodextrin-containing polymer (CAL101) and targeting agent (AD-PEG-Tf)	siRNA	Calando Pharmaceuticals	Intravenous	70 nm	N/A	1:20 (Targeting ligand: siRNA Ratio)	Solid Tumors	To deliver siRNA, to avoid their degradation by non-specific immune system cells. Primary outcome: to determine the tolerability, safety profile and MTD of intravenous CALAA-01	CALAA-01 delivery system had positive anti-tumor results and has been shown to be safe.	NCT00689065 (Phase I)

Table 2.
(Continued)

Name	Formulation	Bioactive compound	Company	Admin. Route	Size	Drug Loading/ Encapsulation (%)	Nanovector /Drug Ratio	Indications	Description	Conclusions	Clinical Trials Identifier (Phase, Status)
CDP791	PEG-VEGFR-2/KDR inhibitor	Carboplatin-Paclitaxel	UCB Pharma	Intravenous	140 kDa	N/A	N/A	NSCLC	The trial examined the safety, tolerability and PK (part 1) and antitumor activity (part 2) in 165 patients with locally advanced or metastatic NSCLC. Primary outcome: tumor response rate at 18 weeks.	N/A	NCT00152477 (Phase II)
								Advanced Renal Cell Carcinoma	Dose escalation study of th CRLX101, in combination with Bevacizumab has beer investigated in advanced renal cell carcinoma. Primary outcome: to determine the safety and efficacy of the combinatior therapy, and determine the optimum dose of camptothecin given in combination with bevacizumab.	Camptothecin, in combination with bevacizumab have a PFS of four months in at least 50% patients, achieving the defined primary endpoint. MTD has been established	NCT01625936 (Phase I/b)
								NSCLC	Primary outcome: to compare OS of patients treated with CRLX101 to those patients treated with best supportive care.	Clinical trial failed to meet its primary endpoint of OS benefit, despite showing a favourable safety profile and tumour reductions	NCT01380769 (Phase II)

Table 2. *(Continued)*

Name [Refs]	Formulation	Bioactive compound	Company	Admin. Route	Size	Drug Loading/ Encapsulation (%)	Nanovector /Drug Ratio	Indications	Description	Conclusions	Clinical Trials Identifier (Phase, Status)
CRLX101 (IT-101)	Beta-Cyclodextrine-PEG	Camptothecin (CPT)	Cerulean Pharma Inc.	Intravenous	20-30 nm	10	N/A	Advanced Gastric, Gastroesophageal, or Esophageal Squamous or Adenocarcinoma	This is a pilot clinical trial in patients with advanced or metastatic stomach, gastroesophageal, or esophageal cancer that has progressed through at least one prior regimen of chemotherapy and cannot be removed by surgery. Primary outcomes: to evaluate pre- and post-treatment biopsies, to assess CRLX101 nanoparticle CPT uptake in tumor and normal tissue.	CRLX101 localize in tumor tissue and not in the non-neoplastic tissue.	NCT01612546 (Phase N/P pilot study)
CT-2103 (Opaxio, Xyotax)	α-poly-L-glutamic acid or poliglumex	Paclitaxel	Cell Therapeutics	Intravenous	48 kDa	37	N/A	Ovarian cancer	To evaluate paclitaxel poliglumex as a first-line maintenance therapy for women with ovarian, fallopian tube or peritoneal cavity cancer, who have achieved complete remission following standard first-line chemotherapy. The primary endpoint of this trial is OS	N/A	NCT00108745 (Phase III, active, not recruiting)

Table 2. *(Continued)*

Name [Refs]	Formulation	Bioactive compound	Company	Admin. Route	Size	Drug Loading/ Encapsulation (%)	Nanovector /Drug Ratio	Indications	Description	Conclusions	Clinical Trials Identifier (Phase, Status)
CT-2103 (Opaxio, Xyotax)	α-poly-L-glutamic acid or poliglumex	Paclitaxel	Cell Therapeutics	Intravenous	48 kDa	37	N/A	In combination with gemcitabine or vinorelbine to treat advanced NSCLC	To compare the effectiveness of polyglutamate paclitaxel with that of gemcitabine or vinorelbine in treating patients who have stage IIIB, stage IV, or recurrent NSCLC	N/A	NCT00054197 (Phase III)
NK911	PEG-poly(aspartic acid)	Doxorubicin	Nippon Kayaku Co.,Ltd.	Intravenous	40 nm	N/A	N/A	Metastatic or recurrent solid tumors	The trial was conducted in Japan to determine the maximum tolerated dose, dose-limiting toxicities and recommended dose	NK 911 improved PK values and produced higher antitumor activity than doxorubicin alone.	N/A (Phase I, marketed in Japan)
NKTR-102	Four arm PEG	Irinotecan	Nektar Therapeutics	Intravenous		N/A	N/A	Metastatic breast cancer	To evaluate the safety and efficacy of NKTR-102 in patients with metastatic or locally advanced breast cancer whose disease has failed prior taxane-based treatment. Primary outcome: ORR	NKTR-102 shows a very high RR, PFS of 5.3 months and OS of 13.1 months.	NCT00802945 (Phase II)
								Colorectal cancer in combination with Cetuximab	To investigate NKTR-102 in combination with Cetuximab as a second-line treatment for colorectal cancer. Primary outcome: to establish recomanded dose (Phase II a) and PFS (phase II b).	Phase II: dose recommended has been establish. Phase II b not enrolled.	NCT00598975 (Phase II)

Table 2. *(Continued)*

Name [Refs]	Formulation	Bioactive compound	Company	Admin. Route	Size	Drug Loading/ Encapsulation (%)	Nanovector /Drug Ratio	Indications	Description	Conclusions	Clinical Trial Identifier (Phase, Status)
NKTR-102	Four arm PEG	Irinotecan	Nektar Therapeutics	Intravenous		N/A	N/A	Metastatic or locally recurrent breast cancer	NKTR-102 was tested in patients who have previously failed treatment with an anthracycline, a taxane, and capecitabine (ATC) in the adjuvant or metastatic setting. Primary outcome is OS.	The trial did not meet statistical significance	NCT0149210 (Phase III, active, not recruiting)
NKTR-105	4 arm PEG	Docetaxel	Nektar Therapeutics	Intravenous		N/A	N/A	Solid tumors	N/A	N/A	N/A (Phase I)
PEG-SN38 (EZN-2208)	4 arm PEG	SN38	Enzon Pharmaceuticals, Inc	Intravenous	40 kDa	3.45	N/A	Advanced Solid Tumors or Lymphoma	To find the highest tolerable dose of EZN-2208 that can be given to patients with advanced cancer or lymphoma. Primary outcome: to determine the MTD	Safety and tolerability have been assessed. MTD was established.	NCT0052039 (Phase I)
ProLindac (AP5346)	Poly(hydroxypropylmethacrylamide) (pHPMA)	Diaminocyclohexane-platinum (DACH-Pt)	Access Pharmaceuticals	Intravenous	25 kDa	10.5 ± 2.2	N/A	Solid tumor including colorectal and ovarian cancer	AP 5346 was in phase II development for the treatment of ovarian cancer and cholangiocarcinoma in Europe. Phase II development in head and neck cancerwas conducted in the US. An IND for the agent was approved for clinical trials in colorectal cancer. However, it appears that the company has decided to focus on gene therapy and cell therapy products and therefore development of the product was discontinued.	N/A	N/A (Phase II

1.4.2 Micelles

In 1913, J.W. McBain introduced the term "micelle" into surface and colloid chemistry in the context of the association of surfactant molecules in aqueous solution. Micelles are colloidal particles formed by amphiphilic molecules (block copolymers or surfactants) that self-assemble to form nanocapsules in water. Micelles contain polar head groups that usually form the outside surface of micelles. The head groups can be cationic, anionic or neutral groups. They face the water because they are polar and hydrophilic. The hydrophobic tails are inside and away from the water since they are nonpolar and suitable for hydrophobic cargo (Figure 4A). Depending on the type of amphiphilic molecules, micelles can be divided into lipid micelles, and polymeric micelles (Figure 4B-C).

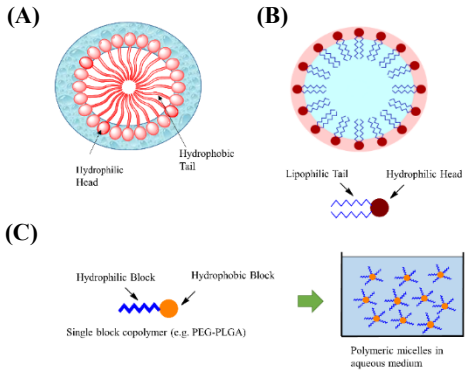

Fig. (4). (A) An example of a micelle in polar solvent, **(B)** Lipid micelle, and **(C)** polymeric micelle.

Different from the lipid bilayer structure of liposomes, the lipid micelles are based on a monolayer structure with hydrophilic heads facing the outside aqueous medium and lipophilic tails forming the inner core. Depending on the composition, concentration of surfactants, temperature and pH, the shape of micelles can be spherical, ellipsoidal, rod-shaped, reversed micelles, or lamellar[88,89]. At low concentration, the amphiphilic molecules align at the interface (liquid/air or liquid/oil), their hydrophilic head oriented toward the aqueous phase and the hydrophobic tail to the other, and reduce the surface tension between them. When the concentration increases, the whole surface will be covered with amphiphilic molecules. At that moment, they start to assemble in a micellar structure. The lowest concentration of monomer at which micelles are formed is called the critical micelle concentration (CMC). The concentration of free amphiphilic molecules is constant as the micelle concentration increases, and they exist in dynamic equilibrium. However, the lipid micelles display two limitations: they possess a low drug loading capacity due to the small hydrophobic core, and they dissociate fastly once diluted in body fluids or in cell culture medium[90].

Polymeric micelles are prepared by a self-assembly process using hydrophilic and hydrophobic block copolymers to form a hydrophilic shell and a hydrophobic core[91,92] (Figure 4C). There are two ways to load drug in amphiphilic micelle structures: drug conjugation and drug encapsulation. Drug conjugation utilizes a non-water soluble drug as a hydrophobic core of the micelle, which is conjugated to the hydrophilic polymer backbone[93]. Drug encapsulation is formed by the encapsulation of hydrophobic drugs into the core of a core-shell nanostructure during the self-assembly process via hydrophobic interactions[94]. PLGA is one of the most popular hydrophobic polymers used as a core for drug encapsulation and breakdown the ester bonds in the body, resulting in a release of the drug. Other studies used a multi-benzene ring as the hydrophobic core, which can bind to a drug contain many benzene rings through π-π interactions under neutral pH, and acidic conditions can decrease these π-π interactions and cause the release of the drug[95]. Currently, several micellar formulations for cancer therapy are under clinical evaluation, but only Genexol-PM has been FDA approved in 2007 for the treatment of BC.

It is based on the development of polymeric micelles formulation of paclitaxel. The formulation of micelles is based on biodegradable amphiphilic diblock copolymer comprised of monomethoxy poly(ethyl-glycol)-block-poly(D,L-lactide) (mPEG-DDLLA). Like Abraxane, this formulation, avoiding the employment of lipid-based solvent, is demonstrated to improve the *in vivo* toxicity, efficacy and biodistribution compared to Cremophor-based paclitaxel[96]. One of the main properties of NPs is that they can be engineered with an antibody, epitope and other biologically active molecules in order produce active targeting to the tumor side. Other micelles formulation under clinical evaluation are summarized in Table 3

Table 3 [80] Micelles on the market and under clinical evaluation. Reproduced from Palazzolo et al.

Name	Formulation	Bioactive compound	Company	Admin. Route	Size	Drug Loading/ Encapsulation (%)	Indications	Description	Conclusions	Clinical Trials Identifier (Phase, Status)
Genexol-PM	mPEG-PDLLA	Paclitaxel	Samyang Biopharma	Intravenous	20-50 nm	16.7	Metastatic breast cancer	To reduce the side effect of cremophor-based paclitaxel and increase the terapeutic index.	Genexol-PM significantly improved OS and ORR compared with generic paclitaxel.	N/A (Approved 2007 (EU, Korea))
							Advanced Urothelial Cancer Previously Treated with Gemcitabine and Cisplatin	To study the efficacy and safety of Genexol-PM in advanced urothelial cancer patients previously treated with gemcitabine plus platinum as adjuvant chemotherapy or first line therapy for metastatic disease. Primary outcome: RR and tumor response.	Genexol-PM was generally well tolerated and demonstrated sufficient antitumor efficacy.	NCT01426126 (Phase II, completed)
							Advanced pancreatic cancer	To determine the efficacy and safety of intravenous treatment of Genexol PM. Primary endpoint: TTP.	The treatment was well tolerated and common toxicities were qualitatively similar to cremophor-based paclitaxel. TTP was 3.2 months.	NCT00111904 (Phase II, completed)
							Taxane-pretreated recurrent breast cancer	To evaluate the RR, toxicity and PFS in patients with taxane-pretreated recurrent breast cancer receiving Genexol-PM. Primary outcome: RR	N/A	NCT00912639 (Phase IV)

Table 3. *(Continued)*

Name	Formulation	Bioactive compound	Company	Admin. Route	Size	Drug Loading/ Encapsulation (%)	Indications	Description	Conclusions	Clinical Trials Identifier (Phase, Status)
NC-4016	Micellar PEG/polyamino acid	Oxaliplatin	Nanocarrier Co., Ltd	Intravenous	30 nm	N/A	Advanced solid tumors, lymphoma	The safety of the drug will be evaluated. Primary outcome: MTD	Recruitment is ongoing.	NCT01999491 (Phase I, recruiting)
NC-6004 (Nanoplatin)	PEG-poly(glutamic acid)	Cisplatin	Orient Europharma Co./ Nanocarrier Co., Ltd	Intravenous	30 nm	39	Advanced solid tumors or NSCLC in combination with gemcitabine	To test safety and fin evidence of the anti-tumor activity of NC-6004 in combination with gemcitabine. Primary outcome: M	N/A	NCT02240238 (Phase I, II, recruiting)
							Pancreatic cancer	To assess efficacy, safety and tolerability. To determine the recommended dose of NC-6004 according to the DLT in combination with Gemcitabine. Primary outcome: DLT and RR.	Efficacy was approximately the same compared to literature data of existing therapies (Abraxane+gemcitabine); OS median: 8.2 months, PFS median: 3.8 months.	NCT00910741 (Phase I, II, recruiting)
							Advanced or metastatic pancreatic cancer in combination with gemcitabine	To evaluate the impact of the addition of NC-6004 to gemcitabine in the treatment of patients with locally advanced or metastatic pancreatic cancer. Primary outcome: OS	N/A	NCT02043288 (Phase III, recruiting)

Table 3. *(Continued)*

Name [Refs]	Formulation	Bioactive compound	Company	Admin. Route	Size	Drug Loading/ Encapsulation (%)	Indications	Description	Conclusions	Clinical Trials Identifier (Phase, Status)
NK012	PEG-poly(glutamic acid)	SN38, active metabolite of irinotecan	Nippon Kayaku Co., Ltd.	Intravenous	20 nm	20	Solid Tumors	To determine if NK012 is safe and effective in the treatment of refractory solid tumors.	NK012 was well tolerated and showed antitumor activity including partial responses and several occurrences of prolonged stable disease across a variety of advanced refractory cancers.	NCT00542958 (Phase I, completed)
							Small Cell Lung Cancer (SCLC)	To determine the dose-limiting toxicity (DLT), evaluate the pharmacokinetic profile, and document any antitumor activity of NK012. Primary outcome: ORR	N/A	NCT00951613 (Phase II, completed)
							Triple Negative Breast Cancer	To determine whether NK012 is safe and effective in the treatment of advanced and metastatic triple negative breast cancer. Primary outcome: ORR	N/A	NCT00951054 (Phase II, completed)
NK-105	mPEG-poly(aspartic acid)	Paclitaxel	Nippon Kayaku Co., Ltd./Nanocarrier Co., Ltd	Intravenous	85 nm	23	Stomach cancer	To evaluate the safety and efficacy of micelle paclitaxel in previously treated patients with advanced or recurrent gastric cancer	N/A	JapicCTI090769 (Phase II)

Table 3. *(Continued)*

Name [Refs]	Formulation	Bioactive compound	Company	Admin. Route	Size	Drug Loading/ Encapsulation (%)	Indications	Description	Conclusions	Clinical Trials Identifier (Phase, Status)
NK-105	mPEG-poly(aspartic acid)	Paclitaxel	Nippon Kayaku Co., Ltd./Nanocarrier Co., Ltd	Intravenous	85 nm	23	Breast cancer	To investigate the efficacy of micelle paclitaxel compared to the marketed formulation of paclitaxel, in patients with metastatic or recurrent breast cancer. Primary outcome: PFS	N/A	N/A (Phase III, active, not recruiting)
Paclical	XR-17 (Oasmia's excipient technology, based on Vitamin A)	Paclitaxel	Oasmia Pharmaceutical AB	Intravenous	20-60 nm	N/A	Ovarian cancer	To study the efficay and safety of two different formulations of paclitaxel, Paclical and Taxol. Primary outcome: PFS, change in AUC, incidence and severity of hypersensitivity reactions.	Paclical showed positive risk/benefit ratio when compared with Taxol and possibly a reduced risk of nephropathy. The product required less infusion time and demonstrated no need for pre-medication with corticosteroids and antihistamines. Primary endpoint of progression-free survival was reached. Both Paclical and Taxol in combination with carboplatin showed the same PFS rates.	NCT00989131

Table 3. *(Continued)*

Name	Formulation	Bioactive compound	Company	Admin. Route	Size	Drug Loading/ Encapsulation (%)	Indications	Description	Conclusions	Clinical Trials Identifier (Phase, Status)
SP1049C	Pluronic L61 and Pluronic F127	Doxorubicin	Supratek Pharma Inc.	Intravenous	30 nm	8.2	Advanced adenocarcinoma of the esophagus and gastroesophageal junction	To demonstrate SP1049C efficacy in non-resectable adenocarcinoma of the esophagus.	Preliminary data from the first group of 10 patients showed partial and minor responses after two of the six-cycle treatments.	N/A (Phase II)

1.4.4 Liposomes

Liposomes are synthetic lipid vesicles with a hydrophilic cavity surrounded by a bilayer of amphiphilic phospholipids[97]. A phospholipid molecule has a phosphate group on one end, called the "head," and two side-by-side chains of fatty acids that make up the lipid "tails". The phosphate group is negatively charged, making the head polar and hydrophilic. The lipid tails, are uncharged, nonpolar, and hydrophobic. Some lipid tails consist of saturated fatty acids and some contain unsaturated fatty acids (Figure 5). Since their discovery by Alec Bangham and colleagues in 1961[98] (published in 1964), the liposomes became an important choice for many drug formulations.

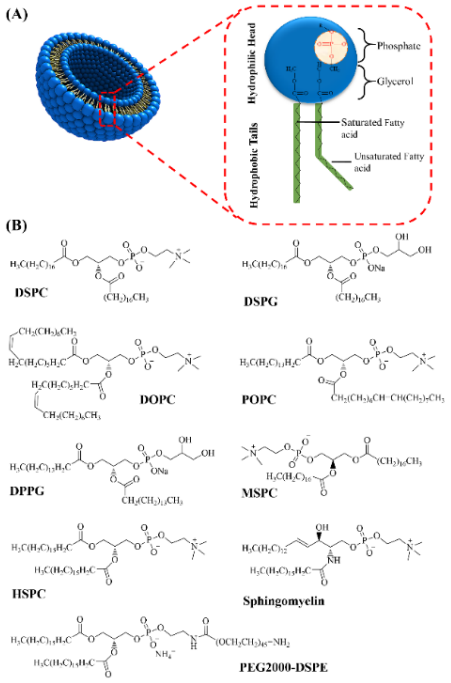

Fig. (5). Schematic illustration of liposomes **(A)** and chemical structures of phospholipids used in the formulation of liposomes **(B).**

Liposome has both a hydrophilic and a hydrophobic regions, permitting the encapsulation and transport of both therapeutic and diagnostic agents via a variety of methods[99]; hydrophobic drugs can be enclosed within the phospholipid bilayers, while hydrophilic drugs can be entrapped in the hydrophilic cavity[100]. To avoid the recognition by RES system and prolong their circulation in the bloodstream, stealth liposomes with PEG molecules (e.g. PEG-DSPE) can be inserted into the liposomes to form a hydrated layer on the liposome surface[101]. Liposomes can be classified according to their lamellarity (uni- and multilamellar), size (small ≤ 100 nm, Intermediate 100-250 nm, and large ≥ 250 nm), and surface charge (anionic, cationic, or neutral)[102,103].

Liposomes were the first platform in nanomedicine and represent a versatile system for drug delivery with lots of compounds effective at a preclinical stage and more than 200 are under clinical evaluation. The first liposome synthesis happened in 1961 in the laboratory of Bengham, in early 70s Gregoriadis (Gregoriadis and Rayman 1971)[104] was one of the first to demonstrate the ability of liposomes to deliver therapeutic drug conducting the first in man study. Two decades later in 1990 Ambisome® (liposomal amphotericin B), the first liposomal drug formulation, was approved by FDA and in 1995 was approved the first anticancer liposome formulation (Doxil®). Synthesized liposomal NPs are characterized by several advantages: first of all, they are able to deliver both hydrophilic and hydrophobic molecules[105], their formulation protect therapeutic cargo from the *in vivo* environment and increase circulation half-life, permeability, biodistribution and targeting specificity[106]. These principles were the basement on which Barenholz built up the study that allowed him to develop the formulation of liposomal doxorubicin (Doxil®)[107]. Doxorubicin is a member of anthracycline class chemotherapeutics utilized against a wide range of cancer including breast, lung, gastric, ovarian, sarcoma, myeloma, leukemias and lymphomas[108]. Unfortunately, its poor selectivity toward cancer cells induces severe systemic side effects, in particular in patients treated with these drugs it has been observed severe heart toxicity, bone marrow toxicity with consequent myelosuppression. The development of Doxil® allowed reducing drastically doxorubicin side effects. The first study carried out on Doxil demonstrated that the new doxorubicin formulation possesses a completely different pharmacokinetics that enhances the circulation time of drugs changing the biodistribution incrementing tumor passive accumulation due to the EPR effect[109]. The two key changes in the history of liposomes are linked to Doxil® which is considered the real breakthrough. The first one is represented by the inclusion of polyethylene glycol in liposome surface to create a "stealth" particle that can escape the detection by the RES system. The second major improvement was the remote loading driven by ammonium sulfate gradient to increase doxorubicin loading within each liposome[107] (Table 4).

Table 4 [80] Liposomes on the market and under clinical evaluation. Reproduced from Palazzolo et al.

Name [Refs]	Formulation	Bioactive compound	Company	Admin. Route	Size	Drug Loading/ Encapsulation (%)	Nanovector/ Drug Ratio	Indications	Description	Conclusions	Clinical Trials Identifier (Phase, Status)
Daunoxome	DSPC, cholesterol (2:1 molar ratio)	Daunorubicin	Galen Pharmaceuticals	Intravenous	40-60 nm	N/A	18.7:1	Advanced HIV-associated Kaposi's sarcoma	To compare the safety and efficacy of liposomal daunorubicin (DaunoXome; NeXstar Pharmaceuticals, Inc, Boulder, CO) with a reference regimen of doxorubicin, bleomycin, and vincristine (ABV) in advanced AIDS-related KS.	DaunoXome was comparable to that of ABV. Response rates, time to treatment failure, and OS were similar on both treatment arms. DaunoXome is a safe and effective primary therapy for advanced AIDS-related KS.	N/A (Approved 1996)
Doxil (USA); Caelyx (EU)	HSPC, Cholesterol, lipid with PEG head group (DSPE-PEG2000) (56:38:6 molar ratio)	Doxorubicin	Johnson & Johnson	Intravenous	100 nm	>90	8.0:1	AIDS-related Kaposi's sarcoma	To improve efficacy of Doxorubicin, reducing toxicity, prolonging TTP and increasing ORR and OS.	Superior efficacy over former conventional therapy.	N/A (Approved FDA 1995, EMA 1996)
								Ovarian cancer		Superior efficacy and improved safety profile over comparator drug (topotecan).	N/A (Approved FDA 1999)
								Breast cancer		Equivalent efficacy and reduced cardiotoxicity compared to free doxorubicin.	N/A (Approved FDA 2003)

Table 4. *(Continued)*

Name [Refs]	Formulation	Bioactive compound	Company	Admin. Route	Size	Drug Loading/ Encapsulation (%)	Nanovector/ Drug Ratio	Indications	Description	Conclusions	Clinical Trials Identifier (Phase, Status)
Doxil (USA); Caelyx (EU)	HSPC, Cholesterol, lipid with PEG head group (DSPE-PEG2000) (56:38:6 molar ratio)	Doxorubicin	Johnson & Johnson	Intravenous	100 nm	>90	8.0:1	Multiple myeloma	To improve efficacy of Doxorubicin, reducing toxicity, prolonging TTP and increasing ORR and OS.	Equivalent efficacy and improved safety profile compared to free doxorubicin combination. Superior efficacy in combination with bortezomib over single agent bortezomib.	N/A (Approved FDA 2007)
Marqibo	Sphingomyelin and cholesterol (57:43 molar ratio)	Vincristine	Talon Therapeutics	Intravenous	100 nm	N/A	N/A	Philadelphia chromosome negative acute lymphoblastic leukemia (ALL)	To improve the PK and pharmacodynamics of vincristine.	This formulation resulted in shorter elimination half-times and slow release into circulation which decrease drug toxicity and adverse side effects.	N/A (Approved 2012)
Myocet	POPC and cholesterol with 55:45 molar ratio	Doxorubicin	Sopherion Therapeutics Inc (USA, Canada), Cephalon Inc (EU)	Intravenous	180 nm	N/A	3.7:1	Metastatic breast cancer	Non-pegylated liposomal Doxorubicin reduces side effects in particular cardiotoxicity.	N/A	N/A (Approved 2000 (EU and Canada))

Table 4. *(Continued)*

Name	Formulation	Bioactive compound	Company	Admin. Route	Size	Drug Loading/ Encapsulation (%)	Nanovector /Drug Ratio	Indications	Description	Conclusions	Clinical Trials Identifier (Phase, Status)
Onivyde (nal-IRI, MM-398, PEP02)	Polyalkylammonium salt of a polymeric (polyphosphate) or nonpolymeric (sucrose octasulfate)	Irinotecan	Merrimack Pharmaceuticals	Intravenous	80-120 nm	800 g irinotecan per mole of phospholipid	N/A	In combination with fluorouracil and Leucovorin, for metastatic adenocarcinoma of pancreas after disease progression following gemcitabine-based therapy.	To improve PK increasing drug encapsulation and loading efficiency. This formulation protects irinotecan in the active lactone configuration, prolonging circulation time, providing sustained release, increasing tumor accumulation via the EPR effect, and reducing host toxicity.	Significant improvement in OS with a 45% improvement (6.1 months) for patients receiving the ONIVYDE combination regimen compared to 4.2 months for patients who received 5-FU and leucovorin alone.	N/A (Approved 2015)
CPX-351	DSPC/DSPG/ Cholesterol (7:2:1 molar ratio)	Cytarabine:Daunorubicin (5:1 molar ratio)	Celator Pharmaceuticals	Intravenous	100 nm	N/A	N/A	Acute Myeloid Leukemia (AML)	To confirm the efficacy of CPX-351 compared to standard chemotherapy treatment with cytarabine and daunorubicin (7+3) as first line therapy in patients 60-75 years old with high risk of (secondary) Acute Myeloid Leukemia. The primary efficacy endpoint will be OS.	Primary endpoint satisfied: the treatment led to statistically significant improvement in OS and RR.	NCT01696084 (Phase III)

Name	Formulation	Bioactive compound	Company	Admin. Route	Size	Drug Loading/ Encapsulation (%)	Nanovector /Drug Ratio	Indications	Description	Conclusions	Clinical Trials Identifier (Phase, Status)
CPX-1	DSPC/DSPG/ Cholesterol (7:2:1 molar ratio)	Irinotecan HCl:Floxuridine (1:1 molar ratio)	Celator Pharmaceuticals	Intravenous	N/A	N/A	N/A	Colorectal cancer	This study, conducted in the US and Canada, consisted of two arms of patients (irinotecan-naive or irinotecan-refractory) who received irinotecan/floxuridine. Primary outcome: response rate will be assessed using RECIST criteria.	N/A	NCT00361842 (Phase II)
CPX-351	DSPC/DSPG/ Cholesterol (7:2:1 molar ratio)	Cytarabine:Daunorubicin (5:1 molar ratio)	Celator Pharmaceuticals	Intravenous	100 nm	N/A	N/A	Acute Myeloid Leukemia (AML)	To confirm the efficacy of CPX-351 compared to standard chemotherapy treatment with cytarabine and daunorubicin (7+3) as first line therapy in patients 60-75 years old with high risk of (secondary) Acute Myeloid Leukemia. The primary efficacy endpoint will be OS.	Primary endpoint satisfied: the treatment led to statistically significant improvement in OS and RR.	NCT01696084 (Phase III)

Name	Formulation	Bioactive compound	Company	Admin. Route	Size	Drug Loading/ Encapsulation (%)	Nanovector /Drug Ratio	Indications	Description	Conclusions	Clinical Trials Identifier (Phase, Status)
EndoTAG-1 (Lipopack)	DOTAP/DOPC/Paclitaxel (50:47:3 molar ratio)	Paclitaxel	MediGene	Intravenous	180-200 nm	N/A	N/A	Triple Receptor Negative Breast Cancer	To assess the efficacy, safety and tolerability of a therapy with EndoTAG-1 + paclitaxel in combination and EndoTAG-1 alone as a rescue therapy for patients with relapsed or metastatic triple receptor negative breast cancer. Primary outcome: 4-month PFS rate.	OS data collected in this trial suggested a promising anti-tumoral effect of EndoTAG-1, especially in the combination therapy with weekly paclitaxel.	NCT00448305 (Phase II)
								Advanced and/or Metastatic Adenocarcinoma of the Pancreas with Gemcitabine Combination Therapy	To evaluate safety, tolerability and efficacy of a 1st line combination treatment with weekly infusions of gemcitabine and twice weekly administration of EndoTAG-1 at three dose levels compared with gemcitabine monotherapy. Primary outcome: PFS, 6-month-survival-rate and OS.	Combination treatment with EndoTAG-1 and gemcitabine resulted in dose-dependent increase of the median OS up to 9.4 months, compared to 7.2 months in the control arm. The 12-month survival rate of patients treated with EndoTAG-1 increased up to 36%, compared to 17% in the control arm. Those patients who had the option to receive repeated treatment cycles with EndoTAG-1 showed an even significantly higher median overall survival up to 13.6 months and a 12-month survival rate of up to 52%.	NCT00377936 (Phase II)

Table 4. *(Continued)*

Name	Formulation	Bioactive compound	Company	Admin. Route	Size	Drug Loading/ Encapsulation (%)	Nanovector/ Drug Ratio	Indications	Description	Conclusions	Clinical Trials Identifier (Phase, Status)
LEP-ETU	DOPC/cardiolipin/cholesterol (90:5:5 molar ratio)	Paclitaxel	INSYS Therapeutics Inc	Intravenous	150 nm	99.3	33.0:1	Metastatic Breast Cancer	To evaluate the safety and efficacy of LEP-ETU in patients with metastatic breast cancer. Primary outcome: ORR after administered over 90 minutes at the MTD (275mg/m2), PFS and OS.	Overall tumor responses with fully audited data were as follows: 16 subjects (46%) with tumor response including 15 partial responses and one complete response; 10 subjects (29%) with stable disease (mean duration, 6 cycles; range, 2-10 cycles); 9 subjects (25%) with progressive disease. LEP was well tolerated with sensory polyneuropathy ≥ grade 3 in only one subject (3%) and neutropenia ≥ grade 3 in 2 subjects (6%), two common toxicities of Taxol® and Abraxane®. No significant infusion-related reactions were observed as indicated by adverse events or prophylactic pre-medication use.	NCT01190982 (Phase II, completed)

Table 4. *(Continued)*

Name	Formulation	Bioactive compound	Company	Admin. Route	Size	Drug Loading/ Encapsulation (%)	Nanovector/ Drug Ratio	Indications	Description	Conclusions	Clinical Trials Identifier (Phase, Status)
Lipoplatin	SPC-3, Cholesterol, DPPG and mPEG2000-DSPE	Cisplatin	Regulon Inc.	Intravenous	110 nm	11.6	10.24:1	NSCLC	To compare the effectiveness of lipoplatin combined with paclitaxel versus cisplatin and paclitaxel in advanced non-squamous NSCLC	Liposomal cisplatin in combination with paclitaxel produce a statistically significant higher response rate than cisplatin combined with paclitaxel in non-squamous NSCLC	N/A (Phase III)
Lipoxal	SPC-3, Cholesterol, DPPG and mPEG2000-DSPE	Oxaliplatin	Regulon Inc.	Intravenous	250 nm	N/A	N/A	Advanced gastrointestinal cancer	Equivalent efficacy with lower toxicity	N/A	N/A (Phase I)
Lipusu	Paclitaxel, Lecithin and Cholesterol (1:12:1.8 w/w)	Paclitaxel	Luye Pharma Group	Intravenous	400 nm	99	15:1	Metastatic Breast cancer	To evaluate the antitumor activity and safety of weekly dose-dense paclitaxel liposome injection compared to 3-weekly regimen. Primary outcome: PFS	N/A	NCT02142790 (Phase IV, recruiting)
								Advanced Solid Tumor After Failure From Conventional Treatments	To determine the MTD, to compare the PK between Lipusu and paclitaxel and to evaluate the effectiveness for cancer treatment. Primary outcome: MTD	N/A	NCT01994031 (Phase IV, recruiting)

Table 4. *(Continued)*

Name	Formulation	Bioactive compound	Company	Admin. Route	Size	Drug Loading/ Encapsulation (%)	Nanovector/ Drug Ratio	Indications	Description	Conclusions	Clinical Trials Identifier (Phase, Status)
LE-SN38	SN38, SPC, Cholesterol and dextrose (1:20:5:100 w/w)	SN38, active metabolite of irinotecan	Neopharm Inc.	Intravenous	231 nm	>85	30.0:1	Metastatic Colorectal Cancer	To study how liposomal SN-38 is effective as a second-line treatment in patients with metastatic colorectal cancer. Primary outcome: objective response rate.	Primary outcome had not yet been achieved.	NCT00311610 (Phase II)
MBP-426	Transferrin (Tf)-conjugated N-glutarylphosphatidylethanolamine	Oxaliplatin	Mebiopharm Co., Ltd	Intravenous	180 nm	N/A	N/A	Advanced or Metastatic Solid Tumors	To determine whether MBP-426 is safe and effective in the treatment of advanced or metastatic solid tumors. Primary endpoind: incidence of dose-limiting toxicity, determination of MTD.	Results showed that liposomal oxaliplatin had a favorable safety profile, with thrombocytopenia as the main dose-limiting toxicity.	NCT00355888 (Phase I, completed)
								Gastric, Gastroesophageal, or Esophageal Adenocarcinoma in combination with leucovorin and 5-FU	Primary outcome: to determine the dose of MBP-426 to be utilized in the Phase II portion of this study administered every 21 days in combination with leucovorin (folinic acid or FA) and fluorouracil (5-FU)	Results presented indicate a recommended dose of liposomal oxaliplatin of 170 mg/m2 as part of the combination therapy. However, there have been no recent reports.	NCT00964080 (Phase I, II)

Table 4. *(Continued)*

Name	Formulation	Bioactive compound	Company	Admin. Route	Size	Drug Loading/ Encapsulation (%)	Nanovector/ Drug Ratio	Indications	Description	Conclusions	Clinical Trials Identifier (Phase, Status)
MM-302	HER2-targeted Liposomes	Doxorubicin	Merrimack Pharmaceuticals	Intravenous	75-110 nm	20,000 molecules of doxorubicin in its core	N/A	Locally advanced/Metastatic Breast Cancer	To demonstrate whether MM-302 plus trastuzumab is more effective than the chemotherapy of physician's choice (CPC) plus trastuzumab in locally advanced/metastatic HER2-positive breast cancer patients. Primary outcome: PFS approx. 2 years	N/A	NCT02213744 (Phase II, III)
								Advanced Breast Cancer in combination with trastuzumab or trastuzumab plus cyclophosphamide in patients with advanced HER2 positive breast cancer	Cohorts of three or more patients have been treated at escalating doses until to identify the MTD of MM-302 monotherapy and in combination with Trastuzumab with or without Cyclophosphamide in patients with advanced HER2 positive breast cancer. Primary outcome: severity and the number of adverse events related to escalating doses of the MM-302, in combination with trastuzumab with or without cyclophosphamide	The data demonstrated that patients treated with MM 302 in combination with cyclophosphamide and trastuzumab showed higher RR, longer PFS when compared with MM 302 and trastuzumab monotherapy. MM 302 in combination with cyclophosphamide was well tolerate.	NCT01304797 (Phase I, active, not recruiting)

Table 4. *(Continued)*

Name	Formulation	Bioactive compound	Company	Admin. Route	Size	Drug Loading/ Encapsulation (%)	Nanovector/ Drug Ratio	Indications	Description	Conclusions	Clinical Trials Identifier (Phase, Status)
OSI-211 (NX211)	HSPC and cholesterol (2:1 molar ratio)	Lurtotecan	OSI Pharmaceuticals	Intravenous	150 nm	N/A	N/A	SCLC	To determine whether OSI-211 is an effective and safe treatment for patients with recurrent small cell lung cancer.	N/A	NCT00046787 (Phase II, completed)
								Fallopian tube cancer, ovarian and peritoneal cavity.	To compare the effectiveness of two treatment regimens of lurtotecan liposome in patients who have advanced or recurrent ovarian epithelial cancer, primary fallopian tube cancer, or peritoneal cancer that has been previously treated with chemotherapy.	N/A	NCT00010179 (Phase II, completed)
								Ovarian Cancer	To test the efficacy and safety of OSI-211 and topotecan in patients with relapsed epithelial ovarian cancer.	N/A	NCT00046800 (Phase II, completed)
SPI-77	SHPC, cholesterol, and DSPE-PEG2000 (51:44:5 molar ratio)	Cisplatin	Alza Pharmaceuticals	Intravenous	110 nm	90	70.0:1	Ovarian cancer	To study the effectiveness of liposomal cisplatin in treating patients who have recurrent ovarian cancer.	Data presented indicate that this formulation has an improved safety profile but it demonstrated reduced efficacy in human testing.	NCT00004083 (Phase II, completed)

Table 4. *(Continued)*

Name	Formulation	Bioactive compound	Company	Admin. Route	Size	Drug Loading/ Encapsulation (%)	Nanovector/ Drug Ratio	Indications	Description	Conclusions	Clinical Trials Identifier (Phase, Status)
ThermoDox	Thermosensitive PEGylated liposomes: DPPC, MSPC and PEG2000-DSPE (90:10:4 molar ratio)	Doxorubicin	Celsion Corporation	Intravenous	100-150 nm	N/A	20:1	Breast cancer in combination with Microwave Hyperthermia (heat)	To evaluate the effects of ThermoDox in combination with therapeutic heating of the chest wall in the treatment of recurrent chest wall (RCW) breast cancer. Primary outcome: to determine the bioequivalence of ThermoDox when used with hyperthermia among patients with RCW breast cancer; to determine efficacy of ThermoDox in combination with Hyperthermia.	The MTD was 50 mg/m2. The ORR was 48% (14/29, 95% CI: 30-66%), with five patients (17%) achieving complete local responses and nine patients (31%) having partial local responses.	NCT00826085 (Phase I, II, active, not recruiting)

1.4.5 Exosomes

Exosomes are membrane vesicles with a diameter of 40-100 nm, a sub-fraction of extracellular vesicles that are secreted by many cell types into the extracellular milieu[110,111]. They are equivalent to cytoplasm enclosed in a lipid bilayer with the external domains of transmembrane proteins localized in the cellular surface. Exosomes are formed inside the cell in compartments known as multivesicular endosomes (MVE), which take up bits of the cytoplasm and its contents into membrane-bound vesicles. Upon fusion of MVBs with the plasma membrane, these internal vesicles are secreted. Although, the biological function of exosomes is still under deep studying, it is known that they can mediate inter-cellular communication, provide a protective effect against or induce intra- and extracellular stress and are involved in the exchange of functional genetic information[110,112]. Exosomes are present in cell culture supernatant and in different biological fluids and they are known to be secreted by most cell types under normal and pathological conditions. So far, exosomes have been found to be released by all cells studied until now such as B-cells, dendritic cells (DCs), T-cells, mast cells, epithelial cells, and platelets and have been found to be present in physiological fluids, such as bronchoalveolar lavage (BAL) fluid, serum, urine, breast milk, cerebrospinal fluid (CSF), saliva, and malignant effusions[113–120]. The presence of exosomes in biological fluids could be exploited for biomarkers in the disease diagnosis[112,119–123]. Due to the strong impact of exosomes in cancer pathogenesis and biological compatibilities (i.e. they are able to cross physiological barriers like the blood-brain barrier), exosomes are strong candidates for advanced therapeutic applications. These biological features include targeting exosomes that appear to be essential in cancer progression, engineering and modifying exosomes as therapeutic devices, and discovering new biomarkers for early diagnosis and molecular targets identifying. Besides cancer, beneficial effects of exosomes in therapy have already shown promise in myocardial ischemia-reperfusion and kidney injury[124], myocardial infarction[125], muscle or bone regeneration[126], arthritis[127], nerve regeneration[128] multiple sclerosis[129], and neurodegenerative diseases, such as Alzheimer's or Parkinson's[130].

Due to their selective cargo loading and resemblance to their producer cells, exosomes have high importance in cancer biomarkers discovery. With increasingly improving isolation protocols from cell culture and patient body fluids and their advanced characterizations, scientists are utilizing exosomes to identify molecules for cancer targeting more effectively and apply more personalized techniques for detection, diagnosis, and prognosis. Protein characterization by mass spectrometry[131],

as well as immunocapture techniques for identifying and quantifying peptide and nucleic acid (miRNA, mRNA, etc..) profiles[132].

Drug loading can be accomplished either endogenously or exogenously. Endogenous or passive loading is carried out by overexpressing the RNA species or molecule of interest in producer cells. This passive loading is enabled by the cell's native exosomal loading mechanisms and results in exosomes that contain the drug prior to isolation. Exogenous, or active, loading begins with exosome collection and requires either co-incubation or electroporation of the exosomes with the drug/molecule of interest[133]. One of the applied techniques was the loading of exosomes with curcumin[134] where they were used firstly in treatment of brain inflammatory diseases. The important results found led to their uses in cancer therapy especially in the treatment of colon cancer[135,136] as Phase I clinical trial (Table 5).

Tabella 5[80] Exosomes undergoing clinical evaluation. Reproduced from Palazzolo et al.

Name	Formulation	Bioactive compound	Company	Admin. Route	Size	Indications	Description	Conclusions	Clinical Trials Identifier (Phase, Status)
GELNs	Grape exosome-like nanoparticles	Curcumin	James Graham Brown Cancer Center	Oral	400 nm	Colon cancer	To estimate the effect of a fixed concentration of curcumin when delivered by plant exosomes compared to oral tablets of curcumin alone in CRC patients. Primary outcome: evaluate the concentration of curcumin in normal and cancerous tissues	N/A	NCT01294072 (Phase I)
INF-γ-Dex	Tumor antigen-loaded dendritic cell derived exosomes	MHC class I- and class II-restricted cancer antigens and INF-γ	Gustave Roussy, Cancer Campus, Grand Paris	Vaccination (intravenous)	100 nm	NSCLC	To boost NK and T cell immune responses in NSCLC as maintenance immunotherapy after chemotherapy. Primary outcome: at least 50% of patients with PFS at 4 months after chemotherapy cessation.	Dex stimulated NK cells but no induction of T cells was seen in patients. Primary endpoint was not reached.	NCT01159288 (Phase II)
Mesenchymal stem cells (MSCs) exosomes	Microvesicles and exosomes	Umbilical cord-blood derived MSC microvesicles as anti-inflammatory agents	General Committee of Teaching Hospitals and Institutes, Egypt	Intravenous	40-100 nm	Diabetes mellitus type 1	To reduce the inflammatory state and improve the β-cell mass as well as the glycemic control of the patients with diabetes mellitus type 1. Primary outcome: total daily insulin dose after exosome treatment	N/A	NCT02138331 (Phase II, III)

1.5 Inorganic NPs in nanomedicine

Inorganic NPs are investigated in preclinical and clinical studies for the detection, diagnosis and treatment of many diseases[137–140]. Inorganic NPs have gained wide attention due to their unique material- and size-dependent physicochemical properties, which are not possible with organic NPs. In addition to stability, ease of synthesis, modification and inertness, the magnetic and optical properties make inorganic NPs attractive for imaging and ablation of malignant tissue. Gold NPs (AuNPs), for example, have unique properties, such as size- and shape-dependent optical and electronic features[141,142]. The surface of AuNPs can be modified with ligands containing phosphines, thiols, and amines, exhibiting affinity for the surface of gold[143]. Other inorganic NPs, typically iron oxide nanoparticles (IONPs) can respond to a magnetic field thus making the theranostic nanomedicine excellent contrast agents in magnetic resonance imaging (MRI) and targeted drug delivery[144–147]. The surface of IONPs is typically coated with silica to promote biocompatibility, decrease toxicity, and provide stability under physiological conditions[148,149]. In addition, quantum dots (QDs) are a promising platform in nanotechnology for biomedical imaging for cancer study because of their unique optical and electronic characteristics. QDs are spherical fluorescent semiconductor NPs with a diameter less than 10 nm. They have a series of advantages compared to traditional organic dyes, such as high quantum yield, long lifetime, and high photostability. However, the potential toxicity caused by the release of heavy metals ions strongly limits their translation towards clinical applications[150–155]. In addition, the surface modification of QDs with biocompatible molecules such as polymers, liposomes, and inorganic silica have been investigated to overcome the problem of toxicity of QDs, the prolonged retention *in vivo* studies and the pH-sensitive photoluminescence of QDs[156–160]. In table 6, a short summary of the inorganic nanomaterial reached clinical application. (Table 6).

Table 6 [161]**.** List of Inorganic nanoparticles for cancer therapy approved by FDA or EMA and those undergoing clinical trials**.** Reproduced from Bayda et al.

Nanoplatforms	Name	Formulation	Company/ Sponsor	Admin. route	Size (nm)	Status	Indications	Clinical Trials identifier *	Refs
Gold NPs/Nanoshell	CYT-6091 (Aurimune)	PEGylated colloidal Gold-rhTNF (recombinant human Tumor necrosis factor)	Cytimmune Sciences	Intravenous	27	Phase I Completed	Solid tumors	NCT00356980	[162,163]
						Phase II, in progress	Non-small lung cancer (NSLC)		
	AuroShell	Silica core coated with gold shell	Nanospectra Biosciences Inc.	Intravenous	150	Phase I Recruiting	Ablation of Prostate Tissue	NCT02680535	[164]
	AuroLase	Silica core coated with gold shell	Nanospectra Biosciences Inc.	Intravenous	150	Completed, pilot study	Head and Neck cancer, single dose of AuroShell + NIR laser 808 nm (AuroLase Therapy, Laser responsive)	NCT00848042	[165,166]
						Active, not recruiting, pilot study	Primary and/or Metastatic Lung Tumors (AuroLase Therapy, Laser responsive)	NCT01679470	
Hafnium oxide (HfO_2) NPs	NBTXR3 (NanoXray)	HfO_2 NPs for radiotherapy	Nanobiotix	Intratumoral	50	Phase I Recruiting	Head and Neck Cancer	NCT01946867	[167]
			PharmaEngine			Phase II/III Recruiting	Adult Soft Tissue Sarcoma	NCT02379845	
			Nanobiotix			Phase I/II Recruiting	Prostate Adenocarcinoma	NCT02805894	
			Nanobiotix	Intralesional (IL) or intraarterial (IA)		Phase I/II Recruiting	Liver cancers	NCT02721056	

Table 6 *(continued)*

Nanoplatforms	Name	Formulation	Company/ Sponsor	Admin. route	Size (nm)	Status	Indications	Clinical Trials identifier *	Refs
Magnetic iron oxide NPs	Magnablate I	Iron NPs. Magnetic responsive for Thermoablation	University College London	Intratumoral	N/A	Phase 0	Prostate cancer	NCT02033447	
	NanoTherm (MFL AS1)	Aminosilane-coated iron oxide NPs in magnetite form (Fe_3O_4).	Magforce Nanotech AG	Intratumoral	10-15	Approved, Europe 2010	Thermal ablation, hyperthermia therapy. Local ablation in glioblastoma		[168–170]

*ClinicalTrials Identifier source: ClinicalTrials.gov

1.6 DNA nanotechnology

One of the hardest challenges that chemists have to face in the synthesis of nanomaterial is to construct material with absolute control over the placement of each component in order to tailor properties for a given application. The manipulation of covalent bond formation between atoms is often used by the synthetic chemist to wield this degree of control. In contrast, supramolecular chemist controls the organization of larger molecular species through the manipulation of non-covalent interaction. A characteristic required for these bonds is to have interactions sufficiently directional in order to obtain a final arrangement and orientations of molecules that can be predicted accurately[171].

If this condition is not met, it is difficult for a system to achieve at a well-defined product and there is a decrease of rational control on the final material. The recent developing in nanomaterials synthesis driven by DNA-based assembly allow developing synthetic methodologies that may compete at the nanoscale the results that small molecule chemist has obtained at the molecular scale[172,173].

For those reasons, many research groups have focused their attention on DNA nanomaterial for the construction of artificial nanostructures not present in biological systems for bio-applications. DNA, being a genetic material possesses biocompatibility and low cytotoxicity, is ideal for applications in the biomedical field[174,175]. Its remarkable molecular recognition properties, and complementary base-pairing, along with its stability, mechanical rigidity, nano-dimensions of the repeating unit, easily custom synthesis with a manipulative length of strands, allow the formation of almost every shape of nanostructures. Moreover, high drug loading efficiency and effective cellular internalization further support DNA origami as a programmable "smart" building block for the construction and development of versatile highly nontoxic drug nanocarriers[174–176]. Due to the aforementioned properties, DNA nanostructures have been synthesized and engineered for various applications, such as scaffolds or templates to arrange organic, inorganic and biomolecules into defined morphology; molecular transporters; highly sensitive molecular- and bio-detection; single molecule spectroscopy; protein structure determination; vehicles for *in vitro* and *in vivo* drug delivery[177].

1.6.1 Former DNA nanostructures

The pyridine and purine bases that constitute the nucleotides in single-stranded DNA are linked to sugar pentose and this latter associated unit is called a nucleoside, which is connected to another nucleoside through the phosphodiester bond. The asymmetric ends of DNA strands are called the 5'

and 3' ends depending on whether the terminal group is a phosphate group or a free hydroxyl group, respectively. The purine bases are classified into two types: Adenine (A) and Guanine (G). They have a structure derived from the fusion of five- and six-membered heterocyclic structure, while the pyrimidines are Cytosine (C) and Thymine (T) and are a six-membered ring (Figure 6).

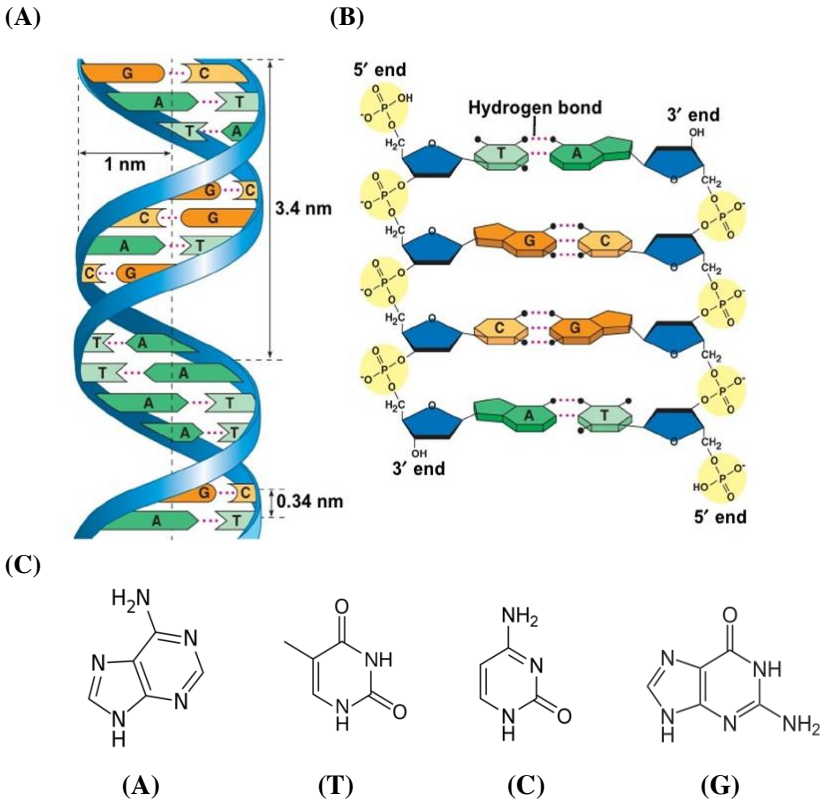

Fig. (6). (A) Key features of DNA structures. (**B)** Chemical structure of DNA stabilized by hydrogen bonds between the bases A-T and G-C. (**C)** Adenine (A), Thymine (T), Cytosine (C) and Guanine (G) of DNA responsible for the robust complementary base pair interactions between DNA strands. Copyright 2002, Pearson Education, Inc. Publishing as Benjamin Cummings

In B-form DNA, the most common form of the double helix, two nucleotide nanowires are twisted around each other with a replicate unit every 3.4 nm while maintaining a distance of 3.4 Å between the consecutive base pairs in a double helix with a diameter of 2 nm. The twist angle between base pairs in solution is ~34.38º with C2'-endo sugar pucker. The persistence length of DNA, which is a measure of stiffness, is 50 nm. Two factors are mainly responsible for the stability of the geometry of the DNA double helix: the presence of hydrogen bonds between complementary bases of the strands, and aromatic π-π stacking between adjacent bases. Two hydrogen bonds are formed between the bases A and T and three between G and C attached to the two strands (Figure 6). While each

hydrogen bond is weak compared to a covalent bond, a large number of hydrogen bonds together represent a strong force that keeps the two strands bound. In addition, other polar groups of the base rings can form external hydrogen bonds with surrounding water that give the molecule extra stability. The hydrogen bond is not the only force that gives stability to the DNA structure. The negativel charge of the phosphate group can interact with positively charged atoms with electrostatic forces. The free energy contribution (-ΔG/kcal mol-1) of the formation of A-T and G-C base pairs due to hydrogen bonds is ~1.34 and 2.17, respectively[178].

A DNA nanostructure is a bottom-up assembly of multiple ssDNA that have to hybridize to other segments or to a scaffold. In 1964, Robin Holliday illustrated a four-armed DNA branched junction, which later become known as the Holliday junction, in which four DNA strands are linked together to form four double helical arms flanking a branch point. A Holliday junction occurs commonly in nature, as it is being the process of genetic recombination called crossing-over involving in passing genetic diversity to the next generation. This specific genetic structure became the foundation of DNA nanotechnology, in which by connecting several Holliday junctions in the form of tiles and yielded DNA lattice in two and three dimensions (Figure 7)[179].

The principle of multiple cross-over junctions is used in some of the first DNA nanostructures to confer sufficient rigidity and to obtain directional interaction. These molecules are composed of coplanar helices containing two or more locations at which the component single strands switch their connectivity from one helix to another[180]. Many of these molecules are present, the one used for the

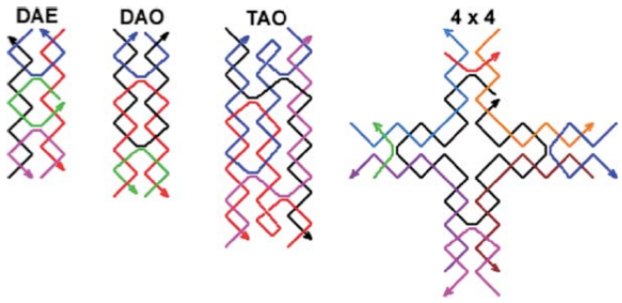

Fig. (7). Schematic drawings of four DNA tiles are shown. Colored lines represent different oligonucleotide strands with arrowheads marking the 3 ends. DAE and DAO are double crossover complexes (also known as DX), TAO is an example of a triple crossover (or TX) tile, and the 4 × 4 tile is composed of four arms each of which contains a four-arm junction.

construction typically have their crossovers formed between strands of opposite polarity. Structural rigidity is achieved by these crossover events between helical domains that reduce the number of possible conformations that still produce a hybridization-driven topology. Structures that present two helical domains and two crossover junctions between them are called *double crossover* (DX) and

those that have three helical domains and between two crossover junctions are known as triple crossover (TX)[180,181]. The rigidity conferred with this strategy is quantified by measuring the persistence length of these molecules; in particular, the persistence length of DX structure is almost the double of an ordinary DNA duplex[182], more complex analogs built of six helices around a central vacancy rotated of 120° from each other have a larger value[183,184]. In these molecules, the DNA helices arranged in antiparallel and coplanar shape mimic a linear coordination geometry, because each helical domain can be ended with a different sticky-end sequence. Two to eight DX or TX molecules have been designed to tile in an alternating brickwork-like pattern to produce 2D crystalline lattices[181,185]. A lot of important advances were obtained assembling DNA-based tiles both in the construction of scaffolds and for the development of dynamic nanomaterials. The formation of a nanomechanical device was introduced using rigid DNA tiles marking the starts of nanorobotics fields in which the use of rigid DNA bonds was extensively used to create a dynamic system that can cover physical tasks very sophisticated[186–189].

The majority of tile-based structure are driven by linear or pseudo-linear bonding modes, more advanced structure constructed by using DNA hybridization have expanded directional interactions to include more complex symmetries. The first step into this concept was carried out by combining several four arm branched junction molecules into a single parallelogram-shaped structure[190]. It was shown that when these junctions are combined into well-defined molecules, they could be assembled into 1D ribbons or 2D lattices depending on the placement of sticky end groups. Yan, Reif and their research group constructed a coplanar arm oriented 90° to one another[191]. Two helical domains constitute each arm of the structure and the antiparallel orientation confers the sufficient rigidity to the structure to maintain the orientation relationship between each of the four arm. If sticky ends sequences are at the end, each structure can be assembled into 1D rolled up tubes or periodic 2D lattices in relation with the number of helical turns of DNA that are in each arm. In this tile, the central strand can be modified to present sequences that are able to capture protein binding domains that allowed this kind of structure to be used to organize proteins and nanoparticles into single component and alternating 2D arrays[192]. Recently, Mao and his collaborators published a work where they presented directional binding domains in three dimensions using structures known as tensegrity triangles[193]. The rigidity of this structure is achieved by the linking of several four-arm branch junctions and conceptually consisting of three double-helical domains oriented to form a triangle-shaped tile. In this tile, the arms are placed in three separate directions like the axes of a coordinate system. In another work is described another version of this molecule presenting a more rigid

structure in which each arm is represented by a DX molecule instead of a single linear duplex, that allowed the generation of ordered 2D arrays of nanoparticles[194]. The same research group described in another work an alternative way to construct 3D wireframe polyhedral structures using DNA tile-based building blocks[195]. Three DX tile arms linked via a central cyclic strand are used to form this structure. In 2012, another work by Yin and coworkers described the extremely complex discrete 2D and 3D objects using single-stranded DNA units[196,197]. To carry out this experiment a library of oligonucleotides is synthesized to hybridize with four independent strands. With this protocol, a rigid bricklike building block has been formed to enable the directional hybridization interaction. The dihedral angle between two adjacent hybridized segments can be determined calculating the number of the basis in each domain. These properties is pivotal for the design strands in order to form 2D or 3D brickwork pattern[196,197]. Through a software is possible to generate a set of single-stranded oligonucleotides that can form extremely complex aperiodic pattern. The yield of these nanoscale object results very low in contrast with DNA origami where the control on the stoichiometry of the product is achieved.

1.6.2 DNA origami

DNA nanotechnology uses the molecular recognition properties of DNA to create artificial DNA structures for technological purposes. It holds great promise for a vast range of applications in different fields such as biology, medicine and material science. In 1982, Nadrian Seeman laid the theoretical framework for the use of DNA as a nanoscale building material. This is due to the DNA's capacity for programmable self-assembly and its high stability[179,198].

In 2006, Paul Rothemund at the California Institute of Technology introduced the term “scaffolded DNA origami”, which has revolutionized the field of structural DNA nanotechnology by enhancing the complexity and size of self-assembled DNA nanostructures in a simple “one-pot” reaction[199] (Figure 8).

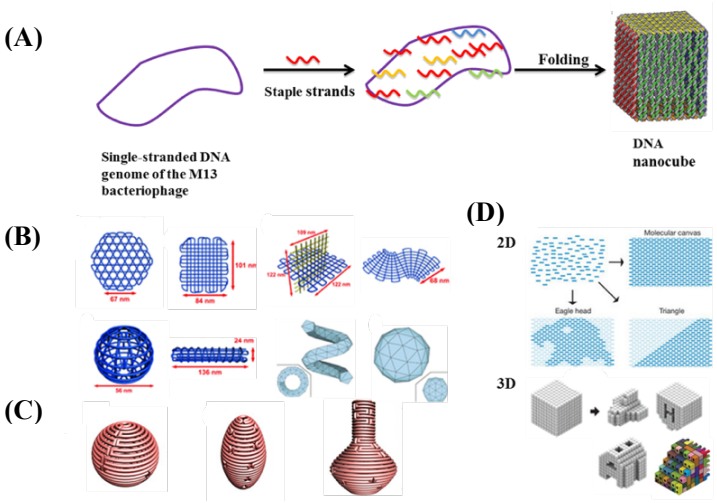

Fig. (8). In DNA origami: (A) a long circular single-strand DNA scaffold is folded into a desired shape with the aid of hundreds of short staple strands. In the above example, circular single-stranded genome of M13 bacteriophage (M13mp18) is folded with the assistance of about 200 staple strands into a DNA nanocube with dimension of 35x36x42 nm during a thermal annealing process. (B) DNA gridiron nanostructures. Reproduced from references [200,201]. (C) 3D structure with complex curvatures. Reproduced from [202]. (D) Design of 2D and 3D DNA canvas using single-stranded tiles/bricks. Reproduced from references [196,197].

Scaffolded DNA origami involve the folding of a long circular single-strand-scaffold viral DNA derived from the bacteriophage M13mp18 composed of 7249 nucleotide sequences with hundreds of short staple strands or helper strands of DNA into the desired shape. The DNA origami technique has been successfully used for the preparation of different 2D and 3D nanostructures and for the nanopatterning of nanoparticles, proteins and other functional molecular components into well-defined arrangements[203] (Figure 9). Staple strands are different, each one and some of them can be designed to present DNA sticky ends

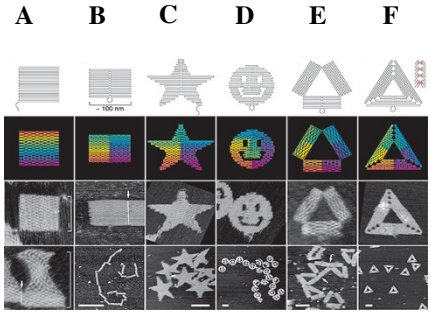

Fig. (9). The first examples of the versatile DNA Origami technique. Top row, folding paths. **A**, square; **B**, rectangle; **C**, star; **D**, disk with three holes; **E**, triangle with rectangular domains; **F**, sharp triangle with trapezoidal domains and bridges between them (red lines in inset). Dangling curves and loops represent unfolded sequence. The lower panels contain the resulting DNA structures as imaged by AFM. All images and panels without scale bars are the same size, 165 nm x165 nm. Scale bars for lower AFM images: **B**, 1 μm; **C–F**, 100 nm. Adapted by permission from reference [196].

in a defined site of the final assembled structure to allow the interaction with other nanoparticles. Moreover, chemically modified staples can be inserted at a predefined position in the DNA nanostructure, which could be used to impart several additional functionalities in the designed DNA nanostructures.

The design of a DNA origami is then fed into computer software called "caDNAno" which calculates the placement of individual staple strands[204]. Each staple binds to a specific region of the DNA template due to Watson-Crick base pairing rules. The scaffold strand and the staple strands are mixed in a one-pot reaction with rapid heating followed by slow cooling allows the various staple strands

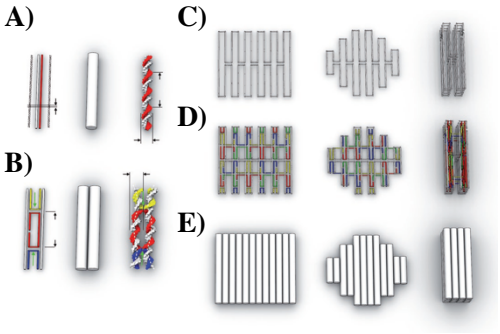

Fig. (10). Scaffold DNA origami design concept: **A)** Schematic representation of DNA double helices. **B)** Two double helices are connected by interhelix crossovers. **C)** Scaffold strand routing to form three different DNA origami objects. **D)** For the same three DNA nanostructures, staples are highlighted with different colours to form the structures. **E)** Cylindrical representation of the three DNA nanostructures. Reproduced from reference [186].

to pull the long scaffold strand into the desired shape. The design concept is illustrated in Figure 10 [205]. The double helix structure of DNA is represented as double helix domains (cylindrical representation) for designing purposes. DNA origami nanostructure rigidity and stability are achieved by the same chemical interaction found in DNA tiles: several crossover events are presents between two neighbor strands linked by hydrogen bonds. In contrast with the construction of DNA tile which are focused on the development of a small number of building blocks able to arrange themselves in a large periodic structure, DNA origami nanotechnology is more concentrated in the synthesis of nanostructure whose size and shape are well defined. The synthesis of a DNA origami structure is obtained through a precise stoichiometry of all the components that allow a high yield of a particular nanoobject. To control the folding of the scaffold in the desired shape there was the need to precisely defined the sequence of the staples that conducted to the development of a lot of open source software that addressed this problem[204,205]. The staple sequences are generated in order to drive the scaffold back and forth to fill an arbitrary shaped 2D area. In this way, computational methods select the appropriate sequences that allow DNA hybridization and crossover junctions to stabilize the structure in the desired folding path. The computational method considers several import parameters including the number of helical twists of DNA between crossover points and the elimination of strain, nicks and seams. With this procedure, the yield of the desired structure reaches almost 60%.

A step-by-step guide to building DNA origami objects is shown in Figure 11[205].

Step 1: Conceive target shape. The work starts with the conception of a target shape with specific functional requirements. Based on the application, it is important to decide on a single-layer or

multilayer structure using square lattice or honeycomb lattice. In Figure 11, Step 1, a 72 nm-tall sculpture of a robot is considered as the target shape using a multilayer honeycomb lattice packing.

Step 2: Design layout, evaluate the design and determine staple sequences. The designing of the internal layout of the DNA origami object can be accomplished with many computational tools (Figure 11, Step 2). Based on cross-over spacing rules, the staple sequence can be determined. Certain applications require site-directed attachment of nanoparticles, proteins or fluorescent dyes. Such attachments need to be considered in this scaffold-staple layout.

Step 3: Prepare scaffold DNA and synthesize staples. The quality of DNA origami folding might depend on the scaffold sequence and the particular cyclic permutation, which means the repeating units of the targeted shape. The single-stranded M13mp18 bacteriophage genome is used as long scaffold strand, which acts as a template for scaffolded DNA origami. This template is commercially available. The scaffold strand could also be prepared by an enzymatic[206] or by a denaturing dialysis method to separate a dsDNA (derived from M13mp18) into two ssDNA scaffolds[207]The staple sequences are generated while designing the DNA origami and are utilized to synthesize the desired oligonucleotides.

Step 4: Pool subsets of concentration-normalized oligonucleotides. This step is important in deciding the right concentration ratio of scaffold strand to staple molecules. For optimal results, this ratio is usually set at 1:5.

Step 5: Run molecular self-assembly reactions. One theory is that the scaffold-staple layout requires a structural solution for the correct mixture of scaffold DNA and staple molecules that minimizes energy through Watson-Crick base pairing. The targeted shape corresponds to a global energy minimum of the system and depends on the solvent and design conditions. The goal of the self-assembly reaction is to reach a minimum energy state in conditions where the targeted structure is folded. The best conditions are identified as a function of the salt concentration and cyclic temperatures.

Step 6: Analyze folding quality and purify the object. The quality assessment of DNA origami folding and purification could be accomplished by gel electrophoresis. The gel has to contain magnesium during running. The reactions could be optimized by searching for the best conditions, which give a high yield of nanostructures and good gel separation from the staples. The reactions are purified from the gel slabs by excising the desired bands followed by the DNA electro-elution method[208]. Another method used to purify and concentrate DNA developed by Stahl et al. is based

on PEG precipitation with high molecular weight. This method was efficient and used to reduce the elution volumes and achieve high recovery yields of up to 97%[209].

Step 7: Single-particle based structural analysis. Single molecule microscope techniques play an important role in the investigation of advanced DNA origami. They can be imaged by negative-stain transmission electron microscopy (TEM) and with atomic force microscopy (AFM) [203,210]. Alloyeau et al. showed that this is also possible for direct imaging along with chemical analysis of unstained DNA origami with transmission electron microscopy[211]. DNA origami nanotechnology became a very powerful technique in the synthesis of complex nanoobject presenting important future as a box with a sequence-specific opening lid[199] and a barrel-shaped structure able to carry molecular cargoes

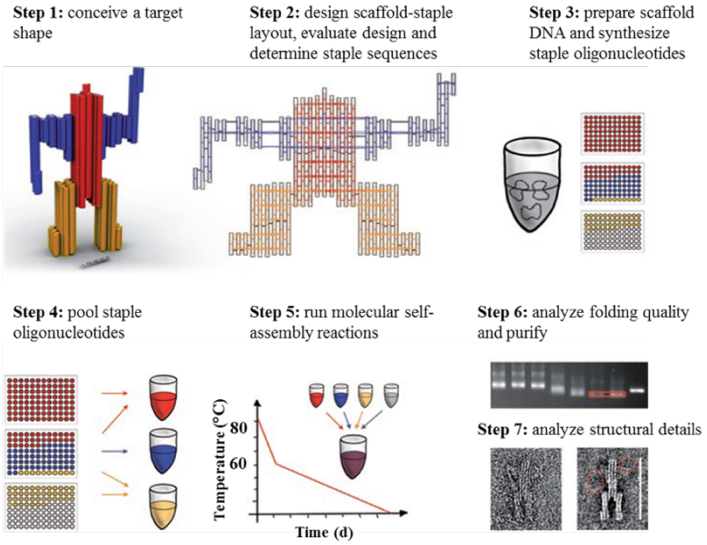

Fig. (11). Step by Step guide of molecular self-assembly with scaffolded DNA origami[186].

and release them through an intracellular logic-gated binding events[212]. In 2009, a step forward in the synthesis of origami has been made obtaining a 3D object. Starting with this new approach a large number of 3D nanostructures have been synthesized expanding the possibility to build new shape. The increasing structural dimensions and complexity required a precise mixture of scaffold and staple and a defined concentration of Na+ and Mg2+ salts to help the synthesis of the structure; in particular, this step can require long annealing times of up to a week under optimize conditions with a yield of the desired product of 7-44% that necessitate a purification step to be isolated[210]. In contrast, Dietz and his research group demonstrated that the folding of complex origami structures is possible even in non-equilibrium conditions with near quantitative yield obtained in minutes[213].

1.6.3 DNA-based drug delivery

Among the wide structure that can be build using DNA nanotechnology, 3D DNA nanostructures possess all the requirement to become universal nanocarriers for smart and targeted drug delivery. In particular, 3D DNA nanostructures possess high stability, high drug loading capability and passive delivery into live cells.

Several DNA-based nanostructures, namely tetrahedral, icosahedral[214], nanotube[183,191,215,216], square and triangle[203] have been developed recently for in vivo and in vitro drug delivery applications. In contrast to dsDNA, DNA nanostructures could be internalized within the cells without any aid from transfection agents[217] and, when densely packaged, could be effectively used for the drug delivery purposes[218].

To be effective as a DDS in mammals, DNA nanostructures should satisfy several important criteria: they have to be stable and intact both in extracellular and intracellular environments, stability should be long enough in the cytoplasm of cells to perform their predefined tasks; they should not induce toxic effect in mammals. For these reasons, several research groups have focused on the stability studies of DNA constructs and on the set up of a new protocol to improve this parameter.

In Table 7, an overview of the different application of DNA nanostructures utilized for drug delivery is provided. Starting from DNA tiles, tetrahedral (N1)[219] and icosahedral (N2)[220] nanostructures were demonstrated to be effective for doxorubicin delivery to breast cancer cells. In particular, the tetrahedral structure was found to be effective on drug-resistant cells. The icosahedral structure was able to efficiently deliver the doxorubicin in a targeted way only after functionalization with aptamer sequences against the tumor surface marker mucin 1 (MUC1). DNA tetrahedral structures have also been shown to demonstrate to protect single-strand sequences against nuclease degradation; in particular, this kind of structure has been employed to increase the *in vivo* circulation half-time of siRNA from 6 to 24 minutes (N3)[174] and deliver Cytosine-phosphate-Guanosine (CpG) to elicit an immunoresponse[221]. Finally, highly biocompatible aptamer-tethered DNA nanotrain against folic acid receptor exhibited high antitumor efficacy and reduced the side effects of doxorubicin in a mouse xenograft tumor model[222]. Very recently, our group has demonstrated that a half icosahedral nanostructure can efficiently deliver doxorubicin to breast and hepatic cancer cells[223].

DNA origami, provides enhanced size, dense packaging of strands and controllable shape and can be used to construct multivalent and multifunctional drug carriers. DNA origami was found to be stable in cell lysates and can be slowly degraded in living cells after 72 hours of treatment, demonstrating its great potential for controlled drug release[224]. This property was demonstrated in an *in vitro*

experiment by Högberg et al. The authors were able to control the kinetics of the release of doxorubicin from DNA origami tubes by regulating the global twist of the structure, showing that the twisted form releases doxorubicin more slowly than the normal structure[225]. The Liedl group constructed a 30-helix DNA origami nanotubes that were functionalized with CpGs oligonucleotides (up to 62 molecules) and tested for their immunostimulatory efficacy in isolated mouse spleen cells. Splenocytes include a subset of immune cells such as dendritic cells and macrophages that initiate and control the immune response. CpG-DNA nanotubes are internalized better than CpG alone and consequently stimulate a strong immune response[226]. DNA barrels have been constructed in a structure capable of selectively interfacing with cells to deliver signaling molecules to cell surfaces[227]. The opening lid is based on a DNA aptamer-based lock mechanism, which opens in response to the binding of antigen keys.

Different DNA nanoshapes (triangle, square and tube) were synthesized and tested for drug delivery *in vitro* and *in vivo* experiments[228,229] (Figure 12). These tests were conducted with the employment of doxorubicin due to the natural interaction between this drugs and DNA. Doxorubicin acts intercalating DNA double strands in G-C base pair[230]. *In vitro* experiments highlighted that DNA origami can circumvent drug resistance in BC resistant cells (res-MCF7). In this work is described

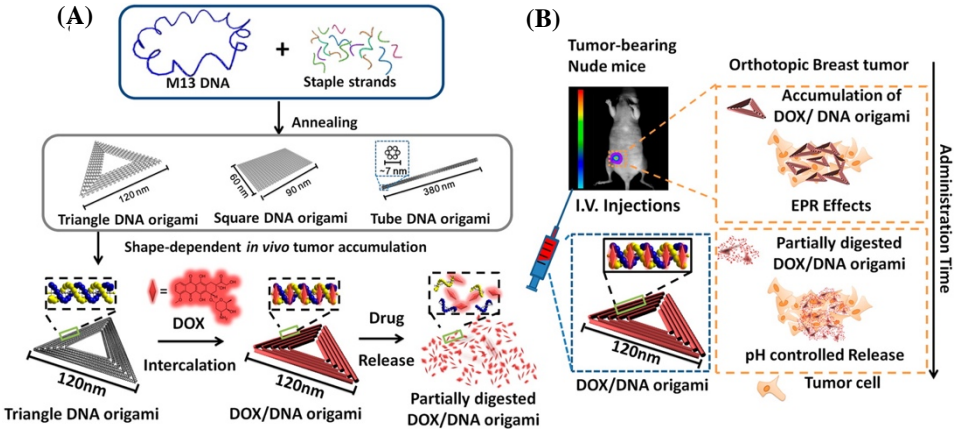

Fig. (12). Schematic design of the DNA carrier-drug complex. **(A)** Long, single-stranded DNA scaffold (M13mp18 phage genomic DNA, blue) hybridizes with rationally designed helper strands to fold into triangular, square, and tube origami shapes. The biodistribution of unstructured M13 DNA and different nanostructures of DNA origami was investigated in subcutaneous breast tumor model. After *in vivo* biodistribution, the triangle-shaped DNA origami demonstrated optimal tumor accumulation; it was then used for doxorubicin intercalation. The Watson-Crick base pairs in the double helices of DNA origami serve as docking sites for doxorubicin intercalation (DOX/DNA origami, red). **(B)** Tail-injected DOX/DNA origami complexes were delivered via blood circulation, accumulating in the breast tumor of nude mice because of EPR effects. Reproduced from reference [210].

the ability of DNA origami to deliver doxorubicin inside the cell while the free doxorubicin cannot enter[228]. This mechanism is related to the capacity of DNA origami to increase lysosomal pH that allows them to remain stable and to enter in the cytoplasm to deliver the drug. *In vivo* experiments demonstrated that the aforementioned structures were able to deliver doxorubicin efficiently to normal and resistant cancer cells[229]. Interestingly, it appears that the triangular structure resided in the tumor for a significantly longer time than the square and tube structures. This might be attributed to the different shape of DNA structures and was probably due to the enhanced retention time inside the tumor (Figure 12).

In most studies, drug loading on DNA nanostructures relies on the intercalation property of doxorubicin molecules with base pairs of DNA duplex[225,228,229]. High loading efficiencies of doxorubicin with different DNA origami structures have been achieved. For instance, in the case of DNA tube, more than 70% loading efficiency was obtained[228].

Thanks to the programmed and well-defined properties of DNA nanostructures, it is possible to precisely control the spatial distribution of cargo molecules over DNA structure. In fact, there is virtually no limit for tethering DNA with various functional molecules through covalent modifications. DNA oligomers with a large variety of functional end groups are commercially available. Amino-functionalized DNA has been employed to bind carboxylic groups and thiol-modified DNA to maleimide groups[231]. Srinivasan et al. have developed a novel procedure for labeling plasmid DNA using QDs. This method involves covalent conjugation of plasmid DNA to phospholipid/polyethylene oxide-encapsulated cadmium selenide/zinc sulfide (CdSe/ZnS) core/shell QDs using a peptide nucleic acid–N-succinimidyl-3-(2-pyridylthio) propionate (PNA–SPDP) linker, which facilitates tagging of the plasmid without interfering with its function. QDs-tagged DNA can transfect cells with high efficiency and intracellular trafficking can be followed through time. The "tagged" plasmid DNA remains functional and serves as a template for gene transcription upon internalization in the nucleus.

The avidin-biotin system has also been used as a non-covalent receptor-ligand system for the binding of DNA to nanoparticles like gold nanoparticles (AuNPs) or QDs[232]. Other than covalent modifications, DNA is negatively charged and is essentially a polyelectrolyte molecule which could bind through the positive charge of the surface such as gold nanoparticles with quaternary ammonium[233]. Additionally, it has been demonstrated that DNA incubated at high stoichiometric excess over gold nanoparticles shows nonspecific adsorption[234].

DNA nanostructures are foreign materials that in theory should be considered as non-self, which could be recognized from the DNA sensing machinery and as a consequence is degraded. DNA is normally confined in the nucleus. When DNA accumulates in the cytoplasm or in endosomes, it is recognized as "anomalous" material. Classical B-form DNA could stimulate immune response through the Toll-like receptor (TLR) pathway. In the endosomes of dendritic cells, TLR9 is activated by anomalous DNA and elicits Type I interferon response. TLR9 preferentially binds unmethylated CpG-rich DNA. These DNA sequences are abundant in numerous pathogen genomes and their binding to the endosomal TLR9 stimulates the immune response. In the cytoplasm, cells are embedded with DNAses, which degrade foreign DNA[235]. Cyclic GMP-AMP synthase (cGAS) and absent in melanoma 2 (AIM2) are a group of sensors that detect DNA in a sequence-independent manner and are localized in the cytoplasm. There is a third group of DNA sensors localized both in nucleus and cytoplasm including interferon-inducible genes 16 (IFI16), RNA polymerase III and the Mre11-Rad50-Nbs1 (MRN) complex. The first hurdle that DNA meets in the blood-stream is represented by DNAse, a few enzymes capable of degrading it, such as deoxyribonuclease II, phosphodiesterase I, DNA hydrolyzing autoantibodies, and neutral deoxyribonuclease I, which is responsible for more than 90% of deoxyribonuclease activity in blood plasma. DNase I is a secreted protein that is released into the alimentary tract and bloodstream. It acts on single-stranded DNA, double-stranded DNA, and chromatin producing fragments of various lenghts[236].

It has been demonstrated that compact structures of DNA present a decreased enzymatic recognition compared to linear DNA. Keum et al.[237]assembled a tetrahedron with edges of about 7 nm containing a centrally located enzyme restriction site, CTNAG (DdeI). It was demonstrated that the tetrahedron structure is less sensitive to DdeI cleavage than the linear DNA presenting the same restriction site. This was probably due to the increased mechanical stability of the ligated DNA. The resistance to non-specific degradation by DNase I was also tested. The tetrahedron structure was digested more slowly than the linear fragment. The explanation of this difference could be attributed to the sensitivity of DNase I activity to local and global helix geometry, which are different between tetrahedral and linear structures. To mimic the physiological condition, the stability of the tetrahedron structure was tested in the presence of 10% FBS. The structure was more resistant to endo- and exo-nuclease cleavage in the serum. The degradation indicated a first-order kinetics and the decay time constant, differed by nearly a factor of 50: 0.8 h for the linear DNA and 42 h for the tetrahedron. The authors hypothesized that the size is an important feature to confer resistance to the enzymatic degradation, but other types of branched geometries, or curvatures, may also mean protection factors.

To overcome the host immunosurveillance, Perrault et al. developed a new system inspired by the envelope of viral particles. In particular, a DNA octahedron of 50 nm was encapsulated in a lipid bilayer in order to mimic virus-like particle. The octahedron structures are composed of bundles of six long double helices (28 nm) engineered with 90° curvatures. The DNA nanostructures could be functionalized by modifying the oligonucleotide structures with high precision. The lipid bilayer was directly assembled around the DNA octahedron, recruited by individual lipid-conjugated oligonucleotides preassembled onto the outer handles. Internal and external diameters were 53 and 76 nm, respectively[238]. In vitro experiments demonstrated that encapsulated DNA drastically decreased the inflammatory response. The production of inflammatory cytokines IL-6 and IL-12 was evident only when the cells were treated with DNA octahedron but not when the structure was encapsulated. Another method to prevent immune response by DNA origami was described by Auvinen et al and consisted in an electrostatic interaction between protein-dendron conjugates and DNA origami building a protein corona coating[239].

Table 7 reproduced from Kumar et al[240].

Structure Characterization									*Biological activity*					
N°	**DNA Nanostructure**	***Characterization***	***Size (nm)***	***Cargo (Loading)***	***Stability***	***Targeting***	***Loading efficiency***	***Release***	***Internalization***	***In vitro tests***		***In vivo tests***		***Biodistribution***
										Cells	**Activity**	**Cells**	**Activity**	
1	Tetrahedral	AFM DLS PAGE (6%)	AFM: height 2-3 nm DLS: 9.08 nm ± 3nm	Doxo	> 4 < 23 hrs **Solution:** 10% human serum **Temp:** 37°C	N/A	26 molecules/ structure **Time:** 1 hr **Temp:** N/A	100% in 10hrs. <10% in 3hrs. **Solution:** PBS pH 7.4 **Temp:** 37°C 60% in 10 hrs **Solution:** PBS pH 5 **Temp:** 37°C	Macropinocytosis and caveolae-mediated endocytosis pathways	Breast cancer MCF7 (drug sensitive) and MCF7-ADR (Doxo resistant).	Doxo-tetrahedral is more effective on cell viability of MCF7-ADR than free doxo. Same efficacy on MCF7 cells.	N/A	N/A	N/A
2	Icosahedral: five- (120 bp) and six- (144 bp) (aptamer) point-star structure	AGE (2%) DLS TEM	**DLS:** - Five stars (28.2 nm ± 3nm) - Six stars (28.6 nm ± 5nm). **TEM**: 25 nm	Doxo	>30min **Solution:** cell culture medium **Temp:** 37°C	Mucin 1 (MUC1). Tumor surface marker	1200 molecules/structure **Time:** 1h incubation **Temp:** room temperature	N/A	Dynamin-dependent and clathrin-mediated endocytosis. Degradation in lysosomes	Breast cancer MCF7 ($MUC1^{+}$), CHO-K1 ($MUC1^{-}$)	Doxo-Aptamer six-point-star structure is more effective on cell viability of MUC1+ cell than free doxo. Same efficacy on MUC- cells.	N/A	N/A	N/A

Structure Characterization									*Biological activity*					
N°	**DNA Nanostructure**	***Characterization***	***Size (nm)***	***Cargo (Loading)***	***Stability***	***Targeting***	***Loading efficiency***	***Release***	***Internalization***	***In vitro tests***		***In vivo tests***		***Biodistribution***
										Cells	**Activity**	**Cells**	**Activity**	
3	Tetrahedral (30bp/edge, Total 6 edges)	AFM DLS PAGE (5%)	**AFM:** height 7.5 nm. **DLS:** 28.6 nm ± 2.38 nm	siRNA against GFP gene. DNA structure conjugated with folic acid.	N/A	Folic acid receptor (FAR)	1-6 siRNA per tetrahedral (1 siRNa/edge)	N/A	N/A	HeLa cells (LUC+). KB cells (HeLa cell contaminant overexpressing folate receptor)	HeLa: LUC expression < 50%. KB: GFP expression <40%	KB xenograft tumours	siRNA no effect on LUC. siRNA-DNA-tetrahedral: IC 50 LUC expression: 1.8 mg/kg. **Inj:** intratumor or tail-vein **Stability:** siRNA 6 min; siRNA-DNA tetrahedral 24 min.	Tumor, Kidney **Time:** 12 hours post injection
4	Tetrahedral	PAGE (3.5%);	N/A	Straptavidin (STV) and CpGs	5hrs **Solution:** FBS 50% **Temp:** room temperature	N/A	N/A	N/A	Endocytosis. Antigen localized in lysosomes after 2 hours	RAW264.7 (macrophage, Abelson murine leukemia virus transformed).	Increased internalization of the complex tetrahedron-STV-CpG by APC cells	BALB/c immunocompetent mice	Mice immunized with the complex tetrahedron-STV-CpG developed a stronger and a longer immunitary response.	N/A

Structure Characterization									*Biological activity*					
N°	**DNA Nanostructure**	***Characterization***	***Size (nm)***	***Cargo (Loading)***	***Stability***	***Targeting***	***Loading efficiency***	***Release***	***Internalization***	***In vitro tests***		***In vivo tests***		***Biodistribution***
										Cells	**Activity**	**Cells**	**Activity**	
5	Aptamer-tethered DNA nanotrain	AFM AGE (3%) TEM	**AFM:** length 100 nm.	Doxo, epirubicin, daunorubicin	>45 hrs **Solution:** PBS+5mM Mg^{2+} **Temp:** N/A	Protein Tyrosin Kinase 7 (PTK7)	N/A	N/A	Endocytosis	CEM cells (human T-cell acute lymphocytic leukemia $PTK7^{+}$) and Ramos (human B lymphocyte Burkitt's lymphoma $PTK7^{-}$)	Drug-Aptamer-DNA-drug is more cytotoxic on $PTK7^{+}$ cells than free drug . Same efficacy on PTK7- cells.	CEM ($PTK7^{+}$) xenograft mouse model	Increased antitumor efficacy and reduced side effects of doxo delivered via Aptamer-DNA nanotrain. **Inj:** I.V.	N/A
6	Open Caged DNA (pyramidal), 408 bp	PAGE (7%)	N/A	Doxo	35 hrs (half-life) **Solution:** cell culture medium+10% FBS **Temp:** 37°C	N/A	172 molecules doxo/structure (at 15% of loading efficiency)	50% of Doxo release from py-Doxo in PBS in 5 hrs and 3 hrs in FBS. Free Doxo in 20 minutes	py-Doxo is able to penetrate inside MDA-MB-231, release Doxo in the nucleus	MDA-MB-231, HepG2	Decrease cell viability compared to free doxo	N/A	N/A	N/A

Structure Characterization									*Biological activity*					
N°	**DNA Nanostructure**	***Characterization***	***Size (nm)***	***Cargo (Loading)***	***Stability***	***Targeting***	***Loading efficiency***	***Release***	***Internalization***	***In vitro tests***		***In vivo tests***		***Biodistribution***
										Cells	**Activity**	**Cells**	**Activity**	
7	Tube with different globlal twist (Straight (S) 10.5 bp/turn and Twist (T) tube 12 bp/turn)	AGE (2%) TEM	**TEM:** length: 138 nm, diameter: 13 nm	Doxo	48hr (T-tube) **Solution:** 10% FBS **Temp:** 37°C	N/A	N/A	80% (T-tube) and 90% (S-tube) in 10 hrs **Solution :** PBS pH 7.4 **Temp:** 37°C	N/A	Breast cancer MDA-MB-231; MDA-MB-468; MCF-7	In all the cell lines tested the T-DNA IC50 is ≈2 times lower than free Doxo. (calculatete d by our group)	N/A	N/A	N/A
8	Tube	AGE (2%) TEM	**TEM:** length: 80 nm, diameter: ≈20 nm	62 CpG sequence specific for mouse Toll like receptor 9	6 hrs **Solution:** cell culture medium **Temp:** 37°C	Toll like recept or 9 (TLR9).	62 binding sites per tube	N/A	N/A	Splenocyt es from female C57BL/6 mice	N/A Immunoresp onse through the TLR9. Nontoxic	N/A	N/A	N/A
9	Hexagonal barrel with aptamer-based lock (antigen keys).	AFM AGE (2%) DLS TEM	**DLS**: 90 nm **TEM**: 35nm x 35 nm x 45 nm	Fab antibody fragment s	N/A	CD33, CDw3 28	N/A	N/A	N/A	NKL	Increase apoptosis	N/A	N/A	N/A

Structure Characterization									*Biological activity*					
N°	**DNA Nanostructure**	***Characterization***	***Size (nm)***	***Cargo (Loading)***	***Stability***	***Targeting***	***Loading efficiency***	***Release***	***Internalization***	***In vitro tests***		***In vivo tests***		***Biodistribution***
										Cells	**Activity**	**Cells**	**Activity**	
10	Triangle and tube	AFM AGE (1%)	**AFM:** -Triangle: edge ≈ 150nm -Tube: lengh ≈ 183 nm	Doxo	N/A	N/A	>200000 molecules (calculated by our group) **Time:** 24 hrs **Temp:** room temperature.	≈15% pH 7.4, 35% pH 5.5 in 48 hrs ≈25% in MCF7 cell lysate >40% with 50U DNAaseI **Solution :** PBS **Temp:** 37°C	Endocytosis and localization of origami in lysosomes after 6 hours of treatement.	Breast cancer MCF7 and MCF7 resistant	MCF-7: 2.5µM and MCF-7 resistant >100µM. DNA origami loaded with doxo enhanced the cells death compared to free doxo on MCF7 doxo resistant cells. No differences between free doxo and origami doxo in regular MCF7.	N/A	N/A	N/A

Structure Characterization									*Biological activity*					
N°	**DNA Nanostructure**	***Characterization***	***Size (nm)***	***Cargo (Loading)***	***Stability***	***Targeting***	***Loading efficiency***	***Release***	***Internalization***	***In vitro tests***		***In vivo tests***		***Biodistribution***
										Cells	**Activity**	**Cells**	**Activity**	
11	Tube, triangle and square	AFM AGE (1%) DLS	**AFM:** -Tube: height: 7 nm, diameter: 380 nm, -Triangle: edge 120 nm, -Square: length*width 90nmx60nm **DLS**: -Triangle: 59 nm -Square: 80.9 nm -Tube: 98.6 nm.	Doxo	24 hrs **Solution:** serum **Temp:** 37°C	N/A	>200000 molecules (calculateted by our group) **Time:** 24 hrs **Temp:** room temperature.	≈20% of Doxo is released in 48 hours at pH 7.4, ≈35% is realeased at pH 5.5 **Solution :** PBS **Temp:** 37°C	N/A	Breast cancer MDA-MB-231	No significant difference compared to the free doxo.	MDA-MB-231 cells Orthotopic breast cancer model	Increased EPR effect of DNA origami. Significant tumor reduction in mice treated with doxo-origami compared to free doxo **Inj:** I.V	Tumor: Triangle > tube >square Tumor > liver > kidney > spleen **Time:** 24 hrs

Structure Characterization									*Biological activity*					
N°	**DNA Nanostructure**	***Characterization***	***Size (nm)***	***Cargo (Loading)***	***Stability***	***Targeting***	***Loading efficiency***	***Release***	***Internalization***	***In vitro tests***		***In vivo tests***		***Biodistribution***
										Cells	**Activity**	**Cells**	**Activity**	
12	Tube (Tile)	AGE (2%) TEM	**TEM**: Length: 27 nm and diameter: 8 nm	siRNA (GFP)	8hrs **Solution:** cell culture medium **Temp:** 37 °C (Degradation depends on Mg^{2+} concentration, oligonucleotide sequences, salt concentration, structural extension)	Folic acid receptor (FAR)	N/A	N/A	Endosomal trapping (no release)	N/A	No effects on GFP expression	N/A	NA	NA

2. Rationale

Surgery together with chemotherapy represent the first line treatment for many tumors[1]. Chemotherapeutic agents (alkylating agent, mitotic inhibitors, anthracyclines, etc.) possess a high cytotoxic effect with an aspecific biodistribution. The poor accumulation in the tumor site is one of the major limits of chemotherapy both with severe and various side effects that can cause myelosuppression, alopecia, gastrointestinal dysfunctions making chemotherapy painful and, in some cases, leading to therapy failure[15]. In order to limit side effects and increase the therapeutic index of anticancer drugs, nanotechnology has shown a key role in this process. Early studies demonstrated that nanoparticles (NPs) drug delivery is able to improve the selectivity of cancer drug on neoplastic cells taking advantages of the enhanced permeability and retention effect (EPR). NPs can also improve some physicochemical aspects of the drug such as water solubility, stability in body fluids, improving the pharmacokinetics and biodistribution parameters and increasing drug half-life[108].

Among approved NPs, liposome technology has become a highly successful and rapidly developing area of preclinical and clinical research. Because of their biocompatibility, biodegradability, low toxicity, and aptitude to trap both hydrophilic and lipophilic drugs[241] and a desirable accumulation in tumoral tissues[242], liposomes are under deep investigation as a drug-delivery system. Many studies have been conducted on liposomes with the goal of decreasing drug toxicity and/or targeting specific cells[243]. Doxil, a liposomal formulation of doxorubicin is for example. Doxorubicin is loaded inside a liposome through a process called remote loading. During the remote loading process, doxorubicin precipitates inside the liposome avoiding its release[107]. Unfortunately, a few drugs have the necessary characteristics to take advantage of this process. The size of liposome (100 nm) is suitable to cross the fenestration of blood vessels in the tumor site and to remain entrapped in the extracellular matrix and the long lasting in blood stream is enhanced by the presence of PEG chain on the surface of the liposome that allows it to escape RES and non-specific immune system[244]. In the last decades, the attention of many research groups has been focusing on DNA nanotechnology that is based on the assembly of artificial DNA nanostructures not present in biological systems, which possess many advantages such as easy custom synthesis, mechanical rigidity and other suitable properties ideal for the applications in the biomedical field. The efficacy of complex DNA nanostructures as an *in vivo* drug delivery vehicle for cancer therapy has been recently highlighted by Zhang et al[229] demonstrating that DNA origamis with triangular shape are able to deliver doxorubicin and passively accumulate in the tumor. Although attractive, DNA is a biodegradable material in biological environments and DNA origami could activate the innate immune system limiting the *in vivo* application. Encapsulation of nanostructured DNA in double layer membranes could avoid DNAse degradation and the immune system response once injected in the blood stream[238]. Another method to prevent immune response

by DNA origami was described by Auvinen et al and consisted in an electrostatic interaction between protein-dendron conjugates and DNA origami building a protein corona coating[239].

3. Aim

The search for safe and effective DDS is the forefront area of research amongst chemist, physicist, engineers and doctors. The field of the development of DDS based on DNA nanotechnology is at early stage and it will require more investigation to fully perceive their applications for cancer therapy. The main goal of this thesis is to experimentally realize the synthesis and development of highly stable and biocompatible DNA nanostructure, using DNA origami technology, as novel DDS and to put the basis for their utilization for site-specific carriers of various diagnostic and therapeutic agents.

The specific aims of this study are:

- To design DNA nanostructure able to fit inside a 100 nm liposomes to load and transport doxorubicin to BC tumors.
- To test *in vitro* the efficacy of the DNA nanostructures based DDS on human BC cell lines.
- To test *In vivo* the antitumor efficacy and biocompatibility of the DDS.

In this work, we present an innovative remote loading system based on a short tube DNA origami (30 nm), which was precisely designed to fit inside a 100 nm liposome. With this new method, the capacity of DNA origami to deliver doxorubicin has been increased also improving the stability of DNA nanostructure in body fluids avoiding inflammation.

4. Materials and Methods

4.1 Reagents

MDA-MB-231, MCF7 (human breast cancer), and LOVO (colorectal cancer) and THP1-Dual^{TM} (monocytic leukemia cell) cell lines were grown as indicated by the suppliers.

Nude mice and FVB mice were purchased from Harlan Laboratories (Udine, Italy). The experimental procedures were approved by the Italian Ministry of Health n°788/2015-PR and performed in accordance with the institutional guidelines. We utilized female mice of 8 weeks of age. Data are reported as mean and standard error of the mean.

Oligonucleotides for the triangle and tubes DNA origamis were purchased from IDT technology (Coralville, Iowa, USA). M13mp18 single strand plasmids were purchased by Bayou Biolabs, LLC, (LA, USA).

4.2 Self-assembling of DNA origami

All DNA origami are assembled on ssDNA M13mp18 as a scaffold at the final concentration of 5nM. Triangle (TrDO) and long tube (LTDO) DNA origami structures were assembled according to Rothemund and Yan's work[203,221]. Annealling and assembling of DNA origami has been performed in 1x TAE- Mg^{2+} buffer (Tris 40 mM; acetic acid 20 mM; EDTA 2mM; magnesium acetate 12,5 mM; pH 8.0) in a thermocycler (Eppendorf Mastercycler®, Hamburg, Germany) by slowly cooling from 90°C to room temperature 12 hours. STDO origami has been designed with CaDNAno software and assembled with the following protocol: 1 x TE (10 mM Tris-HCl and 1 mM EDTA, 16 mM $MgCl_2$, pH 8) in a thermocycler slowly cooling from 65°C to 4°C in 19 hours.

4.3 DNA origami purification

To obtain a pure DNA origami structures eliminating the excess of staple strands and scaffolds, we applied the protocol described by Stahl et al[209] based on DNA PEG precipitation. DNA origami self-assembling mixture weas mixed 1:1 (v/v) with precipitation buffer containing 15% PEG 8000 (w/v), 5 mM Tris-HCl, 1 mM EDTA and 505 mM NaCl all chemicals were purchased by Sigma-Aldrich (Merk, Darmstadt, Germany). Solution was mixed by inversion and spun down at 10000 x g for 25 minutes at room temperature. Supernatant has been discarded and pellet was resuspended in physiological solution.

4.4 Agarose gel electrophoresis (AGE)

Folded DNA structures electrophoresis was carried out in 1% agarose gels in TAE 1x (Tris Acetate EDTA), for two hours at 80 V at room temperature. Gels were stained with SYBR® safe intercalating

agent. Gels images have been acquired through UVP, biospectrum Imaging System, Chemi HR 410, Cambridge, UK.

4.5 TEM analysis

Experiments were carried out using a Philips EM 208 microscope (Philips, Amsterdam, Netherlands). The grid used: FCF 100H-Nikel, 300 Cu Graphene Lacet. Sample stained with a saturated solution of uranyl acetate. Analysis have been performed at 100 kV.

4.6 DNA origami QD labeling

One staple strand has been modified with biotin in each DNA origami structure in order to be able to bind streptavidin-conjugated quantum dot (QD 705, Invitrogen). An equimolar quantity of purified origami and QD were incubated by rotation for 1 hour at room temperature.

4.7 DNA origami stability

DNA origami structure was incubated in DMEM 10% FBS at 37°C. Ten µl of the sample have been collected per each time point and stored at 4°C. At the end of time course, samples were run on 1% agarose gel.

4.8 DLS analysis

Z-average particle size and polydispersity index (PI) were determined by dynamic light scattering (DLS) at 25 °C with a Zetasizer nanosystem (Malvern, UK) using a 10 mV He-Ne laser. Viscosity and refractive index of the physiological solution at 25 °C were used for data analysis using cuvettes with a volume of 100 µl.

4.9 Liposome preparation and DNA origami internalization and purification

1,2-distearoyl-*sn*-glycero-3-phosphocholine (18:0) (DSPC), 1,2-Dipalmitoyl-sn-glycero-3-phosphoethanolamine-PEG 2000 (16:0) (DPPE-PEG), Cholesterol (CHL) and mini-extruder instrument were purchased from Avanti Polar (Avanti Lipids Polar, Alabaster, Alabama, US). DSPC, DPPE-PEG and CHL (55:5:40) powders have been resuspended in chloroform and dried over-night (ON) with a vacuum pump (Genevac, EZ-2, SP scientific, Warminster, PA, USA) to form a "lipid cake". Lipid cake was rehydrated in a DNA origami purified solution and extruded for ten times through 200 and 100 nm Millipore filters (Merck Millipore, Darmstadt, Germany) to load STDO inside (LSTDO). Excess of DNA origami has been eliminated by a cationic resin (IONEX H, C.T.S., Italy) interaction. Cationic resin 500 µg is suspended in 500 µl of mQ water to be hydrated, washed two times and suspended in PBS 1X. This solution was mixed 1:1 to the LSTDO solution and incubated at RT for 1 hour by rotation. After incubation, the solution was centrifuged at 0,2 g for 5

minutes in order to pellet the resin with free DNA origami and supernatant containing the purified LSTDO was collected.

4.10 Doxorubicin intercalation into DNA origami, LSTDO and release

Doxorubicin-HCl was purchased from Accord, (Accord Healthcare Italy S.r.l.). DNA origami was incubated 1:2 (w/w) with doxorubicin for 2 hours in rotation at room temperature. Unloaded doxorubicin was eliminated after centrifugation at 3000 x g for 5 minutes. Origami and doxorubicin pellet were washed with physiological solution until the supernatant appeared clean. LSTDO was loaded with doxorubicin incubating in a solution of doxorubicin 2mg/ml 1:2 (W_{DNA} / W_{Doxo}) ON. The excess of drugs unloaded was eliminated through dialysis in PBS 1X pH 7.4 RT with a 10 kD cutoff semipermeable membrane for 2 hours. Doxorubicin intercalated was dosed by absorbance at 480 nm through a TECAN plate reader. Loading efficiency was calculated with the following formula:

$$\% \text{ loading efficiency} = \frac{weight\ of\ lipos\square mes\ (g)}{weight\ of\ Doxorubicin\ (g)}.$$

The release of doxorubicin and origami-doxo (50 µg/500 µL) was evaluated with a dialysis membrane with a cut-off of 15000 MWCO dipped into 1L of PBS 1X at pH 7.4 or pH 5.5. The cumulative release of DOX was evaluated by measuring the fluorescence intensity (I) at Ex 465/Em 595 nm of DOX inside the dialysis membrane at different time points (0, 0.5, 1, 2, 3, 6, 8, 12, 18 and 24 hours). The percentage of cumulative release was calculated using this equation below:

$$R = \frac{I_0 - I_t}{I_0} \times 100\%$$

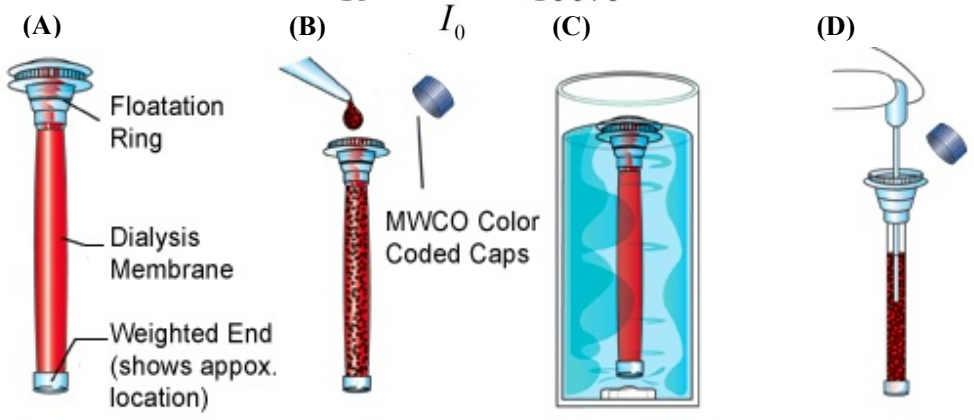

Fig. (13). Schematic picture of dialysis membrane of 20.000 MWCO, indicating the different steps for **(A)** Membrane buffer equilibration. **(B)** Loading with analyzed solution. **(C)** Incubation in PBS 1X pH 7.4 at 37°C **(D)** Sample collection.

4.11 Cell viability assay

Cells were seeded in 96-well plates (Becton Dickinson, NJ, US) at a density of 10^3 cells/well and incubated for 24 h to allow the attachment of cells. The cells were incubated with doxorubicin and origami-doxo at the same drug concentrations for 96 h. The cytotoxicity was evaluated by CellTiter-Glo® Luminescence assay (Promega, Madison, Wisconsin, US) with an Infinite 200 PRO instrument (Tecan Trading AG, Switzerland) (Figure 14).

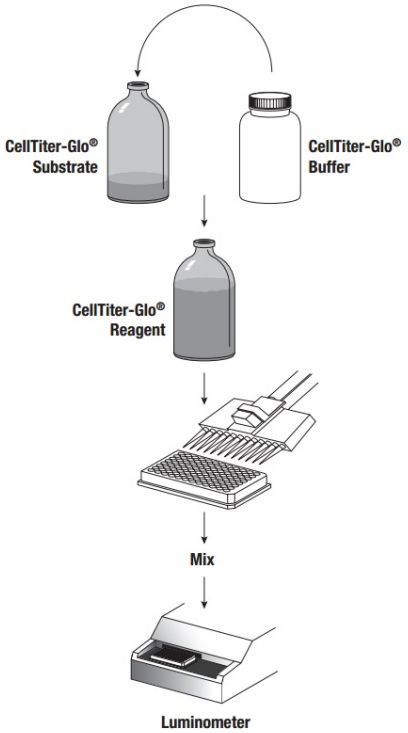

Fig. (14) Flow diagram showing preparation and use of CellTiter-Glo® Reagent.

The CellTiter-Glo® Assay relies on the properties of a proprietary thermostable luciferase (Ultra-Glo™ Recombinant Luciferase), which generates a stable "glow-type" luminescent signal and improves the performance across a wide range of assay conditions. The luciferase reaction for this assay is shown in (Figure 15).

Fig. (15). The luciferase reaction. Mono-oxygenation of luciferin is catalyzed by luciferase in the presence of Mg^{2+}, ATP and molecular oxygen.

4.12 Histopathology

Organs of mice were collected and fixed in phosphate-buffered 10% formalin, embedded in paraffin, sectioned at a thickness of 3 μm, and stained with hematoxylin and eosin (H&E). The tissues were

analyzed with a light microscope using different magnifications. Morphological details were analysed at 40X objective.

4.13 ELISA test

ELISA test was performed on FVB mice injected with free short tube DNA origami, liposomes and liposome with origami inside. The quantity of vector used was calculated referring to the loading efficiency of every single vector in order to inject intravenously the same quantity of vector employed for a treatment of doxo+vector 3 mg/kg. After 6 hours of the injection, mice were sacrificed, and blood was collected by heart punch with a 29g needle 500 ul syringe pre-wet with heparin (Esoclar 5000 UI/ml, Hospira SRL, Italy) with 40 ul of solution left. Samples have been collected in a 1,5 ml eppendorf adding 1:8 ACD-A (Anticoagulant Citrate Solution A, Citralabs, Braintree, UK) solution and centrifuged at 5000 x g to collect plasma. Plasma was analysed with Mouse Inflammatory Cytokines Multi-Analyte ELISArray Kit (SABiosciences, Qiagen, Hilden, Germany) following the protocol precisely.

4.14 Mouse xenograft

$3x10^6$ MDA-MB-231 cells were mixed with 30% of Matrigel (BD Bioscience, CA, US) and implanted orthotopically into 6-week-old female nude mice with a 29G syringe needle in a volume of 100 µl. When tumors reached a measurable size (> 50 mm^3), mice were treated i.v. with 3 mg/kg of doxorubicin, STDOdoxo and LSTDOdoxo once per week for four treatments. Tumor volumes were measured with a calliper instrument and calculated using the formula: $(length \times width^2)/2$.

4.15 Biodistribution

The organs of mice were washed with 10 ml of cold PBS/heparin injected in the heart after sacrifice. Organs were collected after washing and transferred in a 1.5 ml tube containing 500 µl of PBS/BSA 4% and homogenized with Qiagen Tissue Ruptor for 20 seconds at power 4 in ice. Samples were then stored at -80 °C. The concentrations of doxorubicin were measured by liquid chromatography-tandem mass spectrometry (LC-MS/MS). The proteins were precipitated with 2 volumes of cold acetonitrile containing 20 ng/mL daunorubicin as the internal standard. After vortexing and spinning at 13000 rpm for 15 min. at 4 °C, the cleared supernatant was diluted with 2 volumes of 0.2% formic acid and 10 µl were injected on LC-MS/MS system. Chromatographic separation was performed on Accucore-150 30x2.1 mm 2.6 µm C18 column (Thermo Scientific, MA USA), equilibrated with a 0.7 ml/min of 0.2% formic/acetonitrile (95:5) and maintained at 50°C. An elution gradient B from 5% to 80% of acetonitrile over 5 min. was applied and 3 min. of equilibration A 4000 QTRAP MS/MS system equipped with Turbo ESI source (AB Sciex, MA, USA) was applied in positive-ion mode. The transitions of doxorubicin and daunorubicin were monitored in multi-reaction monitoring mode at

m/z 544.1→397.2 and 528.2→321.1, respectively. The spray voltage was set at 5000 V and the source temperature at 400 °C. The curtain gas, nebulizer gas (gas1) and auxiliary gas (gas 2) were set at 20, 50 and 50 arbitrary units, respectively. The declustering potential and collision energy voltages for both doxorubicin and daunorubicin were set at 45 V and 16 V, respectively.

4.16 Statistical Analysis

The statistical significance was determined using a two-tailed t-test. A *p*-value less than 0.05 was considered significant for all comparisons done. Bars represent error standards for tumor volume and body weight. All other bars are standard deviations.

5. Results

5.1 DNA origami synthesis, characterization and stability

DNA origami were assembled in a one-step reaction according to the protocol described in the previous paragraph. The structure has been characterized by AGE, TEM and DLS.

Purification of origami occurred through PEG precipitation as described previously allowing us to eliminate all the excess of staples with almost 90% of structure recovering.

TEM analysis showed that the structures synthesized were the one which is predicted by the informatics design. TEM analysis of STDO made us able to take all the measurements with the following dimensions: length 30,1 nm ± 0,67 nm and width 10,2 nm ± 0,09. Also, TrDO and LTDO were analyzed by TEM confirming that the structures were correctly assembled with the following dimension for TrDO and LTDO: 120 nm each edge and 380 nm length respectively.

DLS analysis showed two peaks. One represents the real hydrodynamic radius and the other shows the hydrodynamic radius of the aggregates made by the structures (Figure 16). DLS results are the

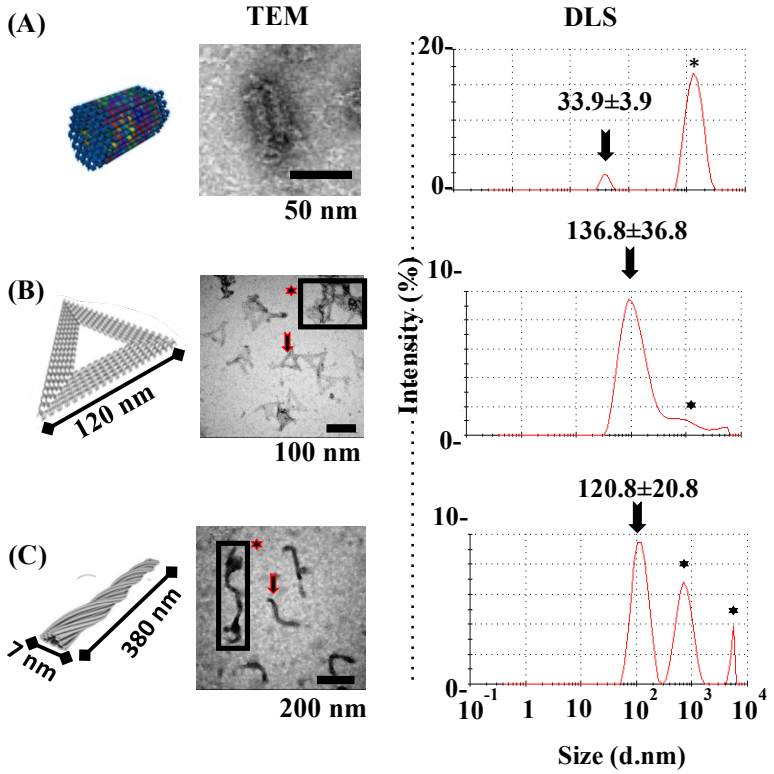

Fig. (16). TEM and DLS characterizations of STDO, TrDO and LTDO. TEM image and DLS analysis of (A) STDO, (B) TrDO and (C) LTDO. Arrows on TEM images and DLS indicate the DNA origami; star, aggregates.

following: STDO 33.9±3.9 nm, TrDO 136.8±36.8 nm and LTDO 120.8±20.8 nm.

Stability test of STDO, TrDO and LTDO in physiological condition showed that STDO is stable for 48 hours vs 8 hours for TrDO and LTDO (Figure 17).

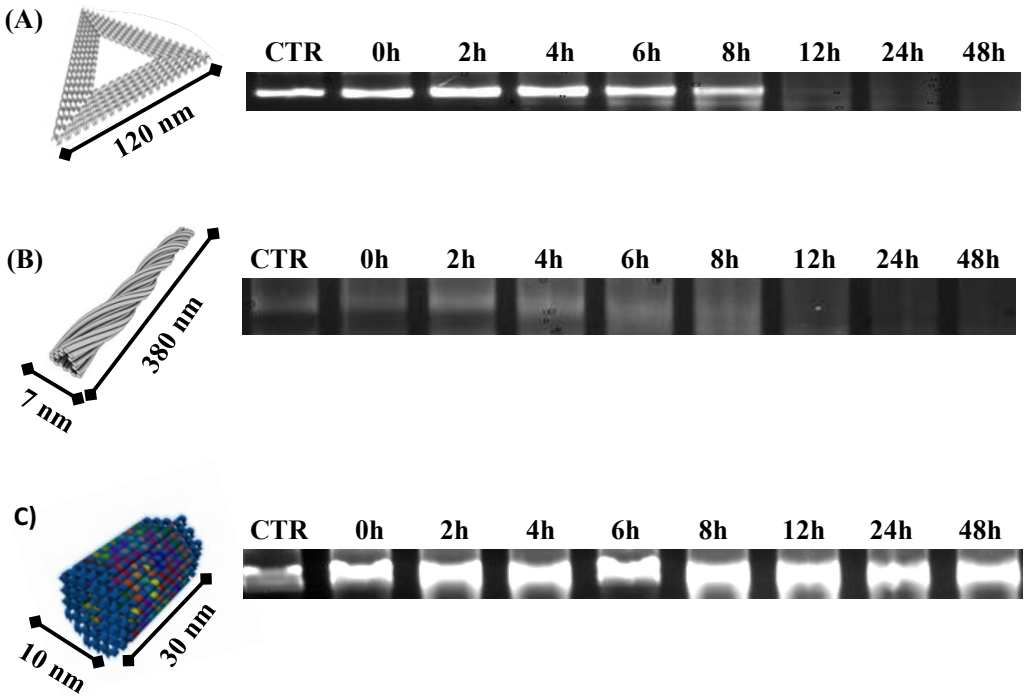

Fig. (17). AGE analysis of DNA origami's stability: **(A)** TrDO. **(B)** LTDO. **(C)** STDO. Stability test was performed in DMEM 10% FBS at 37°C. Samples were collected at indicated time points and run on 1% agarose gel for 1 hour. STDO has a long stability up to 48 hours.

5.2 Three stage nanovector (LSTDO) synthesis and characterization

Lipid cake was resuspended in a physiological solution containing pure STDO in a physiological solution for a final concentration of 2 mg of lipid in 1 ml of 800 μg of STDO, extruded through semipermeable filters of 200 nm and 100 nm. The excess of DNA STDO outside the liposome was eliminated through a cationic exchange resin that catches the free DNA without interfering with liposome. The structure was analysed by TEM and DLS (Figure 18). To be able to see STDO through the lipid membrane we used a STDO modified with QD in order to have a structure more electron-dense bound to STDO to allow us to see them inside liposome. TEM images displayed the correct loading of STDO inside liposome and the efficacy of purification method. DLS measurements support TEM images with the following results: STDO+QDs 37.6±7.6 nm, liposomes 153.0±53.0 nm, LSTDO with excess of STDO (not purified) 170.1±70.1 and LSTDO (purified) 163.9±63.9.

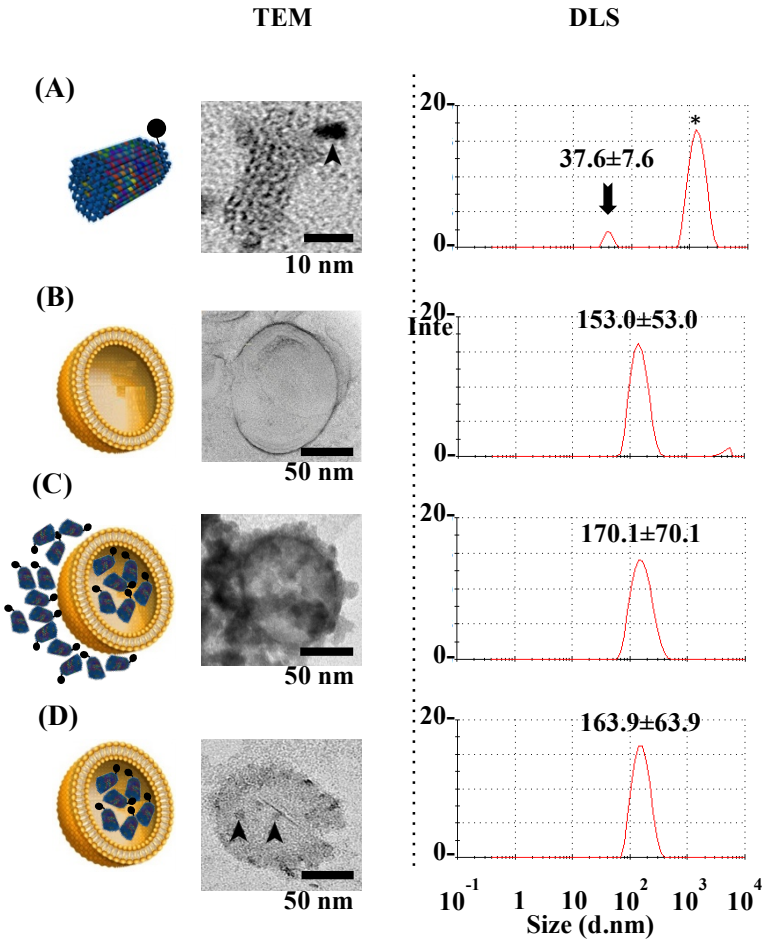

Fig. (18). Characterization of liposomes, STDO+QDs and LSTDO. (A) STDO was synthesized and characterized by TEM and DLS (arrows indicate the correct peak of size distribution). To visualize STDO inside liposome, a Cd-Se QD was conjugated to STDO. (B) Pegylated liposomes were synthesized and (C) loaded with STDO (LSTDO). DLS was enabled to detect only liposomes (LSTDO) (D) The excess of STDO was eliminated incubating LSTDO with a cationic resin that binds unloaded STDO but not liposomes. Arrowheads indicate QD-STDO inside liposomes. Star (*) indicates aggregates.

5.3 Loading-release and cell viability

The doxorubicin loading efficiency percentage inside LSTDO was around 50% (Figure 19 A). Empty liposomes were used as control. We tested the release at 37°C, pH 7.4 and at pH 5.5. The release is faster in acidic condition compared to pH 7.4 (Figure 19 B).

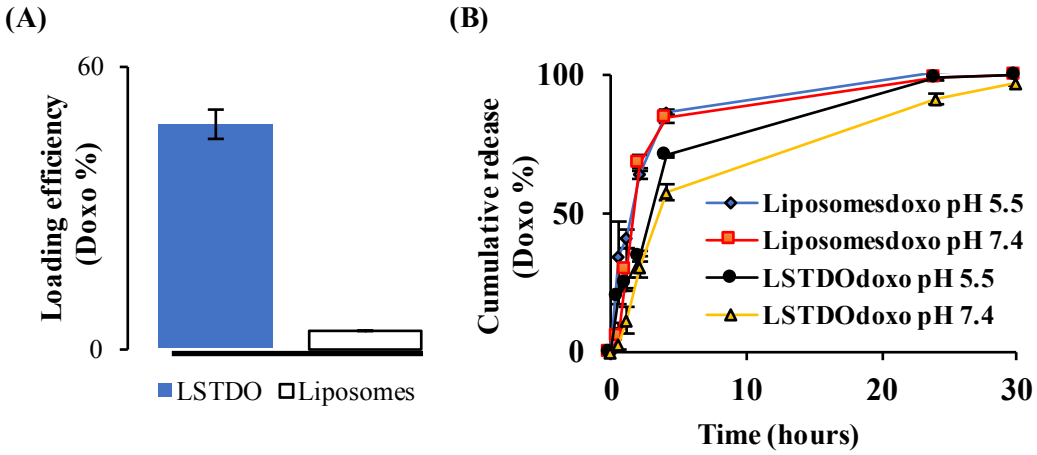

Fig. (19). (A) Doxorubicin loading efficiency of LSTDO. LSTDO and liposomes were incubated for 24 hours with doxorubicin, dialyzed for 2 hours and the doxorubicin was quantified by absorbance at 480 nm (three independent experiments). **(B)** Doxorubicin cumulative release of LSTDO. The release of doxorubicin by LSTDO was assessed by dialysis at pH 7.4 and 5.5 in order to reproduce the physiological conditions of blood and tumor microenvironment (triplicates). LSTDO has a faster kinetic release at pH 5.5.

MDA-MB 231 and MCF7 (breast cancer) and LoVo S (colorectal cancer) cell lines were treated with the same amount of doxorubicin, STDOdoxo and LSTDOdoxo and results showed that there were no significant differences between the three groups (Figure 20).

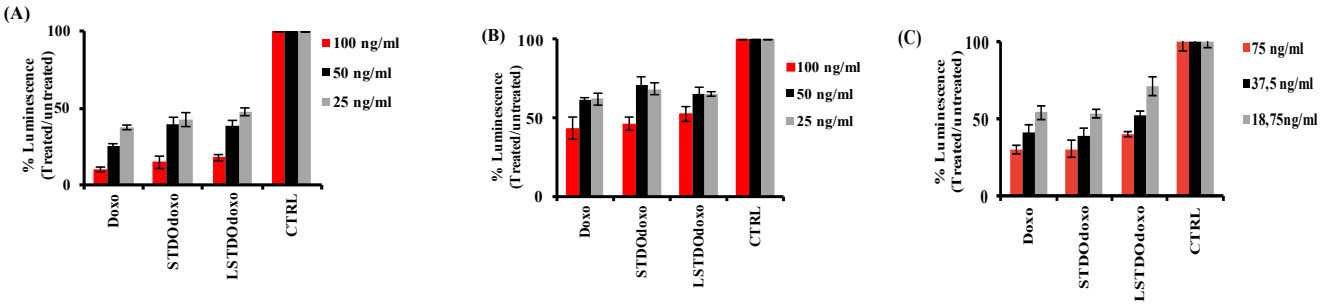

Fig. (20). Cytotoxicity of LSTDOdoxo, STDOdoxo and doxorubicin on **(A)** MCF7, **(B)** MDA-MB-231 BC and **(C)** LoVo colorectal cancer cell lines. Histograms represent the viability of cells and bars represent Standard deviations. Experiments were done in triplicates. No significants differences are reported by these experiments.

5.4 Acute toxicity evaluation

Acute toxicity was performed in nude mice. 15 mg/kg of doxorubicin, STDOdoxo LSTDOdoxo were injected intravenously (iv). The loss of weight was followed for ten days highlighting that the mice treated with STDOdoxo showed a fast weight decrease in five days inducing their sacrifice. The other two groups displayed the same profile of weight loss (Figure 21).

5.5 Histopathology analysis

At the end of acute toxicity experiment organs (liver, spleen, bone marrow, lung, small intestine, kidney, heart, brain and skin) were harvested from mice and analyzed. The only difference detected between the three groups concerned the count of blast cells in bone marrow that was decreased in mice treated with STDOdoxo (Figure 21).

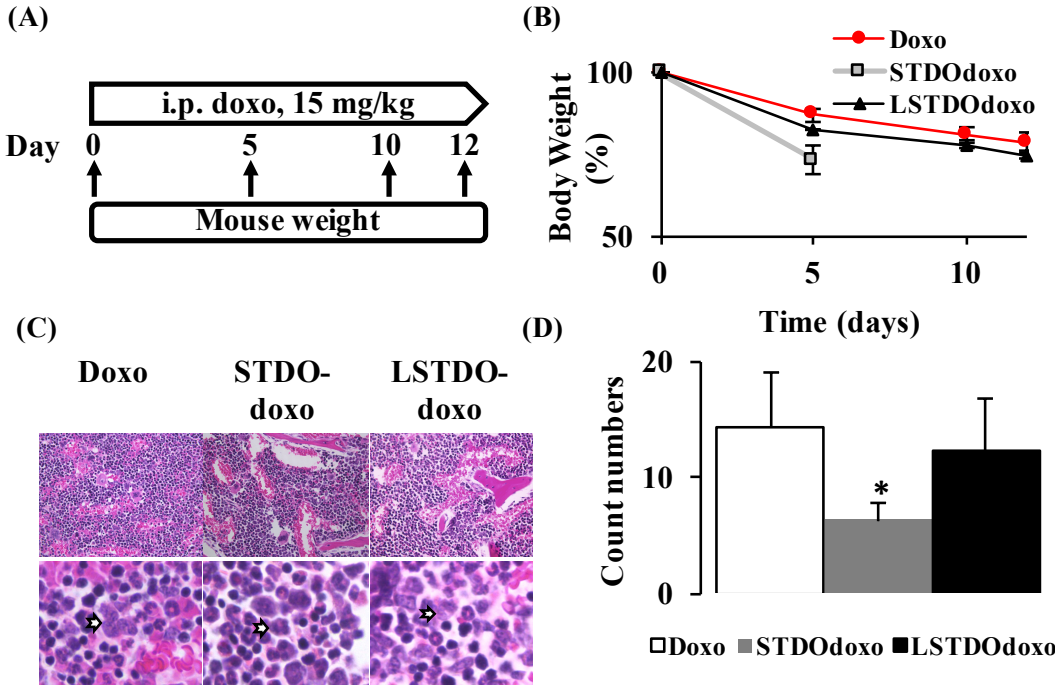

Fig. (21). LSTDOdoxo is less toxic than STDOdoxo *in vivo*. **(A)** Schematic design of the study. Three mice/group were injected i.p. with 15 mg/kg of doxo, STDOdoxo and LSTDOdoxo at day 0 and the body weight was measured at indicated intervals. **(B)** Mice body weight has been followed up for 12 days as an index of illness. Mice treated with LSTDO are comparable to mice treated with doxo. Mice treated with STDOdoxo have a faster weight decrease and were sacrificed ahead of time. **(C)** Mice bone marrows were analyzed by histopathology. Representative H&E staining of bone marrows at 40X magnification (upper panel). The lower panel shows examples of blasts (arrows). The number of blast cells was less in STDOdoxo mice compared to the other treatments **(D)**. (* p-*value* < *0.05*).

5.6 Antitumor efficacy

Antitumor efficacy of our structure was tested on nude mice bearing orthotopic breast cancer tumor induced by the injection of MDA-MB 231 cells. Mice were treated three times once per week with 3 mg/kg of doxorubicin, STDOdoxo and LSTDOdoxo. Tumor growth and mice weight have been followed. Mice treated with LSTDOdoxo showed a slower tumor growth compared to the other two groups with a statistical difference (p-*value*< *0.05*) (Figure 22A-B).

Tumors biodistribution was determined by MS-HPLC analysis (Figure 22C).

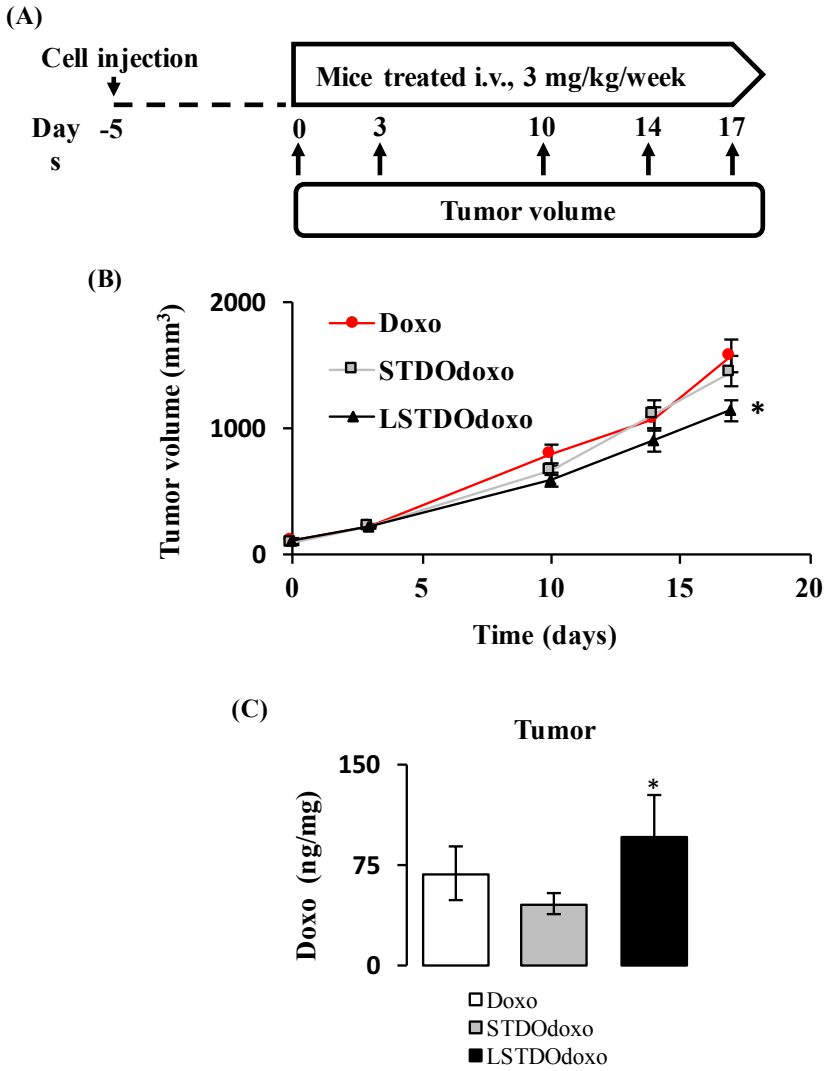

Fig. (22). LSTDOdoxo increases the efficacy of doxorubicin *in vivo*. **(A)** Schematic design of tumor growth study. Mice were treated three times (3 mg/kg, once a week) and tumor volumes (n=8) were followed up. **(B)** After 14 days, mice treated with LSTDOdoxo have a reduced tumor volume compared with mice treated with doxorubicin and STDOdoxo (* p-*value* < *0.05*). **(C)** After 72 hours from doxorubicin injection, mice were sacrificed and the drug was quantified in the tumors (n=8). (* p-*value* < *0.05*).

5.7 ELISA test

Mice (three/group) were treated intravenously with the same amount of STDO, LSTDO and liposome required to a 3mg/kg doxorubicin treatment. After six hours mice were sacrificed and blood collected. ELISA test was performed on plasma and a panel of interleukin (IL-1a, IL-1B, IL-2, IL-4, IL-6, IL-10, IL-12, IL-17A, IFN-γ, TNF-α) was tested. IL-6 was increased in mice treated with STDO compared with the group treated with LSTDO (Figure 23A).

5.8 THP1 activation experiment

THP1 dual cells have been seeded in a 96 mw (100000 cells/well) and treated with STDO, TDO, TrDO, LSTDO and Liposomes (100 and 1 ng). After 24 hours of incubation at 37°C 10 ul of the medium have been collected and put into a 96-well black and the activation of interferon regulatory factor (IRF) was evaluated. Naked DNA nanostructure activate IRF more than LSTDO and liposomes (Figure 23B).

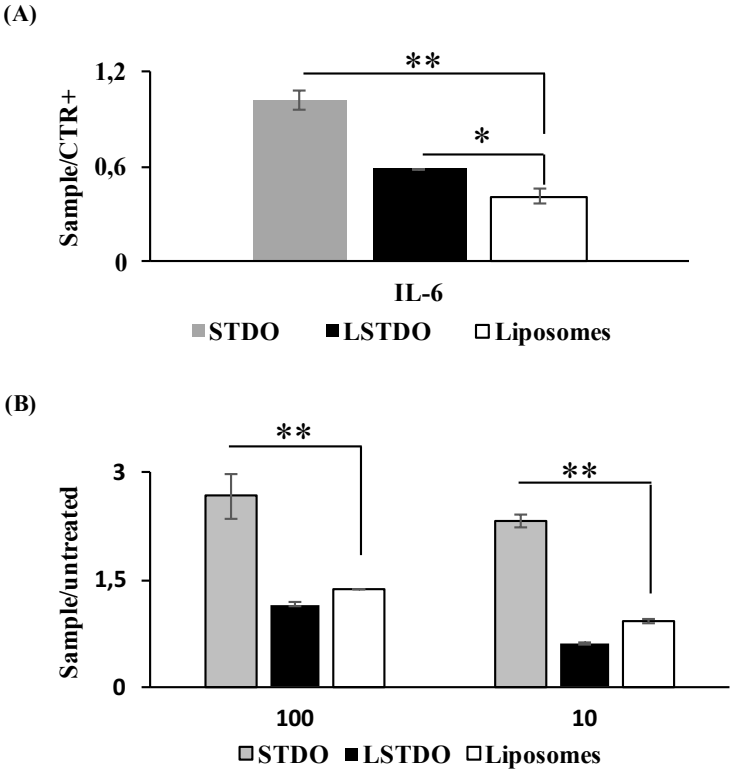

Fig. (23). LSTDO attenuates the inflammation induced by DNA origami. **(A)** ELISA test on FVB/N mice. Mice (two groups of 4 mice) were treated with STDO, LSTDO and liposomes to detect acute inflammation. After six hours of i.v. injection blood was collected and analysed: IL-6 increased in mice treated with STDO (* p-*value* < *0.05*). **(B)** Evaluation of interferon activation in THP1 monocytic cell line. THP1 cell line was modified in order to secrete a luciferase under the control of interferon pathway. Cells were treated with 10 and 100 µg/ml of STDO, LSTDO and liposomes. Interferon production was enhanced by the treatment with STDO (** p-*value* < *0.01; * <0.05*).

6. Discussion

Nanotechnology is a multidisciplinary field involving a wide range of scientific disciplines from physics to medicine going through chemistry, engineering and biology. In the last two decades, nanotechnology rapid developments have allowed the incorporation of multiple therapeutic, sensing and targeting agents into NPs in order to develop nanodevices able to detect, prevent and treat oncological diseases. It is well known that chemotherapeutic agents present severe side effects including bone marrow suppression, cardiac and kidney toxicity, hair loss and mucositis; in addition, these drugs are poorly soluble in biological fluids, are quickly recognized by the mononuclear phagocyte system (MPS) and rapidly cleared from the body[38]. The binding or the encapsulation of drug to nanoparticles can also modify chemical and physical properties such as poor water solubility, drug circulation half-life escaping the non-specific immune system, improving biodistribution and PK[39]. In the application to drug delivery, all these properties are translated in an improvement of selectivity in targeting neoplastic cells by allowing the preferential delivery of drugs to tumors owing to the EPR effect of leaky vasculature increasing the therapeutic index of the anticancer drugs. Summarizing, the drug encapsulation helps for two main purposes: the body is protected against off-site toxicities and the drug is protected against body defence system.

In the last two decades, both inorganic and organic materials have been used to construct nanostructures that facilitate anticancer drug delivery. These technologies represent a promising breakthrough in cancer therapy. However, in some cases, the observed toxicity raises concerns for real applications *in vivo*. In the wide landscape of nanomaterials applied to drug delivery, recently, many research groups have focused their attention on DNA nanotechnology, the construction of artificial DNA nanostructures not present in the biological system, which possess minimal toxicity and other suitable properties ideal for applications in medicine and biomedical field.

DNA, being a biological material, assembled in the correct shape and dimension, should possess high stability, mechanical rigidity, easy custom synthesis with a manipulative length of strands, and multifunctionality. DNA remarkable molecular recognition properties, complementary base-pairing, high loading efficiency, effective cellular internalization and structural features further make it appropriate as a programmable "smart" building block for the construction of organized nanostructures for the development of nanocarriers for various chemotherapeutics for cancer therapy. Different kinds of DNA structures can be build up through a bottom-up assembly of multiple ssDNA that have to hybridize to other segments or to a scaffold. In 1964, Robin Holliday illustrated a four-armed DNA branched junction, which later became known as the Holliday junction, in which four DNA strands are linked together to form four double helical arms flanking a branch point. A Holliday

junction occurs commonly in nature, as it is being the process of genetic recombination called crossing-over involved in passing genetic diversity to the next generation[245]. This specific genetic structure became the foundation of DNA nanotechnology, in which by connecting several Holliday junctions in the form of tiles and yielded DNA lattice in two and three dimensions[179]. In 2006, Paul Rothemund at the California Institute of Technology introduced the term "scaffolded DNA origami", which has revolutionized the field of structural DNA nanotechnology by enhancing the complexity and size of self-assembled DNA nanostructures in a simple "one-pot" reaction. Scaffolded DNA origami involves the folding of a long circular single-strand-scaffold viral DNA derived from the bacteriophage M13mp18 hundreds of short staple strands or helper strands of DNA into the desired shape[203]. The DNA origami technique has been successfully used for the preparation of different 2D and 3D nanostructures and for the nanopatterning of nanoparticles, proteins and other functional molecular components into well-defined arrangements. Chemically modified staples can be inserted at a predefined position in the DNA nanostructure, which could be used to impart several additional functionalities in the designed DNA nanostructures.

Lastly, it was demonstrated that anticancer drugs activity and release kinetics of drugs could be regulated by encapsulating them in DNA origami nanostructures[225]

Small DNA cages have shown to work as effective delivery carriers for anticancer drugs, small interfering RNA, immune stimulating CpGoligo-DNA and antigen molecules, either *in vitro* or *in vivo*[226]. Scaffolded DNA nanostructures, which provides enhanced size and controllable shape, can be used to construct multivalent and multifunctional drug carriers. DNA origami was found to be stable in cell lysates and can be slowly degraded in living cell treatment, demonstrating its stability in physiological condition highlighting its great potential for drug-controlled release[225,229].

Doxorubicin is an anthracycline and is one of the most common utilized chemotherapeutic drugs. Doxorubicin is an intercalating agent acting damaging DNA inducing cells apoptosis[246]. Unfortunately, this potent chemotherapeutic agent presents severe side effects in particular on bone marrow and on heart tissue[247] limiting its treatment dosage. Relating to the intrinsic nature of DNA origami, the question is whether it is possible to tune DNA nanostructures to optimize the delivery of doxorubicin to human cancer cells[248,249] and to reduce side effects. Until now, few structures were designed for drug delivery, starting from the simplest pyramidal to the more complex like a triangle, square and hexagonal origami. Since doxorubicin is the most utilized drug on BC treatment, cell lines derived from this type of tumor were chosen to test the efficacy. The efficacy of DNA-doxo complex was evaluated in cell viability and cytotoxicity experiments[247] and it is demonstrated that doxoDNA is able to circumvent even drug resistence[247].

The *in vivo* application of DNA nanostructures has been shown to improve the pharmacological effect of their cargo[229,250,251]. Among all the described benefits, there is a limitation to the *in vivo* application of DNA nanotechnology. DNA nanostructures are foreign materials that should be considered as non-self, and could be recognized from the DNA sensing machinery to be degraded. The first hurdle that DNA meets in the bloodstream is represented by enzymes capable of degrading it[252,253]. DNA is recognized as "anomalous" material could stimulate immune response through the Toll-like receptor (TLR) pathway and elicits Type I interferon response. It has been demonstrated that compact structures of DNA present a decreased enzymatic recognition compared to linear DNA.
To overcome the host immuno-surveillance, Perrault et al developed a new system inspired by the envelope of viral particles. In particular, a DNA octahedron of 50 nm was encapsulated in a lipid bilayer in order to mimic virus-like particle[238]. *In vitro* experiments demonstrated that encapsulated DNA drastically decreased the inflammatory response. The production of inflammatory cytokines IL-6 and IL-12 was evident only when the cells were treated with DNA octahedron but not when the structure was encapsulated. In a recent work by Auvinen et al[239] demonstrated that also a coating of BSA on DNA origami can prevent the activation of immune system. These results outlined that a three-stage DDS (Membrane-DNA-Drug) could increase the circulation half-life of the DNA nanostructures in the blood and finely control the drug release. In addition, the outer membrane could be engineered by adding specific molecules such as receptors, ligands or antibodies in order to target specific cells. In this thesis is described a new DDS based on DNA origami able to deliver doxorubicin improving its pharmacological profiles and avoiding side effects induced by DNA.

DNA origami synthesis, characterization and stability. To synthesize a very stable DNA nanostructure able to fit inside a liposome of 100 nm to build a biocompatible molecular scale device, we design and synthesize a tubular structure of 30 nm in length (Figure16). The aim was to create a three-stages system in order to set up a new protocol to remote load liposome with doxorubicin. The synthesis of this structure was carried out through the self-assembling of short sequences of ssDNA on the circular ssDNA M13mp18 as scaffold. After the synthesis, we purified the synthesized structure by the excess of staples and the scaffold recovering the 90% of pure STDO using the method described by Stahl et al[209] and we characterized by AGE, TEM and DLS confirming that the structure we obtained is the one that we expected. Since the aim of our project was to set up a DDS based on DNA origami, we assessed the stability in the physiological condition of our structure since it is one of the must-have properties of a good carrier. Comparing with other structures present in literature TrDO and LTDO, our structure is more stable (48 vs 8 hours) (Figure17). We speculated that the compact structure of STDO could limit the access of DNAses preventing its rapid degradation. The

need to fit inside a stealth membrane is related to the fact that DNA is a foreign material that is recognized by the non-specific immune system. DNA once in the bloodstream is also recognized by enzymes capable of degrading it. DNA is normally confined in the nucleus. When DNA accumulates in the cytoplasm or in endosomes, it is recognized as "anomalous" material and could stimulate immune response through the Toll-like receptor (TLR) pathway. Moreover, each nanoparticle before *in vivo* application should satisfy important requirements. The combination between size and surface properties can determine the fate of nanoparticles within the body defining the interactions with their local environment. Surface charge covers a key role in the recognition of nanoparticles by the RES. To avoid or minimize these issues, we decided to load our DNA origami inside stealth PEGylated liposomes. PEG is a linear polyether diol with many suitable features, such as biocompatibility, low toxicity, low immunogenicity and antigenicity[244]. STDO was loaded inside liposomes through resuspension of lipid cake with a solution of purified STDO. Then to obtain a monodisperse population of liposomes of 100 nm we extruded the solution through a 100 nm Millipore filter. The excess of STDO outside liposomes was eliminated through the employment of a cationic resin able to catch DNA and to precipitate it centrifuging the solution at low g owing to the fact that liposomes did not interact with resin and did not form aggregation that allows them to not precipitate at low g[244]. To be able to understand if STDO was inside the liposomes at TEM, we synthesized STDO with a biotinylated staple able to bind a QDs modified with streptavidin. QDs are small nanoparticles of size ranging from 2-10 nm made of binary compounds such as lead sulfide, lead selenide, cadmium selenide, cadmium sulfide, indium arsenide, and indium phosphide. The presence of heavy metal in their structure allowed us to see them through the membrane of liposomes at TEM revealing that the protocol we set up to load STDO inside the liposome and the purification methods are efficient (Figure 18).

Doxorubicin loading, release and *in vitro* efficacy. To load doxorubicin, we exploited the intrinsic property of anthracycline to intercalate DNA. LSTDO was incubated with doxorubicin for 24 hours at room temperature (remote loading). The unloaded doxorubicin was removed by 2-hours dialysis with 15 kD membrane, loading efficiency was about 50% (w/w) (Figure 19A) that is sufficient to use this DDS *in vivo* avoiding the toxicity induced by liposomes[254]. To possess a controlled release is a key feature of a DDS. Following the loading process, the release of doxorubicin was tested. As suggested in literature[225], the release test was performed at 37°C pH 7.4 and 5.5 to reproduce physiological and tumor microenvironment condition. The kinetics of release depends on pH. At lower pH, the doxorubicin was released faster than at pH 7.4 (Figure 19B). The fast and anabolic metabolism of cancer cell stimulates the lowering of pH in the tumor microenvironment, in this condition the structure of DNA origami can be affected and doxorubicin could be released more

quickly than in physiological condition. Doxorubicin is predominantly used in the treatment of breast cancer often in combination with cyclophosphamide in a regimen called AC. For this reason, we test the cytotoxic effect of STDO and LSTDO was tested on the breast (MCF7 and MDA-MB-231) and to confirm the results on colon cancer (LoVo) cell lines. The cell viability experiments showed that there are no statistically significant differences between free doxorubicin, STDO and LSTDO (Figure 20). These results are in line with previous publications[228] and supported by data obtained with liposomal doxorubicin which shown an advantage only in mouse models. Our group has previously demonstrated that doxorubicin encapsulated in exosomes, natural vesicles lined with a bilayer of phospholipids, are able to reduce cardiotoxicity increasing the therapeutic index of this drug only *in vivo*.

***In vivo* toxicity, antitumor efficacy and inflammatory response.** To establish the toxic effect of STDO and doxorubicin, mice were i.p. injected with 15 mg/kg of doxorubicin and the acute toxicity was followed for 12 days (Figure 21). The loss of body weight was monitored as an objective parameter of wellness. STDOdoxo showed a fast weight decrease in five days and the mice were sacrificed. LSTDOdoxo displayed the same profile of weight loss of free doxorubicin. Comparing with STDO, LSTDOdoxo was safer. To gain information on the reason of the observed toxicity, the tissues of mice were analyzed by histopathology. The only difference founded were on bone marrow of mice treated with STDOdoxo in which resulted in a decrease of blast cells.

The antitumor efficacy of LSTDO was tested on nude mice implanted with MDA-MB-231 cells orthotopically in the mammary fat pad. Mice were treated three times, once per week, with 3 mg/kg of doxo, STDOdoxo and LSTDOdoxo. Tumor growth and mice weight were followed. Mice treated with LSTDOdoxo showed a slower tumor growth compared to the other two groups with a statistical difference (p-value< 0.05) (Figure 22). To support our data, the concentration of the doxo was measured in the tumor (Figure 22). As demonstrated by biodistribution analysis LSTDO increases the quantity of doxorubicin in tumor compared to STDO and free drug probably taking advantage of the EPR effect. The increasing of antitumor efficacy by the three-stage vector is coupled by a decreasing in toxicity induced by the naked DNA. To support this thesis, we conducted an ELISA test on the plasma of FVB mice treated with the same amount of vector required for a 3 mg/kg doxorubicin treatment. Results showed that only the STDO induces the release of IL-6 displaying an increasing of inflammation compared to LSTDO and liposome (Figure 23). This result is in line with what demonstrate by Perrault et al[238] in their work where they describe that DNA origami induces less immune response if rounded by a phospholipids double layer; it is also aligned with a work published by Auvinen et al in 2017 in which they set up a new strategy to mask DNA origami nanostructure with albumin decreasing the inflammatory response *in vitro* tests[239].

7. Conclusions

DNA nanotechnology discipline is based on the unique and robust self-assembling properties of DNA through complementary base pair interactions, which allow the programmable design of DNA nanostructures with the required anticipated geometry and functional properties. The modulation of size, shape and charge of DNA nanostructures has been shown to overcome the natural cell membrane barrier allowing the delivery of naked DNA or siRNA that otherwise would not enter the cells. DNA nanostructures could be easily programmed to be a smart delivery system of different cargos. A limitation of low-dense DNA nanostructures is represented by many circulating enzymes such as DNAse that especially in tumour cells and tumour microenvironment are overrepresented and can degrade it quickly. The dense packaging of DNA helices within a DNA nanostructure is one strategy that could increase their stability against DNA-degrading enzymes. Another approach could be to encapsulate DNA structures under a sheet of biocompatible materials like membranes, which will protect them from unspecific degradation[238,255]. From a therapeutic point-of-view, considering the elimination and terminal clearance half-life of most chemotherapeutic drugs, the *in vivo* half-life of DNA-based nanostructures should be higher than 30 hours to enable their feasible clinical applications in drug delivery and formulation. For instance, the terminal clearance half-life of doxorubicin, which is among the most widely used chemotherapeutic agents, is around 30 hours[256].
Another advantage of DNA origami could be represented by the ability to actively release multiple drugs. In the more mature field of liposomes, many research groups are dedicating much effort to loading different drugs inside a single liposome, especially for cancer therapy. As compared to DNA origami, the charge, hydrophobicity and pKa of the drug represent an important limitation for the loading of the liposome. The presence of a huge number of modifiable oligonucleotides ideally represents an advantageous and easy way to load multiple drugs. Tweezer-like DNA nanodevices are able to control the activity of an external enzyme and represent an earlier system to be implemented to design a DNA nanomachine with intrinsic abilities to actively release drugs[257].
The above studies showed that DNA nanotechnology could provide an excellent designing tool for the construction of novel drug delivery vehicles possessing optimal biocompatibility along with high cellular uptake kinetics of drug-loaded DNA nanostructures. DNA nanotechnology enables tuning and optimization for their best performance *in vivo* and *in vitro* experiments by judiciously selecting the shape, size and functionalities of DNA nanostructures owing to the shape and size-dependent EPR effect. However, before *in vivo* applications of any perspective DNA nanostructure, a very careful and rigorous *in vitro* testing is required to avoid any misinterpretation or artefacts in the data[258]. In

addition, the cost of production, the yield and purification steps are still an obstacle. Many laboratories are working in this direction and some improvements were recently achieved[213,257,259].

In this work is demonstrated that DNA origami nanostructure could be utilized to build a valid three stage DDS based on an STDO loaded inside a stealth liposome in order to actively load doxorubicin inside. This DDS has been demonstrated to possess suitable properties for a preclinical application improving the beneficial effect of doxo through a passive accumulation in the tumor microenvironment also decreasing the side effect induced by the administration of exogenous DNA in immunocompetent animals.

The work described is the first step towards a new nanotechnology drug delivery era in which DNA nanostructure will cover a key-role.

Nevertheless, the research area of DNA nanotechnology for drug delivery is still in the initial stage and a breakthrough is still needed in DNA nanotechnology, that could pave the way for the development of smart functional DNA origami for biomedical applications and drug delivery, and in the long term find a way to be translated into clinics to improve the health of patients.

Bibliography

1. Practice & Guidelines | ASCO. Available at: https://www.asco.org/practice-guidelines. (Accessed: 16th November 2017)
2. Definition of first-line therapy - NCI Dictionary of Cancer Terms - National Cancer Institute. Available at: https://www.cancer.gov/publications/dictionaries/cancer-terms?cdrid=346494. (Accessed: 16th November 2017)
3. Wills, L., Clutterbuck, P. W. & Evans, B. D. A new factor in the production and cure of macrocytic anaemias and its relation to other haemopoietic principles curative in pernicious anaemia. *Biochem. J.* **31,** 2136–47 (1937).
4. Farber, S., Diamond, L. K., Mercer, R. D., Sylvester, R. F. & Wolff, J. A. Temporary Remissions in Acute Leukemia in Children Produced by Folic Acid Antagonist, 4-Aminopteroyl-Glutamic Acid (Aminopterin). *N. Engl. J. Med.* **238,** 787–793 (1948).
5. ELION, G. B., SINGER, S. & HITCHINGS, G. H. Antagonists of nucleic acid derivatives. VIII. Synergism in combinations of biochemically related antimetabolites. *J. Biol. Chem.* **208,** 477–88 (1954).
6. Hitchings, G. H. & Elion, G. B. THE CHEMISTRY AND BIOCHEMISTRY OF PURINE ANALOGS. *Ann. N. Y. Acad. Sci.* **60,** 195–199 (1954).
7. HEIDELBERGER, C. *et al.* Fluorinated Pyrimidines, A New Class of Tumour-Inhibitory Compounds. *Nature* **179,** 663–666 (1957).
8. GREENSPAN, E. M., FIEBER, M., LESNICK, G. & EDELMAN, S. Response of advanced breast carcinoma to the combination of the antimetabolite, Methotrexate, and the alkylating agent, thio-TEPA. *J. Mt. Sinai Hosp. N. Y.* **30,** 246–67
9. Canellos, G. P. *et al.* Cyclical combination chemotherapy for advanced breast carcinoma. *Br. Med. J.* **1,** 218–20 (1974).
10. Druker, B. J. *et al.* Effects of a selective inhibitor of the Abl tyrosine kinase on the growth of Bcr-Abl positive cells. *Nat. Med.* **2,** 561–6 (1996).
11. Druker, B. J. *et al.* Activity of a Specific Inhibitor of the BCR-ABL Tyrosine Kinase in the Blast Crisis of Chronic Myeloid Leukemia and Acute Lymphoblastic Leukemia with the Philadelphia Chromosome. *N. Engl. J. Med.* **344,** 1038–1042 (2001).
12. Manning, G., Whyte, D. B., Martinez, R., Hunter, T. & Sudarsanam, S. The Protein Kinase Complement of the Human Genome. *Science (80-.).* **298,** 1912–1934 (2002).
13. DeVita, V. T. On special initiatives, critics, and the National Cancer Program. *Cancer Treat. Rep.* **68,** 1–4 (1984).
14. Krause, D. S. & Van Etten, R. A. Tyrosine Kinases as Targets for Cancer Therapy. *N. Engl. J. Med.* **353,** 172–187 (2005).
15. Chabner, B. A. & Roberts, T. G. Timeline: Chemotherapy and the war on cancer. *Nat. Rev. Cancer* **5,** 65–72 (2005).
16. Floyd, J. D. *et al.* Cardiotoxicity of Cancer Therapy. *J. Clin. Oncol.* **23,** 7685–7696 (2005).
17. Minotti, G., Menna, P., Salvatorelli, E., Cairo, G. & Gianni, L. Anthracyclines: Molecular Advances and Pharmacologic Developments in Antitumor Activity and Cardiotoxicity. *Pharmacol. Rev.* **56,** 185–229 (2004).
18. Van Dyke, T. p53 and Tumor Suppression. *N. Engl. J. Med.* **356,** 79–81 (2007).
19. Shan, K., Lincoff, A. M. & Young, J. B. Anthracycline-induced cardiotoxicity. *Ann. Intern. Med.* **125,** 47–58 (1996).
20. Cavaliere, R. & Schiff, D. Neurologic toxicities of cancer therapies. *Curr. Neurol. Neurosci. Rep.* **6,** 218–26 (2006).
21. Wendling, L. R., Bleyer, W. A., Di Chiro, G. & McIlvanie, S. K. Transient, severe

periventricular hypodensity after leukemic prophylaxis with cranial irradiation and intrathecal methotrexate. *J. Comput. Assist. Tomogr.* **2,** 502–5 (1978).
22. Daniel, D. & Crawford, J. Myelotoxicity From Chemotherapy. *Semin. Oncol.* **33,** 74–85 (2006).
23. Sonis, S. T. *et al.* Perspectives on cancer therapy-induced mucosal injury. *Cancer* **100,** 1995–2025 (2004).
24. Pico, Avila-Garavito & Naccache. Mucositis: Its Occurrence, Consequences, and Treatment in the Oncology Setting. *Oncologist* **3,** 446–451 (1998).
25. Carr, C., Ng, J. & Wigmore, T. The side effects of chemotherapeutic agents. *Curr. Anaesth. Crit. Care* **19,** 70–79 (2008).
26. Ferlay, J. *et al.* Cancer incidence and mortality worldwide: sources, methods and major patterns in GLOBOCAN 2012. *Int. J. cancer* **136,** E359-86 (2015).
27. Sorlie, T. *et al.* Gene expression patterns of breast carcinomas distinguish tumor subclasses with clinical implications. *Proc. Natl. Acad. Sci.* **98,** 10869–10874 (2001).
28. Perou, C. M. *et al.* Molecular portraits of human breast tumours. *Nature* **406,** 747–752 (2000).
29. Kennecke, H. *et al.* Metastatic Behavior of Breast Cancer Subtypes. *J. Clin. Oncol.* **28,** 3271–3277 (2010).
30. Lund, M. J. *et al.* Age/race differences in HER2 testing and in incidence rates for breast cancer triple subtypes. *Cancer* **116,** NA-NA (2010).
31. Metzger-Filho, O. *et al.* Patterns of Recurrence and outcome according to breast cancer subtypes in lymph node-negative disease: results from international breast cancer study group trials VIII and IX. *J. Clin. Oncol.* **31,** 3083–90 (2013).
32. Carey, L. A. *et al.* Race, Breast Cancer Subtypes, and Survival in the Carolina Breast Cancer Study. *JAMA* **295,** 2492 (2006).
33. Bosch, A., Eroles, P., Zaragoza, R., Viña, J. R. & Lluch, A. Triple-negative breast cancer: Molecular features, pathogenesis, treatment and current lines of research. *Cancer Treat. Rev.* **36,** 206–215 (2010).
34. Herschkowitz, J. I. *et al.* Identification of conserved gene expression features between murine mammary carcinoma models and human breast tumors. *Genome Biol.* **8,** R76 (2007).
35. Webster, T. J. Nanomedicine: what's in a definition? *Int. J. Nanomedicine* **1,** 115–6 (2006).
36. Wagner, V., Dullaart, A., Bock, A.-K. & Zweck, A. The emerging nanomedicine landscape. *Nat. Biotechnol.* **24,** 1211–1217 (2006).
37. Bharali, D. J., Khalil, M., Gurbuz, M., Simone, T. M. & Mousa, S. A. Nanoparticles and cancer therapy: a concise review with emphasis on dendrimers. *Int. J. Nanomedicine* **4,** 1–7 (2009).
38. Svenson, S. Clinical translation of nanomedicines. *Curr. Opin. Solid State Mater. Sci.* **16,** 287–294 (2012).
39. Dianzani, C. *et al.* Drug delivery nanoparticles in skin cancers. *Biomed Res. Int.* **2014,** 895986 (2014).
40. Gaudana, R., Jwala, J., Boddu, S. H. S. & Mitra, A. K. Recent Perspectives in Ocular Drug Delivery. *Pharm. Res.* **26,** 1197–1216 (2009).
41. Brannon-Peppas, L. & Blanchette, J. O. Nanoparticle and targeted systems for cancer therapy. *Adv. Drug Deliv. Rev.* **56,** 1649–1659 (2004).
42. Ferrari, M. Frontiers in cancer nanomedicine: directing mass transport through biological barriers. *Trends Biotechnol.* **28,** 181–188 (2010).
43. Tasciotti, E. *et al.* Mesoporous silicon particles as a multistage delivery system for imaging and therapeutic applications. *Nat. Nanotechnol.* **3,** 151–157 (2008).
44. Tanaka, T. *et al.* Nanotechnology for breast cancer therapy. *Biomed. Microdevices* **11,** 49–63 (2009).
45. Etheridge, M. L. *et al.* The big picture on nanomedicine: the state of investigational and

approved nanomedicine products. *Nanomedicine* **9,** 1–14 (2013).
46. Hay, M., Thomas, D. W., Craighead, J. L., Economides, C. & Rosenthal, J. Clinical development success rates for investigational drugs. *Nat. Biotechnol.* **32,** 40–51 (2014).
47. Farokhzad, O. C. *et al.* Targeted nanoparticle-aptamer bioconjugates for cancer chemotherapy in vivo. *Proc. Natl. Acad. Sci. U. S. A.* **103,** 6315–20 (2006).
48. Wang, S. *et al.* Novel methods to incorporate photosensitizers into nanocarriers for cancer treatment by photodynamic therapy. *Lasers Surg. Med.* **43,** 686–695 (2011).
49. Elzoghby, A. O., Samy, W. M. & Elgindy, N. A. Albumin-based nanoparticles as potential controlled release drug delivery systems. *J. Control. Release* **157,** 168–182 (2012).
50. Choi, K. Y. *et al.* Self-assembled hyaluronic acid nanoparticles for active tumor targeting. *Biomaterials* **31,** 106–114 (2010).
51. Agnihotri, S. A., Mallikarjuna, N. N. & Aminabhavi, T. M. Recent advances on chitosan-based micro- and nanoparticles in drug delivery. *J. Control. Release* **100,** 5–28 (2004).
52. Panyam, J. & Labhasetwar, V. Biodegradable nanoparticles for drug and gene delivery to cells and tissue. *Adv. Drug Deliv. Rev.* **55,** 329–347 (2003).
53. Vauthier, C. & Bouchemal, K. Methods for the preparation and manufacture of polymeric nanoparticles. *Pharm. Res.* **26,** 1025–58 (2009).
54. Jain, R. A. The manufacturing techniques of various drug loaded biodegradable poly(lactide-co-glycolide) (PLGA) devices. *Biomaterials* **21,** 2475–2490 (2000).
55. Kumari, A., Yadav, S. K. & Yadav, S. C. Biodegradable polymeric nanoparticles based drug delivery systems. *Colloids Surfaces B Biointerfaces* **75,** 1–18 (2010).
56. Nair, L. S. & Laurencin, C. T. Biodegradable polymers as biomaterials. *Prog. Polym. Sci* **32,** 762–798 (2007).
57. Fasano, M. *et al.* The extraordinary ligand binding properties of human serum albumin. *IUBMB Life* **57,** 787–96 (2005).
58. Gong, J. *et al.* Synthesis, characterization, drug-loading capacity and safety of novel octyl modified serum albumin micelles. *Int. J. Pharm.* **376,** 161–168 (2009).
59. Ghosh, P. K. Hydrophilic polymeric nanoparticles as drug carriers. *Indi an J. Biochem. Biophys.* **37,** 273–282 (2000).
60. Kamaly, N., Xiao, Z., Valencia, P. M., Radovic-Moreno, A. F. & Farokhzad, O. C. Targeted polymeric therapeutic nanoparticles: design, development and clinical translation. *Chem. Soc. Rev.* **41,** 2971–3010 (2012).
61. Li, J., Stayshich, R. M. & Meyer, T. Y. Exploiting sequence to control the hydrolysis behavior of biodegradable PLGA copolymers. *J. Am. Chem. Soc.* **133,** 6910–3 (2011).
62. Bertin, A. Emergence of Polymer Stereocomplexes for Biomedical Applications. *Macromol. Chem. Phys.* **213,** 2329–2352 (2012).
63. Rancan, F. *et al.* Investigation of polylactic acid (PLA) nanoparticles as drug delivery systems for local dermatotherapy. *Pharm. Res.* **26,** 2027–36 (2009).
64. Karavelidis, V., Karavas, E., Giliopoulos, D., Papadimitriou, S. & Bikiaris, D. Evaluating the effects of crystallinity in new biocompatible polyester nanocarriers on drug release behavior. *Int. J. Nanomedicine* **6,** 3021–32 (2011).
65. Danhier, F. *et al.* PLGA-based nanoparticles: An overview of biomedical applications. *J. Control. Release* **161,** 505–522 (2012).
66. Makadia, H. K. & Siegel, S. J. Poly Lactic-co-Glycolic Acid (PLGA) as Biodegradable Controlled Drug Delivery Carrier. *Polymers (Basel).* **3,** 1377–1397 (2011).
67. Amann, L. C., Gandal, M. J., Lin, R., Liang, Y. & Siegel, S. J. In vitro-in vivo correlations of scalable PLGA-risperidone implants for the treatment of schizophrenia. *Pharm. Res.* **27,** 1730–7 (2010).
68. Faisant, N., Siepmann, J. & Benoit, J. P. PLGA-based microparticles: elucidation of mechanisms and a new, simple mathematical model quantifying drug release. *Eur. J. Pharm. Sci.* **15,** 355–366 (2002).

69. Ramchandani, M. & Robinson, D. In vitro and in vivo release of ciprofloxacin from PLGA 50:50 implants. *J. Control. release* **54,** 167–175 (1998).
70. Becker, R., Dembek, C., White, L. A. & Garrison, L. P. The cost offsets and cost–effectiveness associated with pegylated drugs: a review of the literature. *Expert Rev. Pharmacoecon. Outcomes Res.* **12,** 775–793 (2012).
71. Kommareddy, S., Tiwari, S. B. & Amiji, M. M. Long-circulating polymeric nanovectors for tumor-selective gene delivery. *Technol. Cancer Res. Treat.* **4,** 615–25 (2005).
72. Esmaeili, F. *et al.* PLGA nanoparticles of different surface properties: Preparation and evaluation of their body distribution. *Int. J. Pharm.* **349,** 249–255 (2008).
73. Wani, M. C., Taylor, H. L., Wall, M. E., Coggon, P. & McPhail, A. T. Plant antitumor agents. VI. Isolation and structure of taxol, a novel antileukemic and antitumor agent from Taxus brevifolia. *J. Am. Chem. Soc.* **93,** 2325–2327 (1971).
74. Rowinsky, E. K. & Donehower, R. C. Paclitaxel (taxol). *N. Engl. J. Med.* **332,** 1004–14 (1995).
75. Paál, K., Müller, J. & Hegedûs, L. High affinity binding of paclitaxel to human serum albumin. *Eur. J. Biochem.* **268,** 2187–2191 (2001).
76. Hawkins, M. J., Soon-Shiong, P. & Desai, N. Protein nanoparticles as drug carriers in clinical medicine. *Adv. Drug Deliv. Rev.* **60,** 876–85 (2008).
77. Purcell, M., Neault, J. F. & Tajmir-Riahi, H. A. Interaction of taxol with human serum albumin. *Biochim. Biophys. Acta - Protein Struct. Mol. Enzymol.* **1478,** 61–68 (2000).
78. John, T. A., Vogel, S. M., Tiruppathi, C., Malik, A. B. & Minshall, R. D. Quantitative analysis of albumin uptake and transport in the rat microvessel endothelial monolayer. *Am. J. Physiol. Lung Cell. Mol. Physiol.* **284,** L187-96 (2003).
79. Desai, N. Increased Antitumor Activity, Intratumor Paclitaxel Concentrations, and Endothelial Cell Transport of Cremophor-Free, Albumin-Bound Paclitaxel, ABI-007, Compared with Cremophor-Based Paclitaxel. *Clin. Cancer Res.* **12,** 1317–1324 (2006).
80. Palazzolo, S. *et al.* The Clinical translation of Organic Nanomaterials for Cancer Therapy: A Focus on Polymeric Nanoparticles, Micelles, Liposomes and Exosomes. *Curr. Med. Chem.* **24,** (2017).
81. Miele, E., Spinelli, G. P., Miele, E., Tomao, F. & Tomao, S. Albumin-bound formulation of paclitaxel (Abraxane ABI-007) in the treatment of breast cancer. *Int. J. Nanomedicine* **4,** 99–105 (2009).
82. Yardley, D. A. Nab-Paclitaxel mechanisms of action and delivery. *J. Control. Release* **170,** 365–372 (2013).
83. Abraxane Approval.
84. Paclitaxel (Abraxane). Available at: http://www.fda.gov/drugs/informationondrugs/approveddrugs/ucm323668.htm. (Accessed: 21st June 2016)
85. FDA approves Abraxane for late-stage pancreatic cancer.
86. Gentzler, R. D. *et al.* Carboplatin/ nab -Paclitaxel and Pembrolizumab for Patients with Advanced Non–Small Cell Lung Cancer (NSCLC): Phase 1 Results. *Int. J. Radiat. Oncol.* **98,** 236 (2017).
87. Ho, C. *et al.* Phase I/II trial of pemetrexed plus nab-paclitaxel in advanced solid tumor patients with emphasis on non-small cell lung cancer. *Invest. New Drugs* **31,** 1587–1591 (2013).
88. Arleth, L. *et al.* Detailed structure of hairy mixed micelles formed by phosphatidylcholine and PEGylated phospholipids in aqueous media. *Langmuir* **21,** 3279–90 (2005).
89. Holmberg, K., Jönsson, B., Kronberg, B. & Lindman, B. SURFACTANTS AND POLYMERS IN AQUEOUS SOLUTION.
90. Feng, L. & Mumper, R. J. A critical review of lipid-based nanoparticles for taxane delivery. *Cancer Lett.* **334,** 157–175 (2013).

91. Adams, M. L., Lavasanifar, A. & Kwon, G. S. Amphiphilic block copolymers for drug delivery. *J. Pharm. Sci.* **92,** 1343–1355 (2003).
92. Rösler, A., Vandermeulen, G. W. . & Klok, H.-A. Advanced drug delivery devices via self-assembly of amphiphilic block copolymers. *Adv. Drug Deliv. Rev.* **53,** 95–108 (2001).
93. Veronese, F. M. *et al.* PEG-doxorubicin conjugates: influence of polymer structure on drug release, in vitro cytotoxicity, biodistribution, and antitumor activity. *Bioconjug. Chem.* **16,** 775–84
94. Lalatsa, A., Schätzlein, A. G., Mazza, M., Le, T. B. H. & Uchegbu, I. F. Amphiphilic poly(l-amino acids) — New materials for drug delivery. *J. Control. Release* **161,** 523–536 (2012).
95. Lim, E.-K. *et al.* pH-Triggered Drug-Releasing Magnetic Nanoparticles for Cancer Therapy Guided by Molecular Imaging by MRI. *Adv. Mater.* **23,** 2436–2442 (2011).
96. Kim, S. C. *et al.* In vivo evaluation of polymeric micellar paclitaxel formulation: Toxicity and efficacy. *J. Control. Release* **72,** 191–202 (2001).
97. Zamboni, W. C. Liposomal, nanoparticle, and conjugated formulations of anticancer agents. *Clin. Cancer Res.* **11,** 8230–4 (2005).
98. BANGHAM, A. D. & HORNE, R. W. NEGATIVE STAINING OF PHOSPHOLIPIDS AND THEIR STRUCTURAL MODIFICATION BY SURFACE-ACTIVE AGENTS AS OBSERVED IN THE ELECTRON MICROSCOPE. *J. Mol. Biol.* **8,** 660–8 (1964).
99. Barenholz, Y. Liposome application: problems and prospects. *Curr. Opin. Colloid Interface Sci.* **6,** 66–77 (2001).
100. Torchilin, V. P. Recent advances with liposomes as pharmaceutical carriers. *Nat. Rev. Drug Discov.* **4,** 145–60 (2005).
101. Huang, L. & Liu, Y. In vivo delivery of RNAi with lipid-based nanoparticles. *Annu. Rev. Biomed. Eng.* **13,** 507–30 (2011).
102. Jesorka, A. & Orwar, O. Liposomes: technologies and analytical applications. *Annu. Rev. Anal. Chem. (Palo Alto. Calif).* **1,** 801–32 (2008).
103. Irache, J. M., Esparza, I., Gamazo, C., Agüeros, M. & Espuelas, S. Nanomedicine: Novel approaches in human and veterinary therapeutics. *Vet. Parasitol.* **180,** 47–71 (2011).
104. Gregoriadis, G. The carrier potential of liposomes in biology and medicine (first of two parts). *N. Engl. J. Med.* **295,** 704–10 (1976).
105. Allen, T. M. & Cullis, P. R. Liposomal drug delivery systems: from concept to clinical applications. *Adv. Drug Deliv. Rev.* **65,** 36–48 (2013).
106. Allen, T. M., Cheng, W. W. K., Hare, J. I. & Laginha, K. M. Pharmacokinetics and pharmacodynamics of lipidic nano-particles in cancer. *Anticancer. Agents Med. Chem.* **6,** 513–23 (2006).
107. Barenholz, Y. Doxil?? - The first FDA-approved nano-drug: Lessons learned. *J. Control. Release* **160,** 117–134 (2012).
108. Min, Y., Caster, J. M., Eblan, M. J. & Wang, A. Z. Clinical Translation of Nanomedicine. *Chem. Rev.* **115,** 11147–11190 (2015).
109. Gabizon, A. *et al.* Prolonged circulation time and enhanced accumulation in malignant exudates of doxorubicin encapsulated in polyethylene-glycol coated liposomes. *Cancer Res.* **54,** 987–92 (1994).
110. Simons, M. & Raposo, G. Exosomes – vesicular carriers for intercellular communication. *Curr. Opin. Cell Biol.* **21,** 575–581 (2009).
111. Stoorvogel, W., Kleijmeer, M. J., Geuze, H. J. & Raposo, G. The biogenesis and functions of exosomes. *Traffic* **3,** 321–30 (2002).
112. Nieuwland, R. & Sturk, A. Why do cells release vesicles? *Thromb. Res.* **125,** S49–S51 (2010).
113. Zhou, Q. *et al.* Immune-related microRNAs are abundant in breast milk exosomes. *Int. J. Biol. Sci.* **8,** 118–23 (2012).
114. Street, J. M. *et al.* Identification and proteomic profiling of exosomes in human cerebrospinal

fluid. *J. Transl. Med.* **10,** 5 (2012).
115. Qazi, K. R. *et al.* Proinflammatory exosomes in bronchoalveolar lavage fluid of patients with sarcoidosis. *Thorax* **65,** 1016–24 (2010).
116. Lässer, C. *et al.* Human saliva, plasma and breast milk exosomes contain RNA: uptake by macrophages. *J. Transl. Med.* **9,** 9 (2011).
117. Keller, S., Ridinger, J., Rupp, A.-K., Janssen, J. W. G. & Altevogt, P. Body fluid derived exosomes as a novel template for clinical diagnostics. *J. Transl. Med.* **9,** 86 (2011).
118. Gallo, A., Tandon, M., Alevizos, I. & Illei, G. G. The majority of microRNAs detectable in serum and saliva is concentrated in exosomes. *PLoS One* **7,** e30679 (2012).
119. Dimov, I., Jankovic Velickovic, L. & Stefanovic, V. Urinary exosomes. *ScientificWorldJournal.* **9,** 1107–18 (2009).
120. Bard, M. P. *et al.* Proteomic analysis of exosomes isolated from human malignant pleural effusions. *Am. J. Respir. Cell Mol. Biol.* **31,** 114–21 (2004).
121. Admyre, C. *et al.* Exosomes - nanovesicles with possible roles in allergic inflammation. *Allergy* **63,** 404–8 (2008).
122. Little, K. M., Smalley, D. M., Harthun, N. L. & Ley, K. The plasma microparticle proteome. *Semin. Thromb. Hemost.* **36,** 845–56 (2010).
123. Vidal, M. Exosomes in erythropoiesis. *Transfus. Clin. Biol.* **17,** 131–137 (2010).
124. Vicencio, J. M. *et al.* Plasma Exosomes Protect the Myocardium From Ischemia-Reperfusion Injury. *J. Am. Coll. Cardiol.* **65,** 1525–1536 (2015).
125. Sahoo, S. & Losordo, D. W. Exosomes and cardiac repair after myocardial infarction. *Circ. Res.* **114,** 333–44 (2014).
126. Kumar, S. Bone defect repair in mice by mesenchymal stem cells. *Methods Mol. Biol.* **1213,** 193–207 (2014).
127. Arntz, O. J. *et al.* Oral administration of bovine milk derived extracellular vesicles attenuates arthritis in two mouse models. *Mol. Nutr. Food Res.* **59,** 1701–12 (2015).
128. Ching, R. C. & Kingham, P. J. The role of exosomes in peripheral nerve regeneration. *Neural Regen. Res.* **10,** 743–7 (2015).
129. Sáenz-Cuesta, M., Osorio-Querejeta, I. & Otaegui, D. Extracellular Vesicles in Multiple Sclerosis: What are They Telling Us? *Front. Cell. Neurosci.* **8,** 100 (2014).
130. Haney, M. J. *et al.* Exosomes as drug delivery vehicles for Parkinson's disease therapy. *J. Control. Release* **207,** 18–30 (2015).
131. Kreimer, S. *et al.* Mass-spectrometry-based molecular characterization of extracellular vesicles: lipidomics and proteomics. *J. Proteome Res.* **14,** 2367–84 (2015).
132. Zarovni, N. *et al.* Integrated isolation and quantitative analysis of exosome shuttled proteins and nucleic acids using immunocapture approaches. *Methods* **87,** 46–58 (2015).
133. EL Andaloussi, S., Mäger, I., Breakefield, X. O. & Wood, M. J. A. Extracellular vesicles: biology and emerging therapeutic opportunities. *Nat. Rev. Drug Discov.* **12,** 347–57 (2013).
134. Zhuang, X. *et al.* Treatment of brain inflammatory diseases by delivering exosome encapsulated anti-inflammatory drugs from the nasal region to the brain. *Mol. Ther.* **19,** 1769–79 (2011).
135. Wang, Q. *et al.* Delivery of therapeutic agents by nanoparticles made of grapefruit-derived lipids. *Nat. Commun.* **4,** 1867 (2013).
136. Mu, J. *et al.* Interspecies communication between plant and mouse gut host cells through edible plant derived exosome-like nanoparticles. *Mol. Nutr. Food Res.* **58,** 1561–73 (2014).
137. Huang, H.-C., Barua, S., Sharma, G., Dey, S. K. & Rege, K. Inorganic nanoparticles for cancer imaging and therapy. *J. Control. Release* **155,** 344–357 (2011).
138. Tang, F., Li, L. & Chen, D. Mesoporous Silica Nanoparticles: Synthesis, Biocompatibility and Drug Delivery. *Adv. Mater.* **24,** 1504–1534 (2012).
139. Giljohann, D. A. *et al.* Gold nanoparticles for biology and medicine. *Angew. Chem. Int. Ed. Engl.* **49,** 3280–3294 (2010).

140. McCarthy, J. R. & Weissleder, R. Multifunctional magnetic nanoparticles for targeted imaging and therapy. *Adv. Drug Deliv. Rev.* **60,** 1241–1251 (2008).
141. Eustis, S. & El-Sayed, M. A. Why gold nanoparticles are more precious than pretty gold: noble metal surface plasmon resonance and its enhancement of the radiative and nonradiative properties of nanocrystals of different shapes. *Chem. Soc. Rev.* **35,** 209–217 (2006).
142. Iwaki, M., Iwane, A. H., Ikezaki, K. & Yanagida, T. Local heat activation of single myosins based on optical trapping of gold nanoparticles. *Nano Lett.* **15,** 2456–2461 (2015).
143. Daniel, M.-C. & Astruc, D. Gold nanoparticles: assembly, supramolecular chemistry, quantum-size-related properties, and applications toward biology, catalysis, and nanotechnology. *Chem. Rev.* **104,** 293–346 (2004).
144. Estelrich, J., Sánchez-Martín, M. J. & Busquets, M. A. Nanoparticles in magnetic resonance imaging: from simple to dual contrast agents. *Int. J. Nanomedicine* **10,** 1727–1741 (2015).
145. Na, H. Bin, Song, I. C. & Hyeon, T. Inorganic Nanoparticles for MRI Contrast Agents. *Adv. Mater.* **21,** 2133–2148 (2009).
146. Timko, B. P. & Kohane, D. S. Prospects for near-infrared technology in remotely triggered drug delivery. *Expert Opin. Drug Deliv.* **11,** 1681–1685 (2014).
147. Abdalla, M. O. *et al.* Enhanced noscapine delivery using uPAR-targeted optical-MR imaging trackable nanoparticles for prostate cancer therapy. *J. Control. Release* **149,** 314–322 (2011).
148. Cole, A. J., Yang, V. C. & David, A. E. Cancer theranostics: the rise of targeted magnetic nanoparticles. *Trends Biotechnol.* **29,** 323–332 (2011).
149. Shubayev, V. I., Pisanic, T. R. & Jin, S. Magnetic nanoparticles for theragnostics. *Adv. Drug Deliv. Rev.* **61,** 467–477 (2009).
150. Winnik, F. M. & Maysinger, D. Quantum dot cytotoxicity and ways to reduce it. *Acc. Chem. Res.* **46,** 672–680 (2013).
151. Gao, X., Cui, Y., Levenson, R. M., Chung, L. W. K. & Nie, S. In vivo cancer targeting and imaging with semiconductor quantum dots. *Nat. Biotechnol.* **22,** 969–976 (2004).
152. Choi, H. S. & Frangioni, J. V. Nanoparticles for biomedical imaging: Fundamentals of clinical translation. *Mol. Imaging* **9,** 291–310 (2010).
153. Naahidi, S. *et al.* Biocompatibility of engineered nanoparticles for drug delivery. *J. Control. Release* **166,** 182–194 (2013).
154. Hilderbrand, S. A. & Weissleder, R. Near-infrared fluorescence: application to in vivo molecular imaging. *Curr. Opin. Chem. Biol.* **14,** 71–79 (2010).
155. He, X., Gao, J., Gambhir, S. S. & Cheng, Z. Near-infrared fluorescent nanoprobes for cancer molecular imaging: status and challenges. *Trends Mol. Med.* **16,** 574–583 (2010).
156. Ye, L. *et al.* A pilot study in non-human primates shows no adverse response to intravenous injection of quantum dots. *Nat. Nanotechnol.* **7,** 453–458 (2012).
157. Su, Y. *et al.* In vivo distribution, pharmacokinetics, and toxicity of aqueous synthesized cadmium-containing quantum dots. *Biomaterials* **32,** 5855–5862 (2011).
158. Liu, Y.-S. *et al.* pH-sensitive Photoluminescence of CdSe/ZnSe/ZnS Quantum Dots in Human Ovarian Cancer Cells. *J. Phys. Chem. C. Nanomater. Interfaces* **111,** 2872–2878 (2007).
159. Loginova, Y. F. *et al.* Biodistribution and stability of CdSe core quantum dots in mouse digestive tract following per os administration: advantages of double polymer/silica coated nanocrystals. *Biochem. Biophys. Res. Commun.* **419,** 54–59 (2012).
160. Lee, C.-M. *et al.* Surface engineering of quantum dots for in vivo imaging. *Nanotechnology* **21,** 285102 (2010).
161. Bayda, S. *et al.* Inorganic Nanoparticles for Cancer Therapy: a Transition from Lab to Clinic. *Curr. Med. Chem.* **25,** (2017).
162. Libutti, S. K. *et al.* Phase I and pharmacokinetic studies of CYT-6091, a novel PEGylated colloidal gold-rhTNF nanomedicine. *Clin. Cancer Res.* **16,** 6139–6149 (2010).
163. CytImmune Company.

164. Nanospectra Biosciences Company.
165. AuroLase® Therapy.
166. Pillai, G. Nanomedicines for Cancer Therapy : An Update of FDA Approved and Those under Various Stages of Development. *SOJ Pharm Pharm Sci* **1,** 1–13 (2014).
167. Marill, J. *et al.* Hafnium oxide nanoparticles: toward an in vitro predictive biological effect? *Radiat. Oncol.* **9,** 150 (2014).
168. Rivera Gil, P., Hühn, D., del Mercato, L. L., Sasse, D. & Parak, W. J. Nanopharmacy: Inorganic nanoscale devices as vectors and active compounds. *Pharmacol. Res.* **62,** 115–125 (2010).
169. Bregoli, L. *et al.* Nanomedicine applied to translational oncology: A future perspective on cancer treatment. *Nanomedicine* **12,** 81–103 (2016).
170. Clinical treatment with NanoTherm™ therapy.
171. Liu, B., Leontis, N. B. & Seeman, N. *Nanobiology : journal of research on nanoscale living systems. NANOBIOLOGY* **3,** (Carfax Pub. Co, 1994).
172. Macfarlane, R. J., O'Brien, M. N., Petrosko, S. H. & Mirkin, C. A. Nucleic acid-modified nanostructures as programmable atom equivalents: forging a new "table of elements". *Angew. Chem. Int. Ed. Engl.* **52,** 5688–98 (2013).
173. Aldaye, F. A., Palmer, A. L. & Sleiman, H. F. Assembling materials with DNA as the guide. *Science* **321,** 1795–9 (2008).
174. Li, J., Fan, C., Pei, H., Shi, J. & Huang, Q. Smart Drug Delivery Nanocarriers with Self-Assembled DNA Nanostructures. *Adv. Mater.* **25,** 4386–4396 (2013).
175. Chao, J. *et al.* Structural DNA nanotechnology for intelligent drug delivery. *Small* **10,** 4626–35 (2014).
176. Zhang, F., Nangreave, J., Liu, Y. & Yan, H. Structural DNA nanotechnology: state of the art and future perspective. *J. Am. Chem. Soc.* **136,** 11198–211 (2014).
177. Niemeyer, C. M. Self-assembled nanostructures based on DNA: towards the development of nanobiotechnology. *Curr. Opin. Chem. Biol.* **4,** 609–18 (2000).
178. Protozanova, E., Yakovchuk, P. & Frank-Kamenetskii, M. D. Stacked–Unstacked Equilibrium at the Nick Site of DNA. *J. Mol. Biol.* **342,** 775–785 (2004).
179. Seeman, N. C. DNA in a material world. *Nature* **421,** 427–31 (2003).
180. Seeman, N. C. Nanomaterials Based on DNA. *Annu. Rev. Biochem.* **79,** 65–87 (2010).
181. Thomas H. LaBean, † *et al.* Construction, Analysis, Ligation, and Self-Assembly of DNA Triple Crossover Complexes. (2000). doi:10.1021/JA993393E
182. Sa-Ardyen, P., Vologodskii, A. V. & Seeman, N. C. The Flexibility of DNA Double Crossover Molecules. *Biophys. J.* **84,** 3829–3837 (2003).
183. Mathieu, F. *et al.* Six-Helix Bundles Designed from DNA. *Nano Lett.* **5,** 661–665 (2005).
184. Wang, T., Schiffels, D., Cuesta, S. M., Fygenson, D. K. & Seeman, N. C. Design and characterization of 1D nanotubes and 2D periodic arrays self-assembled from DNA multi-helix bundles. *J. Am. Chem. Soc.* **134,** 1606–16 (2012).
185. Winfree, E., Liu, F., Wenzler, L. A. & Seeman, N. C. Design and self-assembly of two-dimensional DNA crystals. *Nature* **394,** 539–44 (1998).
186. and, W. B. S. & Seeman*, N. C. A Precisely Controlled DNA Biped Walking Device. (2004). doi:10.1021/NL049527Q
187. Yurke, B., Turberfield, A. J., Mills, A. P., Simmel, F. C. & Neumann, J. L. A DNA-fuelled molecular machine made of DNA. *Nature* **406,** 605–8 (2000).
188. Yan, H., Zhang, X., Shen, Z. & Seeman, N. C. A robust DNA mechanical device controlled by hybridization topology. *Nature* **415,** 62–5 (2002).
189. Gu, H., Chao, J., Xiao, S.-J. & Seeman, N. C. A proximity-based programmable DNA nanoscale assembly line. *Nature* **465,** 202–5 (2010).
190. Chengde Mao, Weiqiong Sun, and & Seeman*, N. C. Designed Two-Dimensional DNA Holliday Junction Arrays Visualized by Atomic Force Microscopy. (1999).

doi:10.1021/JA9900398
191. Yan, H., Park, S. H., Finkelstein, G., Reif, J. H. & LaBean, T. H. DNA-templated self-assembly of protein arrays and highly conductive nanowires. *Science* **301,** 1882–4 (2003).
192. Zhang, J., Liu, Y., Ke, Y. & Yan, H. Periodic square-like gold nanoparticle arrays templated by self-assembled 2D DNA Nanogrids on a surface. *Nano Lett.* **6,** 248–51 (2006).
193. Liu, D., Wang, M., Deng, Z., Walulu, R. & Mao, C. Tensegrity: construction of rigid DNA triangles with flexible four-arm DNA junctions. *J. Am. Chem. Soc.* **126,** 2324–5 (2004).
194. Zheng, J. *et al.* Two-dimensional nanoparticle arrays show the organizational power of robust DNA motifs. *Nano Lett.* **6,** 1502–4 (2006).
195. He, Y. *et al.* Hierarchical self-assembly of DNA into symmetric supramolecular polyhedra. *Nature* **452,** 198–201 (2008).
196. Wei, B., Dai, M. & Yin, P. Complex shapes self-assembled from single-stranded DNA tiles. *Nature* **485,** 623–6 (2012).
197. Ke, Y., Ong, L. L., Shih, W. M. & Yin, P. Three-dimensional structures self-assembled from DNA bricks. *Science* **338,** 1177–83 (2012).
198. Seeman, N. C. Nucleic acid junctions and lattices. *J. Theor. Biol.* **99,** 237–247 (1982).
199. Andersen, E. S. *et al.* Self-assembly of a nanoscale DNA box with a controllable lid. *Nature* **459,** 73–76 (2009).
200. Han, D. *et al.* DNA Gridiron Nanostructures Based on Four-Arm Junctions. *Science (80-.).* **339,** 1412–1415 (2013).
201. Benson, E. *et al.* DNA rendering of polyhedral meshes at the nanoscale. *Nature* **523,** 441–444 (2015).
202. Han, D. *et al.* DNA Origami with Complex Curvatures in Three-Dimensional Space. *Science (80-.).* **332,** 342–346 (2011).
203. Rothemund, P. W. K. Folding DNA to create nanoscale shapes and patterns. *Nature* **440,** 297–302 (2006).
204. Douglas, S. M. *et al.* Rapid prototyping of 3D DNA-origami shapes with caDNAno. *Nucleic Acids Res.* **37,** 5001–5006 (2009).
205. Castro, C. E. *et al.* A primer to scaffolded DNA origami. *Nat. Methods* **8,** 221–229 (2011).
206. Ducani, C., Kaul, C., Moche, M., Shih, W. M. & Högberg, B. Enzymatic production of 'monoclonal stoichiometric' single-stranded DNA oligonucleotides. *Nat. Methods* **10,** 647–52 (2013).
207. Yang, Y., Han, D., Nangreave, J., Liu, Y. & Yan, H. DNA Origami with Double-Stranded DNA As a Unified Scaffold. *ACS Nano* **6,** 8209–8215 (2012).
208. Bellot, G., McClintock, M. A., Lin, C. & Shih, W. M. Recovery of intact DNA nanostructures after agarose gel–based separation. *Nat. Methods* **8,** 192–194 (2011).
209. Stahl, E., Martin, T. G., Praetorius, F. & Dietz, H. Facile and Scalable Preparation of Pure and Dense DNA Origami Solutions. *Angew. Chemie Int. Ed.* **53,** 12735–12740 (2014).
210. Douglas, S. M. *et al.* Self-assembly of DNA into nanoscale three-dimensional shapes. *Nature* **459,** 414–418 (2009).
211. Alloyeau, D. *et al.* Direct imaging and chemical analysis of unstained DNA origami performed with a transmission electron microscope. *Chem. Commun.* **47,** 9375 (2011).
212. Douglas, S. M., Bachelet, I. & Church, G. M. A logic-gated nanorobot for targeted transport of molecular payloads. *Science* **335,** 831–4 (2012).
213. Sobczak, J.-P. J., Martin, T. G., Gerling, T. & Dietz, H. Rapid folding of DNA into nanoscale shapes at constant temperature. *Science* **338,** 1458–61 (2012).
214. Zhang, C. *et al.* Conformational flexibility facilitates self-assembly of complex DNA nanostructures. *Proc. Natl. Acad. Sci. U. S. A.* **105,** 10665–9 (2008).
215. Rothemund, P. W. K. *et al.* Design and Characterization of Programmable DNA Nanotubes. *J. Am. Chem. Soc.* **126,** 16344–16352 (2004).
216. Liu, D., Park, S. H., Reif, J. H. & LaBean, T. H. DNA nanotubes self-assembled from triple-

crossover tiles as templates for conductive nanowires. *Proc. Natl. Acad. Sci. U. S. A.* **101,** 717–22 (2004).
217. Walsh, A. S., Yin, H., Erben, C. M., Wood, M. J. A. & Turberfield, A. J. DNA Cage Delivery to Mammalian Cells. *ACS Nano* **5,** 5427–5432 (2011).
218. Li, J. *et al.* Self-Assembled Multivalent DNA Nanostructures for Noninvasive Intracellular Delivery of Immunostimulatory CpG Oligonucleotides. *ACS Nano* **5,** 8783–8789 (2011).
219. Kim, K.-R. *et al.* Drug delivery by a self-assembled DNA tetrahedron for overcoming drug resistance in breast cancer cells. *Chem. Commun. (Camb).* **49,** 2010–2 (2013).
220. Chang, M., Yang, C.-S. & Huang, D.-M. Aptamer-Conjugated DNA Icosahedral Nanoparticles As a Carrier of Doxorubicin for Cancer Therapy. *ACS Nano* **5,** 6156–6163 (2011).
221. Liu, X. *et al.* A DNA nanostructure platform for directed assembly of synthetic vaccines. *Nano Lett.* **12,** 4254–9 (2012).
222. Zhu, G. *et al.* Self-assembled, aptamer-tethered DNA nanotrains for targeted transport of molecular drugs in cancer theranostics. *Proc. Natl. Acad. Sci. U. S. A.* **110,** 7998–8003 (2013).
223. Kumar, V. *et al.* Enhanced Chemotherapeutic Behavior of Open-Caged DNA@Doxorubicin Nanostructures for Cancer Cells. *J. Cell. Physiol.* **231,** 106–10 (2016).
224. Mei, Q. *et al.* Stability of DNA Origami Nanoarrays in Cell Lysate. *Nano Lett.* **11,** 1477–1482 (2011).
225. Zhao, Y.-X. *et al.* DNA origami delivery system for cancer therapy with tunable release properties. *ACS Nano* **6,** 8684–91 (2012).
226. Schüller, V. J. *et al.* Cellular immunostimulation by CpG-sequence-coated DNA origami structures. *ACS Nano* **5,** 9696–702 (2011).
227. Ding, B., Seeman, N. C., Zhang, D. Y. & Winfree, E. Operation of a DNA Robot Arm Inserted into a 2D DNA Crystalline Substrate. *Science (80-.).* **314,** 1583–1585 (2006).
228. Jiang, Q. *et al.* DNA origami as a carrier for circumvention of drug resistance. *J. Am. Chem. Soc.* **134,** 13396–403 (2012).
229. Zhang, Q. *et al.* DNA origami as an in vivo drug delivery vehicle for cancer therapy. *ACS Nano* **8,** 6633–43 (2014).
230. Tam, D. Y. & Lo, P. K. Multifunctional DNA Nanomaterials for Biomedical Applications. *J. Nanomater.* **2015,** 1–21 (2015).
231. Srinivasan, C. *et al.* Labeling and Intracellular Tracking of Functionally Active Plasmid DNA with Semiconductor Quantum Dots. *Mol. Ther.* **14,** 192–201 (2006).
232. Levy, M., Cater, S. F. & Ellington, A. D. Quantum-Dot Aptamer Beacons for the Detection of Proteins. *ChemBioChem* **6,** 2163–2166 (2005).
233. And, G. W. & Murray*, R. W. Controlled Assembly of Monolayer-Protected Gold Clusters by Dissolved DNA. (2003). doi:10.1021/NL034922M
234. Pellegrino, T., Sperling, R. A., Alivisatos, A. P. & Parak, W. J. Gel electrophoresis of gold-DNA nanoconjugates. *J. Biomed. Biotechnol.* **2007,** 26796 (2007).
235. Paludan, S. R. *et al.* Immune sensing of DNA. *Immunity* **38,** 870–80 (2013).
236. TAMKOVICH, S. N. *et al.* Circulating DNA and DNase Activity in Human Blood. *Ann. N. Y. Acad. Sci.* **1075,** 191–196 (2006).
237. Keum, J.-W. & Bermudez, H. Enhanced resistance of DNA nanostructures to enzymatic digestion. *Chem. Commun. (Camb).* 7036–8 (2009). doi:10.1039/b917661f
238. Perrault, S. D. & Shih, W. M. Virus-inspired membrane encapsulation of DNA nanostructures to achieve in vivo stability. *ACS Nano* **8,** 5132–40 (2014).
239. Auvinen, H. *et al.* Protein Coating of DNA Nanostructures for Enhanced Stability and Immunocompatibility. *Adv. Healthc. Mater.* 1700692 (2017). doi:10.1002/adhm.201700692
240. Kumar, V. *et al.* DNA Nanotechnology for Cancer Therapy. *Theranostics* **6,** 710–25 (2016).
241. Johnston, M. J. W. *et al.* Characterization of the drug retention and pharmacokinetic

properties of liposomal nanoparticles containing dihydrosphingomyelin. *Biochim. Biophys. Acta - Biomembr.* **1768,** 1121–1127 (2007).
242. Hofheinz, R.-D., Gnad-Vogt, S. U., Beyer, U. & Hochhaus, A. Liposomal encapsulated anti-cancer drugs. *Anticancer. Drugs* **16,** 691–707 (2005).
243. Omri, A., Suntres, Z. E. & Shek, P. N. Enhanced activity of liposomal polymyxin B against Pseudomonas aeruginosa in a rat model of lung infection. *Biochem. Pharmacol.* **64,** 1407–13 (2002).
244. Immordino, M. L., Dosio, F. & Cattel, L. Stealth liposomes: review of the basic science, rationale, and clinical applications, existing and potential. *Int. J. Nanomedicine* **1,** 297–315 (2006).
245. Saccà, B. & Niemeyer, C. M. DNA origami: the art of folding DNA. *Angew. Chem. Int. Ed. Engl.* **51,** 58–66 (2012).
246. Wang, S. *et al.* Doxorubicin Induces Apoptosis in Normal and Tumor Cells via Distinctly Different Mechanisms: INTERMEDIACY OF H2O2- AND p53-DEPENDENT PATHWAYS. *J. Biol. Chem.* **279,** 25535–25543 (2004).
247. Chatterjee, K., Zhang, J., Honbo, N. & Karliner, J. S. Doxorubicin cardiomyopathy. *Cardiology* **115,** 155–62 (2010).
248. Arora, H. C. *et al.* Nanocarriers enhance Doxorubicin uptake in drug-resistant ovarian cancer cells. *Cancer Res.* **72,** 769–78 (2012).
249. Kellogg, G. E., Scarsdale, J. N. & Fornari, F. A. Identification and hydropathic characterization of structural features affecting sequence specificity for doxorubicin intercalation into DNA double-stranded polynucleotides. *Nucleic Acids Res.* **26,** 4721–32 (1998).
250. Lee, H. *et al.* Molecularly self-assembled nucleic acid nanoparticles for targeted in vivo siRNA delivery. *Nat. Nanotechnol.* **7,** 389–393 (2012).
251. Liu, X. *et al.* A DNA nanostructure platform for directed assembly of synthetic vaccines. *Nano Lett.* **12,** 4254–9 (2012).
252. Tamkovich, S. N. *et al.* Circulating DNA and DNase activity in human blood. *Ann. N. Y. Acad. Sci.* **1075,** 191–6 (2006).
253. Samejima, K. & Earnshaw, W. C. Trashing the genome: the role of nucleases during apoptosis. *Nat. Rev. Mol. Cell Biol.* **6,** 677–88 (2005).
254. Parnham, M. J. & Wetzig, H. Toxicity screening of liposomes. *Chem. Phys. Lipids* **64,** 263–74 (1993).
255. Toffoli, G. *et al.* Exosomal doxorubicin reduces the cardiac toxicity of doxorubicin. *Nanomedicine (Lond).* (2015). doi:10.2217/nnm.15.118
256. Greene, R. F., Collins, J. M., Jenkins, J. F., Speyer, J. L. & Myers, C. E. Plasma pharmacokinetics of adriamycin and adriamycinol: implications for the design of in vitro experiments and treatment protocols. *Cancer Res.* **43,** 3417–21 (1983).
257. Liu, M. *et al.* A DNA tweezer-actuated enzyme nanoreactor. *Nat. Commun.* **4,** 2127 (2013).
258. Kocabey, S. *et al.* Cellular Uptake of Tile-Assembled DNA Nanotubes. *Nanomater. (Basel, Switzerland)* **5,** 47–60 (2014).
259. Fu, Y. *et al.* Single-step rapid assembly of DNA origami nanostructures for addressable nanoscale bioreactors. *J. Am. Chem. Soc.* **135,** 696–702 (2013).